CFD ANALYSIS FOR BEYOND BUBBLY GAS-LIQUID TWO-PHASE FLOWS IN A LARGE DIAMETER PIPE

by

SUNGJE HONG

A DISSERTATION

Presented to the Faculty of the Graduate School of the

MISSOURI UNIVERSITY OF SCIENCE AND TECHNOLOGY

In Partial Fulfillment of the Requirements for the Degree

DOCTOR OF PHILOSOPHY

in

NUCLEAR ENGINEERING

2023

Approved by:

Joshua P. Schlegel, Advisor
Ayodeji B. Alajo
Shoaib Usman
Syed B. Alam
Subash L. Sharma

ABSTRACT

Due to the complexity of multiphase flow phenomena, numerical analysis for multiphase turbulent flow is not as reliable as single-phase computational fluid dynamics (CFD). A literature review has revealed that the current efforts on multiphase flow simulation have focused on small diameter channels under very restricted flow conditions and have been conducted without identifying some important procedures. To expand CFD applications to a wide range of two-phase flow conditions in large diameter channels, this study aims to validate the current CFD models for vertical concurrent air-water two-phase flow simulations beyond bubbly flows. First, a numerical model developed to describe dynamical changes of interfacial area concentration (IAC) of bubbles, known as two-group interfacial area transport equation (2G IATE), is evaluated for a wide range of flow regimes in a large diameter pepe. This evaluation includes examinations of mass and momentum exchange, and interaction mechanisms between gas phases and between gas and liquid phases. Second, the interfacial force closure models, which are a key for the accurate prediction of two-phase flow parameters on the Eulerian-Eulerian framework, are validated and an appropriate choice of closure models for the flow regimes beyond bubbly flows is proposed. Third, CFD models affecting the turbulence mixing effect are compared and the effect of bubble-induced turbulence (BIT) generated by small and large bubbles is investigated. The three important aspects addressed for the validation of the CFD models for high void fraction and high velocity flow conditions in a large diameter pipe are the first effort to validate the current CFD models for beyond bubbly flows and for a large diameter pipe.

ACKNOWLEDGMENTS

First and foremost, praises and thanks to the God, the Almighty, for His blessings throughout my research work to successfully complete this journey.

I would like to express my deepest gratitude to major adviser, Professor Joshua Paul Schlegel for his continuous guidance, feedback, encouragement, and support. His insights into the two-phase flow dynamics and computational analysis are the fundamental ingredient of this research.

Sincere appreciation is extended to Professor Subash Sharma at University of Massachusetts Lowell for his valuable comments, encouragement, and overall patience. His enthusiasm for research motivated me to keep working on my research topic.

I would like to express special thanks to Professors Ayodeji Babatunde Alajo, Shoaib Usman, and Syed Alam who encouraged and supported me over the years in many ways. It was my pleasure to assist you as a graduate teaching assistant.

I am fortunate to be a member of the Thermal-Hydraulic Experiment, Modeling, and Engineering Simulation (THEMES) Laboratory and appreciate of all of the THEMES Lab. members that I have had the privilege to work with. In particular, Dr. Palash Kumar Bhowmik deserves recognition for his invaluable guidance early in the author's graduate studies. Also, I am indebted to Dr. Shaikat Mahmood Galib for making my life easier and enjoyable during our time as office mates and his continued support.

Last but not least, I would like to express my sincere appreciation to my lovely wife for her endless love and understanding over the years, my two sons for encouraging me to live in happiness, and my parents for their love and sacrifices for being willing to be the root of everything for me.

TABLE OF CONTENTS

Page

LIST OF ILLUSTRATIONS

LIST OF TABLES

NOMENCLATURE

Symbol	Description
a_i	Interfacial area concentration [m^{-1}]
C	Model constant [-]
C_D	Drag coefficient [-]
d_B	Bubble diameter [m]
D_c	Critical bubble diameter [m]
$D_{c,max}$	Maximum cap bubble diameter [m]
$D_{d,max}$	Maximum distorted bubble diameter [m]
D_h	Hydraulic diameter [m]
D_{sm}	Bubble Sauter mean diameter [m]
g	Gravitational acceleration constant [ms^{-2}]
j	Volumetric flux [ms^{-1}]
$\Delta\dot{m}_{12}$	Net inter-group volumetric mass transfer rate due to bubble interactions [kg s^{-1}]
M_i	Generalized interfacial drag force [-]
M_γ	Moment of the size distribution [-]
n	Bubble number density [m^{-3}]
∇p	Pressure gradient of phase k [Pa]
$P(d)$	Bubble/droplet size distribution [-]
R	Production rate of bubbles [m^{-3}]
S_γ	S-gamma model (order of moment) [-]
$S_{m,\gamma}$	Modification term for benchmarking two-group IATEs [-]
u_r	Relative velocity [ms^{-1}]

$\bar{u}_r$	Average relative velocity of bubbles [ms^{-1}]
$\bar{u}_{rw}$	Average relative velocity between the liquid in the wake and the surrounding liquid [ms^{-1}]
$\bar{u}_{w12}$	Average local relative wake velocity [ms^{-1}]
v	Velocity [ms^{-1}]
We	Weber number [-]

Greek symbols

α	Volume fraction [%]
η	Void fraction source/sink rate [s^{-1}]
ε	Turbulent kinetic energy dissipation rate per unit mixture mass [$m^2\ s^{-3}$]
γ	Order of moment [-]
λ	Coalescence efficiency once collision occurs [-]
ρ	Density [kgm^{-3}]
$\Delta\rho$	Density difference between two phases [kgm^{-3}]
σ	Surface tension [$kg\ s^{-2}$]
$\bar{\bar{\tau}}_k$	Shear stress tensor [$kgm^{-1}s^{-2}$]
τ_k^t	Turbulent Reynolds stresses [$kgm^{-1}s^{-2}$]
ϕ	Interfacial area concentration source/sink rate [$m^{-1}s^{-1}$]
χ	Inter-group transfer coefficient accounting for the inter-group void transport at the group boundary due to the expansion and compression [-]

Subscripts

1	Value for Group 1
2	Value for Group 2
1,2	Interaction between bubble groups

2,1	Interaction between bubble groups
B	Bubble/droplet
c	Critical value
cr	Critical value
D	Drag
f	Fluid (liquid)
g	Fluid (gas)
i	Interfacial
j	Index for source or sink terms
k	Index for phase
m	Mixture value
max	Maximum value
n	Group-n bubbles
RC	Random collision
SI	Surface instability
SO	Shearing off
TI	Turbulence impact
WE	Wake entrainment
sm	Sauter mean diameter
wb	Wall boiling

Superscripts

*	Dimensionless value
1	Value for Group 1
2	Value for Group 2
1,2	Interaction between bubble groups

2,1	Interaction between bubble groups
br	Bubble breakup
cl	Bubble coalescence
t	Turbulent

1. INTRODUCTION

Two-phase flows have been focused on various industries due to its efficient mass and energy transfer characteristics. Especially, understanding characteristics of the highly turbulent gas-liquid two-phase flows with high void fraction of gas phase in large diameter channels, for example churn-turbulent flow, is crucial for the efficient operation and safety of reactors in various fields including pharmaceuticals, petrochemical engineering, and nuclear power industry.

The two-phase flows are characterized by the existence of numerous interfaces and discontinuities in fluid properties at the interface. The interaction between the two immiscible phases causes the interfaces to change dynamically, which may result in enhancement or reduction in the efficiency of transfer of energy or mass in the two-phase flows. Therefore, identifying flow structure and the knowledge of a flow pattern are important for operating reactors.

Formation of gas phase in gas-liquid two-phase flows the flow structure are characterized by interfacial area concentration (IAC or a_i) of gas phase. Traditional approaches to identifying IAC relied on visual observation and the IAC has been calculated by empirical correlations. However, these conventional methods were dependent on flow regime and hard to reflect dynamic change of interfacial structure. To overcome these issues, numerical analysis for multiphase turbulent flow has been highlighted to model the realistic flow structures and identify the IAC.

As new trials for the better numerical techniques are proposed and computational power increases, it is evident that numerical methodology is anticipated to provide considerable details with adequate accuracy. Computational fluid dynamics (CFD) is a

desirable methodology in terms of its applicability to various industries and has been focused as a primary method for two-phase flow analysis to analyze flow characteristics as well as heat and mass transfer phenomena. The development of and the application of the CFD are a general trend since it allows for researchers and engineers to reduce the number of trials of experimental studies and can provide more economical and efficient way of design and engineering work.

Modeling flow structures and IAC of two-phase flows by using CFD is particularly important for nuclear industry with respect to nuclear reactor safety. Two-phase flow may occur in case of transients and accidents, such as the loss of coolant accident (LOCA) and trip of reactor core pumps (RCPs) for pressurized water reactors (PWR), which can lead to departure from nucleate boiling (DNB) and dry out for boiling water reactors (BWR). The nucleate boiling is one of the most important phenomena during abnormal reactor conditions, which affects reactivity of the reactor core due to the presence of voids characterized by the void coefficient and impacts neutronics performance of the reactors. CFD has been an attractive tool for investigating IAC of the various flow regimes, such as bubbly flow, cap/slug flow, churn-turbulent flow, and annular flow by implementing the state-of-the-art numerical models.

To simulate spatial and temporal change of the IAC, different sets of mathematical models for IAC prediction have been proposed coupled with various numerical techniques for resolving conservation equations, particle interaction mechanisms and treating turbulence phenomena as introduced in the following subsections. However, there are no general consensus of the models to be used for a wide range of flow conditions. Therefore, the models for the IAC should be evaluated for

beyond bubbly flows. Further the closure models of gas-liquid interactions should be tackled. When it comes to iterative finite-volume method for solving interfacial forces, which indicate momentum exchanges between the gas-liquid two phases, the magnitude of the interfacial force terms can cause convergence issues (Stewart and Wedroff, 1974) and uncertainties related to the closure models in predicting two-phase flow parameters. From the point of view, it is necessary to evaluate the closure models of interfacial forces and particle (or bubble) induced turbulence especially for the flows in a large diameter pipe since the channel diameter affects two-phase flow structure and nature of flow characteristics.

1.1. MAJOR METHODS FOR MULTIPHASE CFD MODELING

There are three major approaches for multiphase CFD modeling, i.e. two-fluid model (TFM) based approaches and direct numerical approaches. The TFM based on Eulerian-Eulerian (E-E) approach is known to be the most practical model to be used in industries due to its balance between accuracy and efficiency in solving macroscopic formulation of gas-liquid two phase flow system. Basically, the TFM solves the conservation equations of mass, momentum, and energy for each phase as a Eulerian-Eulerian approach, which treats both gas and liquid phases as the interpenetrating continua. This two fluid framework uses ensemble and time averaging process for the two sets of conservation equations for the two phases. This feature makes TFM the most widely used numerical analysis method and effective formulation in terms of computational power and correctness of predicting thermal hydraulic parameters.

Direct numerical approach is a method to solve Navier-Stock's equation in the computational mesh. There are different method to tackle the direct numerical approach. In terms of investigating turbulence physics, direct numerical simulation (DNS) and large eddy simulation (LES) are used for the direct numerical approach.

DNS solves all range of turbulent scales from smallest turbulent dissipation scales (Kolmogorov microscales) to the integral scale without any turbulence model which implies that the model can result in the most realistic prediction of the complex two-phase flow phenomena with no assumptions of any turbulent closure models, such as modeling eddy viscosity model. This feature provides higher degrees of freedom for comprehensive parametric studies and insights to understanding various flow phenomena since researchers can change thermal hydraulic parameters and evaluate how the changes affect other parameters.

LES model is to directly resolve larger turbulence scales, which contain most energy of the turbulence and are dominant in transferring momentum and turbulent mixing, by spatially filtering out the smallest scales of turbulence. This model requires the sub-grid scale (SGS) model only for the small length scales that leads to a reduction in computational power compared to DNS. Due to the small scales' isotropic and homogeneous characteristics, it is easier to model the SGS motions than resolving all length scales. However, there is no a general set of SGS closure models for the two-phase LES.

Volume-of-fluid (VOF) model uses a surface-tracking method in a fixed Eulerian grid by tracking and locating free surface (interface between the fluids) in the two-phase flows. This method follows three main steps: a scheme to locate the interface, an

algorithm to track the moving sharp interface through a computational grid, and applying boundary conditions at the interface. In this model, a single set of momentum equation is shared by the fluids and the volume fraction of all the fluids in each computational cell is tracked throughout the domain.

The direct numerical approaches, as described above, are highly dependent on mesh size, which means that the fine computational meshes are needed to capture characteristics of the smallest length scales of turbulence and generate the sharp interface enough to reflect realistic interfacial area of gas phase for accurate simulation. Even though the direct numerical approaches can result in details of a very complex physical two-phase flow phenomena with the best numerical accuracy, this requirement generally causes an extensive computational cost and limits the range of its applicability to the low Reynolds number flow conditions or a small number of particles to be calculated. Therein, at the present computational power and calculation level, the TFM based approach is unique for practical design applications.

However, due to the complexity of multiphase flow phenomena, the numerical analysis for multiphase turbulent flow is not as reliable as single-phase CFD. The application of computational multiphase fluid dynamics (CMFD) using TFM with E-E framework to nuclear reactor safety (NRS) analysis has been extensively investigated (Oberkampf and Trucano, 2002; Schwer, 2009; Bestion, 2012). In the application of the CMFD, there is a general framework of proposed systemic steps for the model development and evaluation: (1) the necessary flow interaction phenomena and processes should be identified. This includes mass, momentum and heat transfer, turbulence mixing effect, interaction mechanisms between gas phases and between gas and liquid phases,

(2) the proper CFD model should be selected, which covers status of phases, treatment of phase interface, and turbulent models, (3) the suitable closure models for interfacial momentum exchange, turbulence and wall transfers, (4) validation and verification of the models against both separate effect tests (SET) and mixed effect tests (MET), and (6) uncertainty analysis (Bestion, 2012).

In view of the general framework of the systematic steps of the CFD analysis, three important aspects are addressed for the validation of the CFD models for high void fraction and high velocity flow conditions in a large diameter pipe.

1.1.1. Model Evaluation of Interfacial Area Concentration Transfer Mechanism. In this study, first, an evaluation of the bubble interaction phenomena **is** conducted. IAC is a key parameter that represents physical interaction area between two-phase flows and characterizes the internal structures of the flows. Future, accurate prediction of IAC can improve the performance of two-fluid model.

Prediction of an IAC in two-phase flows has been an issue over several decades in various fields such as bubble column reactors in chemical engineering, heat exchangers in thermal engineering, accident conditions of nuclear reactor systems in nuclear engineering, etc. due to efficiency of reactor or system and safety of the reactor operation. Mechanistic models for dynamic prediction of IAC have been proposed by many researchers (Ishii, 1975; Kocamustafaogullari and Ishii, 1995; Ishii Millies et al., 1996; Morel et al, 1999; Lehr and Mewes, 2001; Krepper et al., 2008; Hibiki, 2011; Liao et al., 2011) to overcome several shortcomings of a static categorization of the two-phase flow structure (Ishii and Mishima, 1984 ; Kelly, 1997) and replace the traditional approach to identifying flow regimes of the two-phase flow.

There are two most popular models to predict some important parameters that represent flow characteristics, such as void fraction distribution, Sauter mean diameter, and IAC: Interfacial area transport equation (IATE) and MUltiple-Size-Group (MuSiG) model. IATE and MUSIG models are based on the same fundamental approach, which is addressing the distribution of particles in a spatial coordinates. The IATE model is directly derived from Boltzmann transport equation and MuSiG model stems from population balance equation (PBE) that is originated from the Boltzmann equation.

1.1.1.1. Population Balance Equation (PBE). Adapting population balance equation (PBE) can be a solution to reflect bubble breakup and coalescence phenomena. Diameters of particles continuously change due to various bubble interaction mechanisms. The evolution of bubble size distribution resulting from coalescence and breakup mechanisms can be modeled by the PBE. The interest in PBE has led to several numerical techniques to solve the PBE: Monte Carlo method, the discrete classes method, and the method of moments (MoM) based models. The Monte Carlo method is a statistical ensemble approach and has advantages of flexibility and accuracy to track particle changes in multidimensional system. However, this model requires extensive computation time to track changes of particle size when it comes to a large number of particles. The method of discrete classes classifies the particle size which varies continuously into a number of classes. This method has received particular interest since it is apprehensive to be implemented into CFD program. The class method can provide high accuracy and predict particle size distribution directly, but there are some limitations of high computational cost, the need of a large number of particle size classes for the accuracy, and potential errors in discretization. The MoM based models are the method

based on the idea of transforming problems into lower-order of moments of the size distribution. The order of the moments depend on features of the problems, but usually two or three moments of size distribution are used for number density, size, and volume distributions of the particles.

Therefore, this model can reduce the dimensionality of the problem significantly, is relatively simple to solve, and can handle a wide range of bubble sizes with reduced computational cost. However, the model does not provide exact particle size distribution.

1.1.1.2. Interfacial Area Transport Equation (IATE). IATE is a mechanistic model that allows predicting changes in the two-phase flow structure dynamically, and the development of the IATE opens a possibility in numerical analysis to better reflect the dynamic evolution of interfacial structure. Present commercial CFD tools and current nuclear reactor system analysis codes usually accept the two-fluid model for two-phase flow analysis, which solves conservation equations separately for each phase and requires the accuracy of constitutive models of interfacial transfer terms. Due to the proportional relationship between IAC and momentum transfer closure models, the two-fluid model heavily depends on better estimation of the IAC. An intensive attempt to benchmarking the IATE has been applied for the prediction of evolution of the IAC (Cheung et al., 2007; Lee et al., 2013; Sun et al. 2003; Tian et al., 2015; Wang and Ishii, 2021). However, there are still many difficulties in modeling the IATE. Two main challenges are to establish bubble interaction mechanisms and relationships between behavior of bubbles and turbulence. In order to resolve the challenges, an extensive experimental data

set is required, which causes another issue in model development and validation. The current potential studies of experiment will be discussed in the section 1.3.

1.1.1.3. MUltiple-Size-Group (MuSiG) model. MuSiG model (Lo, 1996) is one category of PBE. In the model, the bubble size distribution is separately assigned into bins, and the bubbles in each bin interact through kernels for the coalescence and breakup interaction mechanisms. The inhomogeneous MuSiG (iMuSiG) model (Krepper et al., 2008) has developed to account for different slip velocity conditions as the size of particle increases and to expand capability of MuSiG model to the flows with inhomogeneous particle distribution. PBE is applied to each bin of the groups and the different velocity groups are associated with the group numbers. Mass transfer between the sub-size groups (bins) is also described by considering the cases when the mass exchange due to the particle coalescence and breakup interactions make particles to have greater or less velocity than the particle's current velocity group. Even though recently the method of discrete classes has been used (Pohorecki et al., 2001; Olmos et al., 2001;Yeoh and Tu, 2004 and 2005; and Frank et al., 2005), the (i)MuSiG model has difficulties in dealing with the large number of inter-group transfer kernels and limitation of generally using no more than two velocity fields, which is the same approach with 2G IATE but requires more expensive computational cost.

Thus, class methods have shortcomings related to numerical complications and is more computationally expensive due to many interdependent momentum equations to accurately describe the bubble size and velocity distribution.

1.1.1.4. S-Gamma (*Sγ*) model. S-Gamma (*Sγ*) model, which was proposed by Simon Lo and Preetham Rao (2007) on the basis of the method of moments (MoM)

approach with assumption of singe-size approach for dispersed bubbles is an alternative method to solve PBE of a large number of population classes. By assuming a pre-defined shape of particle size distribution (log-normal distribution), *Sγ* model can reduce computational effort. Simon Lo and Dongsheng Zhang (2008) evaluated applicability of *Sγ* model by implementing the model into STAR-CCM+ code against experimental data of Hibiki et al. (2001). Many studies showed that the *Sγ* model successfully predicted bubble size, void fraction, and bubble interaction area density. Simon Lo et al. (2012) presented the improvement of sub-cooled boiling model in predicting bubble diameter and void fraction distribution by adapting *Sγ* model. Colombo, M and Fairweather, M (2016) tried to catch bubble characteristics with respect to two bubble classes, spherical and cap bubbles, by using two *Sγ* models for each bubble group. They compared results with seven experimental data and the results showed good agreement with experiments. Byong-jo Yun et al. (2012) examined *Sγ* model to improve the prediction capability of subcooled boiling flows by adjusting model coefficient for source and sink terms with an advanced wall boiling model and showed that *Sγ* model predicted well experimental data. However, since the *Sγ* model is developed for mono-dispersed bubbly flows, the model is restricted to the flows of one bubble group that includes only spherical shapes of bubbles. Therefore, the *Sγ* model is not applicable to high void fraction flow conditions or beyond bubbly flows in which large bubbles with non-spherical shapes and different velocity characteristics from the small bubbles exist.

From the discussion above, it can be concluded that the IATE model and MoM based PBE model can be primary options for two-phase flow analysis as a good balance between accuracy and computational time to cover a wide range of flow conditions rather

than (i)MuSiG model requiring more computational power. In this study, two-group (2G) IATE is benchmarked with MoM based *Sγ* PBE model to evaluate the IATE model and local phase distributions for beyond bubbly flows in a large diameter channel. Two-group bubble classes are applied by using two separate *Sγ* models, implementing two-group IATE, and introducing mass and momentum source terms for intergroup mass transfer between two-group bubble classes. The results are compared against the existing experimental data (Schlegel et al., 2012).

1.1.2. Closure Models of Momentum Conservation Equation. Second, closure models for the interfacial momentum exchange are investigated. A numerical analysis of two-phase flows has been broadly used in various fields including nuclear, chemical, medicine, and so on, for their specific purposes under unique flow conditions. Closure models for the interfacial forces in TFM, which is required for the accuracy of the TFM to account for the momentum exchange at the interface between the two phases, have been developed under limited conditions, such as single particle flow and low velocity conditions or flows in a small diameter pipe ,etc. Moreover, most of the closure models have been used for or validated for low gas volume flow rate conditions. In this paper, different closure models of interfacial drag force and lift force as main contributors of local void fraction distribution and phase interactions between gas phases as well as gas and liquid phases are compared for high gas volume flow rates, which covers bubbly flow to churn-turbulent flow regimes, in a large diameter channel to validate the current drag and lift coefficient models developed under the certain flow conditions and to give an insight to determine proper closure models for a wide range of flow regimes in a large diameter pipe. For the drag coefficient models, Schiller-Naumann model, Ishii-Zuber

model, Tomiyama model, and Buffo model are compared, and for the lift coefficient models, Tomiyama model, Hibiki model, Shaver-Podowski model, and constant value of 0.1 are evaluated based on two-group IATE (2G IATE) with *Sγ* model of population balance equation (PBE) against the experimental dataset obtained by Schlegel et al. (2012).

1.1.3. Effect of Bubble Induced Turbulence. Lastly, turbulence effect on bubble interaction mechanisms and interfacial forces is evaluated. In view of bubble flow characteristics in large diameter channels, turbulent characteristics induced by bubbles are different from that in small diameter channels. However, very few studies exist for the effect of bubble-induced turbulence (BIT) for beyond bubbly flows in a large diameter channel. In this paper four different lift coefficient models (Tomiyama, 2002; Hibiki, 2007; Constant value 0.01; Shaver and Podowski, 2015) were compared and the effects of BIT were estimated with and without different BIT conditions for group-1 (G1) and group-2 (G2) bubbles to identify the effect on local phase distributions. Four different superficial velocity flow conditions of gas and liquid phases were adapted for model comparison with experiment dataset developed by Schlegel et al. (2012). The assessment reveals that the lift coefficient models have limitations on predicting void fraction near the pipe wall and a direct approach for modeling BIT significantly impacts local profiles of dispersed phase compared to that an indirect approach, a linear algebraic model, does. The significance of BIT by G2 bubbles is enhanced at lower JL and JG conditions as well as under higher level of void fraction for G2 bubbles condition. As

increase more liquid velocity, effect of BIT model for G2 bubbles was more significant and made local phase distributions more flatten.

1.2. CHALLENGES IN MODELING TWO-PHASE FLOWS IN A LARGE DIAMETER CHANNEL

Numerical modeling inherently possesses errors in its process of calculation. In CFD simulations, the errors are divided into the two main categories as shown in Figure 1.1 indicating a general framework for computational model verification and validation (V&V). One is model error, which arises from mathematical modeling process by approximating physical processes. The other one is numerical error that is caused by the discretization of the flow geometry and numerical solution. Therefore, it is important to verify if the assumptions or backgrounds of developing the mathematical models are applicable to the simulation cases. For the application of CFD to two-phase flow analysis, Bestion et al. (2009, 2012) proposed the general steps to follow. The main concerns of the general methodology are of identification of flow process, selection appropriate numerical and computational models, and model V&V.

1.2.1. Differences in Flow Characteristics between in a Small and a Large Diameter Pipes. Flow characteristics in a pipe are highly dependent on size of the pipe. The size of the pipe can be referred to as a small diameter pipe and a large diameter pipe with respect to the critical size of a bubble that can be maintained as the maximum size of the stable bubble before it breaks up. Figure 1.2. shows the visualization of different flow regimes under the same flow conditions in small and large diameter channels. There are some key features of the two-phase flows in the small and the large diameter pipe, respectively. In the small diameter channel, stable slug bubbles can be observed, whereas

it is hard for slug bubbles to maintain their shape in a large diameter channel. Eventually cap bubbles are formed since size of the bubbles is not restricted by the channel, leading to the instability of the upper surface of the bubble. Due to the differences, dominant bubble interaction mechanisms can vary, and change of IAC due to the different shapes of bubbles may affect change in bubble-eddy interactions. Further, the IATE has been developed based on averaging methods and coefficients used for source and sink terms of bubble interaction mechanisms in the IATE vary with flow conditions and geometry of the channel.

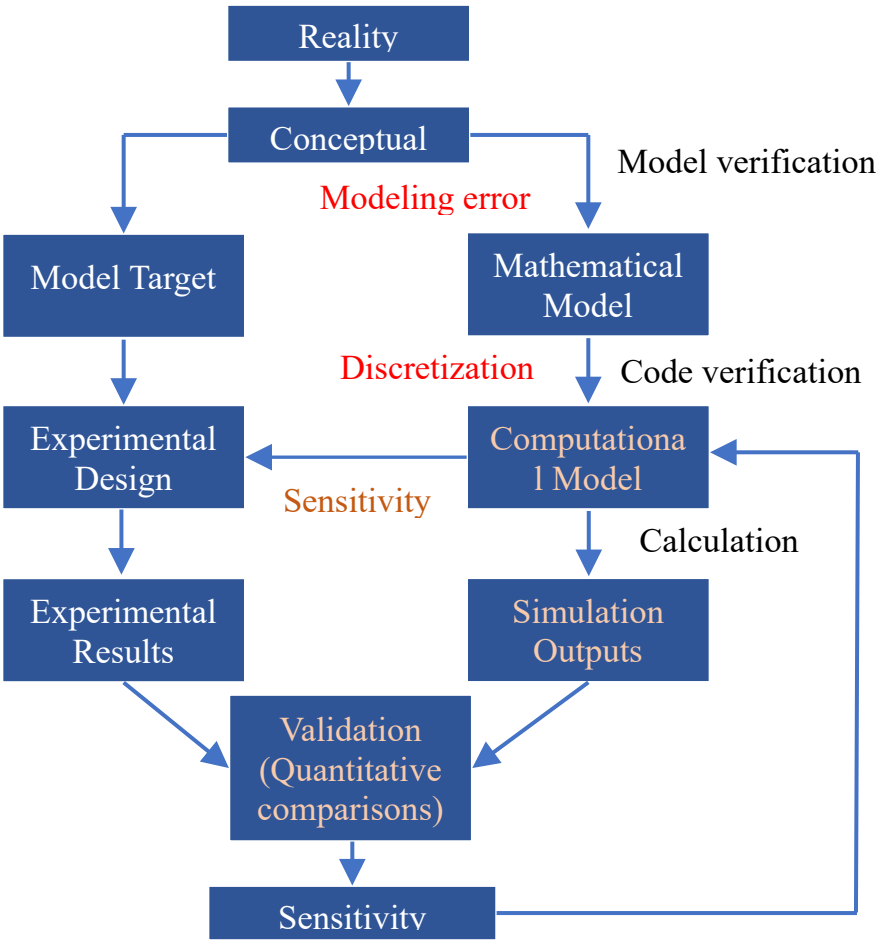

Figure 1.1. General Framework for Computational model Verification and Validation (V&V) (Bestion et al., 2009, 2012).

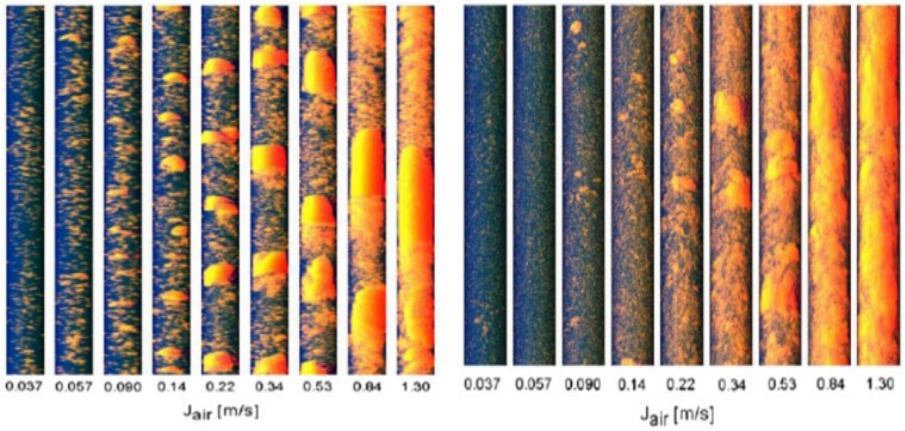

(a) (b)

Figure 1.2. Virtual Side Projections of the Void Distribution in the (a) DN50 (nominal diameter of 50 cm) and (b) DN200 Test Sections with J_L = 1 m/s (Prasser et al., 2007).

In view of bubble flow characteristics in large diameter channels, turbulent characteristics induced by bubbles are different compared to that in small diameter channels. Since large cap bubbles have higher relative velocity than small spherical bubbles does, higher turbulence is generated in the wake of large cap bubbles. This results in larger length scales of turbulence generation that carry small bubbles and different interactions between bubbles and between dispersed phase and continuous phase due to the enhanced turbulent mixing.

Moreover, transitions between flow regimes in a large diameter pipe is more gradual than the transitions in a small diameter pipe. In large diameter channels, large cap bubbles are generated by collapse of slug bubbles as well as coalescence of smaller bubbles, and the quantity of the large cap bubbles are much greater than the number of slug bubbles in small diameter channels. Moreover, while slug bubbles in small diameter channels are bounded in size by the channel wall, which leads to high concentration of small bubbles near the wall region and a small production of bubble induced turbulence,

large cap bubbles in large diameter channels are smaller than the slug bubbles and more numerous and are distributed in the whole area of the flow channel. This causes flatter void fraction distribution in radial direction in a large diameter pipe than the profile in a small diameter pipe. In addition, the large cap bubbles increase in the interfacial surface area of the dispersed phase due to its numbers. This dominance of large cap bubbles results in a larger contribution to production of turbulence. This effect was observed by Ohnuki and Akimoto (1998).

Therefore, it is vital to identify applicability of the IATE to CFD application and validity of numerical models developed for 1D analysis and for bubbly flows in a small diameter pipe to be used for beyond bubbly flows in a large diameter pipe for 2D and 3D analysis.

1.2.2. Limitations of the Current Validation Efforts. 1D system codes based on the empirical work have been used to investigate two-phase flow parameters, such as void fraction (α), Sauter mean diameter, and IAC, for the nuclear reactor safety (NRS) analysis. However, due to the lack of possibility of the 1D system code to predict the change of flow pattern as well as spatial and temporal evolution of flow structures, 3D CFD has been highlighted to resolve the issues with combinations of additional transport equations for particle number density, void and IAC transport. Recently, the 2G IATE has been developed as introduced in the previous section and validated by various researchers (Sun et al., 2003; Krepper et al., 2009; Rzehak and Krepper, 2013; Wang and Sun, 2014; Lee et al., 2013; Sharma et al., 2017 and 2019; Parekh and Rzehak, 2018; Liao et al., 2019; Kuidjo et al., 2023).Even though enthusiastic efforts have been focused on developing and validating the mechanistic models for the analysis of the two-phase

flow, Current studies mostly have focused on low void fraction conditions for a narrow range of flow conditions or used only some of the interfacial force closure models or analyzed with a full set of the closure models but missing the validation procedure for the closure models, and there is a gap between the research and actual flow phenomena existing in the reactors in terms of applicability of the analysis. Moreover, the effect of the small and large bubbles on turbulence characteristics has not been thoroughly studied yet. The recent efforts on computational simulation for gas-liquid two-phase flows in a large diameter pipe is shown in Table 1.1. Therefore, there are still some critical issues on validating the state-of-the-art numerical models and the modeling approaches.

1.3. THE CURRENT POTENTIAL EXPERIMENTAL DATA SETS

Two-fluid model has been implemented not only in the system code, such as TRACE (USNRC, 2008) and RELAP5 (Thermal Hydraulics Group, 1998), but also commercial and open source of CFD codes, such as ANSYS, STAR-CCM+, and OpenFOAM, for the safety analysis of nuclear power plants and constitutive models were validated based on the experimental data. However, two major restrictions to modeling high void fraction with high velocity flow condition in a large diameter pipe can be pointed out. First, again, the interfacial force closure models have been developed under very limited flow conditions in a small diameter channel. Second, there is a distinct lack of experimental data to validate the model, especially for beyond bubbly flows, such as cap/slug flow and churn-turbulent flow regimes. Table 1.2 shows the current potential experimental data for the flows in large diameter pipes (Schlegel et al., 2012, 2014). Yoneda et al. (2002) , Sun et al. (2002), Shen et al (2006), Shawkat et al. (2008), Shen et

Table 1.1. Literature Reviews - Simulations for Large Diameter Pipe.

Author	Geometry	Flow Conditions	Flow Regimes	Simulation Code	Turbulence Model	Method	Interfacial forces/Models	Coalescence model	Breakup model
Krepper et al. (2008)	Pipe D=195.3 L=7800	J_G=0.14 - 0.2194 J_L=1.017	Bubbly	Ansys CFX-4	SST	iMUSIG	C_D: Tomiyama C_L: Tomiyama C_{WL}: Tomiyama C_{TD}: Burns	Prince and Blanch	Luo and Svendson
Deju et al. (2012)	pipe D=195.3 L=9000	J_G =0.14 - 0.2194 J_L =1.017	Bubbly	Ansys CFX-11	κ-ω SST	DQMoM	C_D: Ishii-Zuber C_L : Tomiyama C_{WL} : Antal C_{TD} : Burns	Hibiki and Ishii	Hibiki and Ishii
Cheung et al. (2012)	pipe D=195.3 L=9000	J_G =0.0096 - 0.0898 J_L =1.017	Cap bubbly	Ansys CFX-11	κ-ω SST	ABND	C_D : Ishii-Zuber C_L : Tomiyama C_{WL} : Antal C_{TD} : Burns	Prince and Blanch	Luo and Svendson
Deju et al. (2013)	pipe D=195.3 L=9000	J_G =0.14 - 0.2194 J_L =1.017	Bubbly	Ansys CFX-11	κ-ω SST	ABND, MUSIG, DQMoM	C_D : Ishii-Zuber C_L : Tomiyama C_{WL} : Antal C_{TD} : 1	Yao and Morel, Prince and Blanch	Yao and Morel Luo and Svendson
Liao et al. (2015)	Pipe D=195.3 L=7800	J_G =0.0069-0.0413 J_L =0.405-1.611	Bubbly and Cap bubbly	Ansys CFX-14.5	SST	iMUSIG	C_D : Ishii-Zuber C_L : Tomiyama C_{WL} : Hosokawa C_{TD} : Burns	Prince and Blanch	Luo and Svendson
Swiderski et al. (2016)	Pipe D= 200 L=1800	J_G = 0.0275 - 0.113 J_L =0.25 - 0.986	Bubbly	TransAT	κ-ε	DQMoM	C_D : Tomiyama C_L : Tomiyama C_{WL} : Antal	Coulaloglou and Tavlarides	Laakkonen

al. (2012), and Tian et al. (2015) were focused on bubbly flow regimes or up to cap/slug flow regime. Smith et al. (2002), Prasser (2007), and Lucas et al. (2010) expanded the range of dataset to churn-turbulent flow regime. Although some of the works in the Table 1.2 covered beyond bubbly flows, such as cap/slug flow and churn-turbulent flow regimes, their data set are in the range of the data set obtained by Schlegel et al. (2012, 2014). Further, the reported data obtained by Lucas et al. (2010) that cover a similar range of flow conditions to the data of Schlegel et al. (2012, 2014) was obtained at only two fixed superficial liquid velocities, and when it comes to the setup for the measurement, the data may be hard to reflect the actual evolution of typical boiling flows. The Schlegel data are, therefore, the most suitable data set for the analysis of the model validation under a wide range of flow conditions beyond bubbly flow regimes.

The dataset collected by Schlegel et al. (2012, 2014) describes the local database for vertical upward air-water two-phase flows and consists of intensive local distributions of two-phase parameters in a wide range of flow regimes from bubbly flows to churn-turbulent flows. Test section used in the experiment is a vertical round pipe with the inner diameter of 0.152 m. During the experiment, water was circulated upwards through the pipe by centrifugal pump for liquid velocities of up to 2 m/s and air was injected using an injector unit for gas velocities up to 10 m/s to allow experiment to investigate the effect of varied inlet conditions on the flow.

Table 1.2. The-State-of-the-art Experimental Data sets for Large Diameter Channels (Shen et al., 2018).

Author	Geometry [m]		Gas/Liquid [-]	z/D_h [-]	P [Mpa]	$<J_G>$ [m/s]	$<J_L>$ [m/s]	Measured parameters	Techniques
Ohnuki and Akimoto (2000)	Round pipe	D_h=0.2	Air/Water	10, 60	0.1	0.03–4.7	0.06–1.06	Flow regime map, α, v_{gz}, D_{av}, v_f, $\widetilde{v_f}$	Double-sensor probe, X-type hot-film probe
Yoneda et al. (2002)	Round pipe	D_h=0.155	Steam/Water	0.48, 2.42, 4.35	Max. 0.5	0.01–0.25	0.21–0.59	α, v_{gz}, a_i	Double-sensor probe
Smith (2002)	Round pipe	D_h=0.1016	Air/Water	5, 20, 30	0.1	0.048–7.0	0.058–2.0	α, v_{gz}, a_i , α_1, a_{i1}, v_{gz1}, α_2, a_{i2}, v_{gz2}	Four-sensor probe
	Round pipe	D_h=0.1524		4, 11, 18	0.1	0.04–1.0	0.05–1.0		
Sun et al. (2002)	Round pipe	D_h=0.1016	Air/Water	3, 18, 33	0.1	0.048–0.121	0.058–1.021	α, v_{gz}, a_i	Four-sensor probe
Shen et al. (2006)	Round pipe	D_h=0.2	Air/Water	12, 60	0.1	0.0322–0.218	0.148–1.12	α, v_{gz}, a_i	Four-sensor probe
Prasser (2007)	Round pipe	D_h=0.195	Air/Water	1.1–40	0.1	0.0094–0.53	1.02	α, v_{gz}, a_i , D_{av}	Wire-mesh sensor
Schlegel et al. (2012)	Round pipe	D_h=0.152	Air/Water	2.17, 14.1, 28.0	0.1	0.13–11.21	0.21–1.81	α, v_{gz}, a_i α_1, a_{i1}, v_{gz1}, α_2, a_{i2}, v_{gz2}	Four-sensor probe
Schlegel et al. (2014)	Round pipe	D_h=0.152	Air/Water	28	0.28	0.13–11.21	0.21–1.81	α, v_{gz}, a_i α_1, a_{i1}, v_{gz1}, α_2, a_{i2}, v_{gz2}	Four-sensor probe
	Round pipe	D_h=0. 203		21	0.28	0.28–3.87	0.42–0.46		
	Round pipe	D_h=0.304		14	0.28	0.3–2.33	0.46–0.48		
Shen et al. (2012)	Round pipe	D_h=0.2	Air/Water	41.5, 82.8, 113	0.1	0.0127–0.373	0.0505–0.312	α, v_{gz}, a_i , α_1, a_{i1}, v_{gz1}, α_2, a_{i2}, v_{gz2}	Four-sensor probe
Tian et al. (2015)	Round pipe	D_h=0.1016	Air/Water	2, 29	0.1	0.004–0.095	0.071–0.213	α, v_{gz}, a_i	Four-sensor probe

Measurements were performed at three axial locations (The height-to-diameter (z/D) ratio = 2.17, 14.1 and 28.0) using electrical conductivity four-sensor probes based on the design of Kim, et al. (2000). The local data measured by the four-sensor probes contains the IAC, Sauter mean diameter (D_{sm}), void fraction (α), and velocity of gas phase at the three measurement locations. Measured void fractions ranged from 10 to 90%. Benchmark experiment has found that a relative uncertainty in the local void fraction measurement ranges from 5% to 25% for very low total volumetric fluxes and the upper limit of total volumetric flux, respectively.

1.4. STATEMENT OF OBJECTIVES

A general goal of this work is to evaluate the-state-of-the-art CFD models that are necessary to solve two-phase flow problems and calculate local distributions of the two-phase flow parameters. Many studies, which are addressed in the previous introduction parts, assumed that the numerical models they decided to use were proper for their works, even though the models were developed under different geometric and flow conditions.

In this dissertation, three fundamental models to solve PBE, spatial and temporal transports of void fraction and IAC, and momentum and turbulence exchanges were analyzed to improve multiphase flow modeling for large diameter pipes in CFD.

The principal objectives of this research are as follows:

- Benchmark two-group interfacial area transport equation (2G IATE) and bubble interaction mechanisms developed by Smith et al. (2012) for beyond bubbly flows. In order to implement the 2G IATE proposed by Ishii and Kim

(2009) on the framework of the S_γ model in STAR-CCM+ CFD code, user-defined-functions (UDFs) is used in the STAR-CCM+ commercial CFD code.

- Determination of proper PBE model. As a representative of MoM and Class Method, the two PBE model, S_γ model and MuSiG model, respectively, were compared to find which approach works better for a wide range of flow conditions in a large diameter pipe.
- Determination of suitable interfacial force closure models. Two main interfacial forces were evaluated with different momentum closure coefficient models.
- Evaluation of the effect of the BIT. The effect of direct and indirect approaches to handling bubble-induced turbulence (or mixing) model were analyzed.
- Figuring out the feedback of the model comparisons to the local distributions of the two-phase flow parameters, such as void fraction and IAC.

1.5. RESEARCH CONTRIBUTIONS

This study concerned a wide range of flow regimes from bubbly to churn-turbulent flow regimes under various flow conditions. From the evaluations of the fundamental model comparison, the following specific contributions have been highlighted:

- CFD modeling for flow regimes beyond bubbly flows
- Implementing five major bubble coalescence and breakup mechanisms (RC, WE, TI, SO, and SI).

- Evaluation of 2G IATE with PBE using MoM of particle size distributions and local phase distributions of void fraction and interfacial area concentration
  - Effect of 2G IATE
- Investigation of closure models for interfacial closures for local phase distribution in a large diameter pipe
  - Effect of lift force coefficient models on void fraction distributions
  - Effect of small and large bubbles on turbulence in a large diameter channel for beyond bubbly flows
  - Comparison of different conditions of BIT
  - Prediction of turbulent parameters according to BIT conditions based on PBE
  - Identification of effect of direct approach and indirect approach for considering BIT modeling
- Help for understanding non-linear feedback loop among lateral redistribution forces and turbulence characteristics induced by small and large bubbles
- Support of the understanding of complex multiphase flows for the design, process optimization and safety analysis of related apparatuses and processes.

1.6. OUTLINE FOR THE VALIDATION PROCESS

This evaluation work followed the general framework of the systemic steps as shown in Figure 1.3. First, to set a frame of the modeling for the evaluations, PBE models were compared based on the same boundary conditions, momentum forces, and bubble interaction mechanisms.

Second, source terms to be derived and added to the default frame of model were identified. Third, all source terms were derived and implemented to reflect 2G IATE and the five major bubble interaction mechanisms into the PBE model that was certified by the first step. Through the tree steps, a frame of simulation model was fixed. For the next step to evaluate flow interaction phenomena and the effect of momentum exchanges, four different coefficient models of the interfacial closure model, such as interfacial drag and lift forces, were chosen, and the model equations were implemented into the STAR-CCM+ code. Five, the effects of the BIT were investigated with direct and indirect approaches of considering turbulence source terms. The implementation work was done by using USDs and the local distributions of the void fraction and IAC were evaluated for all comparison works. This dissertation is composed of three topics. First topic covers evaluation of two-group interfacial area transport equation coupled with S_γ PBE for beyond bubbly flows in a large diameter pipe. This topic provides the effect of 2G IATE model and inter-group mass transfer model on the prediction in the distribution of void fraction and IAC for each bubble group. Second topic is about comparison study on drag and lift interfacial forces for beyond bubbly flows in a large diameter pipe. Different drag and lift coefficient models were compared and the best options of coefficient model for the drag and lift interfacial forces were suggested for the beyond bubbly flow regimes. The last topic covers a study on the effect of bubble-Induced Turbulence on two-phase flow parameters for beyond bubbly flows in a large diameter channel. The effect of BIT was evaluated with two approaches to considering source terms in two-equation turbulence model.

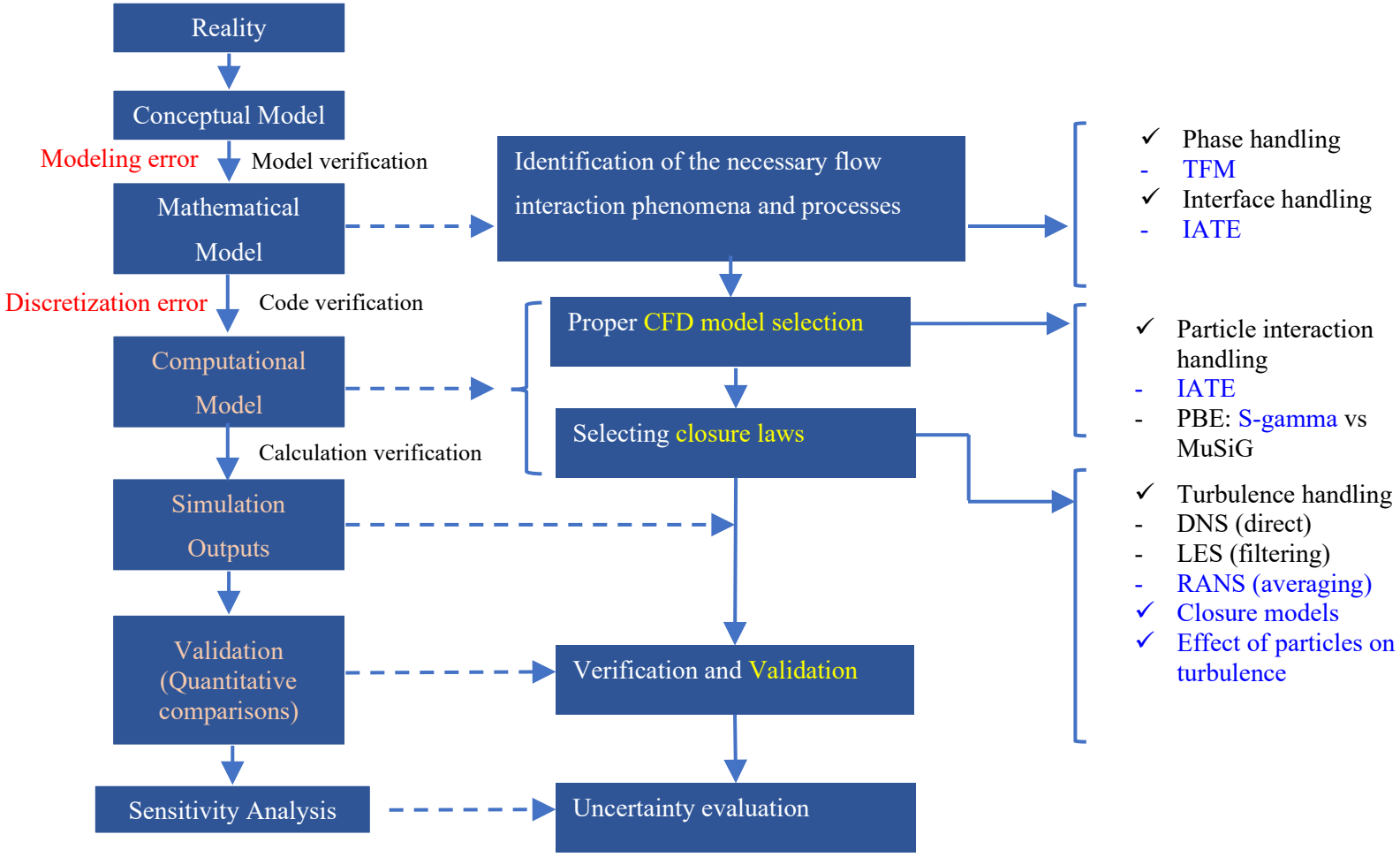

Figure 1.3. General Methodology for Two-Phase CFD Application to Nuclear Reactor Safety (Bestion et al., 2009, 2012).

2. TWO PHASE FLOW PARAMETERS

Two phase phenomena is especially important for safe operation of nuclear power plant. Two-phase flow may occur in case of transients and accidents, such as the loss-of-coolant-accident (LOCA) and trip of reactor cooling pumps (RCPs) for pressurized water reactors (PWRs), which can lead to departure from nucleate boiling (DNB) and dry out for boiling water reactors (BWRs). The nucleate boiling is one of the most important phenomena during abnormal reactor conditions, which affects reactivity of the reactor core due to the presence of voids characterized by the void coefficient. The void generation and its behavior affect not only the thermal-hydraulic characteristics due to the redistribution of the coolant flow through the core but also the nuclear characteristics due to the void reactivity feedback mechanism. The understanding of flow regimes is also very important for BWRs, where the accurate knowledge of the correct distribution of the void fraction allows the prediction of moderator density curves that strongly affect the neutronics performance and local power production, as well as the heat transfer within the power production of reactor core.

Two phase flows are characterized by some important parameters, which is known as two phase flow parameters. There are a number of parameters, such as void fraction, superficial velocity, interfacial area concentration (IAC), Sauter mean diameter, quality, distribution parameter, etc., critical to the numerical evaluation. In this study, void fraction and IAC are focused because of the reasons that the two parameters are the main factors that determine flow regime. Moreover, Sauter mean diameter can be calculated by using the two parameters, and the local distribution of the two properties

directly affects reactor performance and safety of the reactor. Figure 2.1 represents the differences of the parameters for the various size of bubbles in the continuous phase.

Sauter mean diameter is defined as the surface-volume mean diameter or the volume/surface area ratio. The variation of bubble diameter affects the interfacial momentum transfer since the interfacial forces and turbulent structure are strongly dependent on bubble size. It determines the bubble rising velocity and the gas residence time, which in turn governs the gas hold-up, the interfacial area, and subsequently the gas-liquid mass transfer rate. Void fraction is a fundamental multiphase characteristics, which influences the overall performance of system, affects the pressure drop, and can significantly modify the flow structure. IAC is defined as the sum of the interfaces per unit volume. The IAC characterizes the kinematic effect, and it is strongly related to the two-phase flow structure.

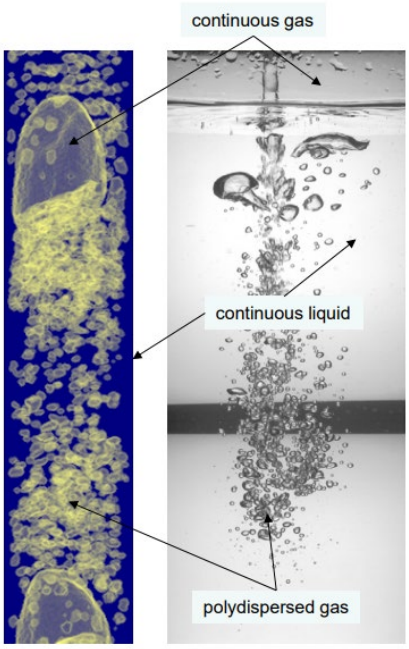

Figure 2.1. Two-Phase Flow Parameters of a Gas Phase in Different Sizes (Lucas and Laurien, 2015).

3. TWO PHASE FLOW MODELING

3.1. BACKGROUND

Two-phase flows have been focused by various industries, such as pharmaceuticals, petrochemical engineering, and nuclear power industry, due to its efficient mass and energy transfer characteristics. Especially, understanding characteristics of the highly turbulent gas-liquid two-phase flows with high void fraction of gas phase in large diameter channels, for example churn-turbulent flow, is crucial for the efficient operation and safety of reactors in large-diameter bubble-column reactors and in highly exothermic processes, such as Fischer–Tropsch synthesis and hydrogenation MAC. Especially, in terms of safety, the two-phase flows grab a special attention for nuclear power plant because the different two-phase flow structures exist not only in the most two popular types of light water reactor, boiling water reactor (BWR) during normal and transients or accident conditions and pressurized water reactor (PWR) during accident scenarios, but also in the advanced BWR designs using natural circulation for cooling the nuclear reactor during the accident conditions.

The region, where the two-phase flows present in the reactor core for both reactor types, can be considered as a large diameter pipe. A dimensional criteria for a large and a small diameter pipe has been accepted as a channel diameter that stable slug bubbles are not capable of maintaining their shapes. In view of bubble flow characteristics in large diameter channels, turbulent characteristics induced by bubbles are different from that in small diameter channels. The detail descriptions of the difference can be found in the papers, Schlegel et al., (2016); Shen et al., (2018).

Computational power has been used to predict the two-phase flow phenomena. For the analysis of the systemic impact, one-dimensional based predictive codes, such as RELAP and TRACE, are used, and the three-dimensional (3D) CFD codes, such as CFX, and STAR-CCM+, are adopted based on the two-fluid model for the evaluation of the local two-phase flow characteristics. However, the characteristics of two-phase flows vary depending on size of channels, and it is hard to expect accurate flow regimes due to the complexity of interphase interaction.

Present commercial CFD tools and current nuclear reactor system analysis codes usually accept the two-fluid model for two-phase flow analysis due to its balance between accuracy and efficiency in solving macroscopic formulation of gas-liquid two phase flow system with appropriate closure relations for the two-fluid model. The two-fluid model solves conservation equations separately for each phase and requires the accuracy of constitutive models of interfacial transfer terms. Because of the proportional relationship between IAC (or a_i) and momentum transfer closure models, the two-fluid model heavily depends on better estimation of the IAC. An intensive attempt to benchmarking the IATE has been applied for the prediction of evolution of the IAC.

The IAC is a key parameter that represents physical interaction area between two-phase flows and characterizes the internal structures of the flows. Prediction of an IAC in two-phase flows has been an issue over several decades in various fields such as bubble column reactors in chemical engineering, heat exchangers in thermal engineering, accident conditions of nuclear reactor systems in nuclear engineering, etc. to comprehend details of the flow phenomena.

Describing flow structures and identifying IAC have been achieved by visual observations in experiment point of view by taking photos and treating them with mathematical methods for sampling and tracking and have been calculated by empirical correlations separately derived from individual flow regimes in modeling perspective, respectively (Ishii and Mishima, 1984). However, these traditional methods have several shortcomings (Ishii et al., 1998). Some main drawbacks are that the conventional methods heavily rely on statistical approach and the modeling framework of thermal-hydraulic system analysis code identifies flow structure based on flow regimes and transition criteria, which are obtained from the existing experimental data. The process of identifying flow regime can be very subjective. Moreover, errors in finding transition criteria and the interfacial area correlations can be huge. However, these approaches are highly dependent on the flow regime with significant potential errors, and hard to reflect dynamic change of interfacial structure.

Mechanistic models for dynamic prediction of IAC have been proposed by many researchers (Ishii, 1975; Kocamustafaogullari and Ishii, 1995; Millies et al., 1996; Morel et al, 1999; Lehr and Mewes, 2001; Krepper et al., 2008; Ishii and Hibiki, 2011, Liao et al., 2011) to overcome the several shortcomings of a static categorization of the two-phase flow structure (Ishii and Mishima, 1984; Kelly, 1997) and replace the traditional approaches to identifying flow regimes of the two-phase flow.

To accommodate a spatial and temporal evolution of interfacial structure, the IATE proposed by Kocamustafaogullari and Ishii (1995) is a mechanistic model that allows predicting dynamical changes in the two-phase flow structure. Wu et al. (1998) developed one-group IATE, which is applicable to homogeneous two-phase flows, such

as bubbly flow regimes, by assuming all bubbles have spherical or distorted shape and move at the same velocity. The one-group IATE has been improved (Hibiki and Ishii (2000), Ishii et al. (2002) and Kim et al. (2003)) for bubbly flows in different sizes and shapes of channels and benchmarked for one-dimensional analysis with three dominant bubble coalescence and breakup mechanisms of random collision (RC), wake entrainment (WE), and turbulence impact (TI) (Ishii et al., 2002; Sun et al., 2002; Kim et al., 2003). Later, in need of better descriptions for bubbles of different sizes and shapes that show different behavior in terms of interaction mechanisms and relative motion, Fu et al. (2003a, 2003b) proposed two-group (2G) IATE to expand applicability to a wide range of flow conditions. Extensive efforts to theoretically improved the 2G IATE (Kim and Ishii (2004), Sun et al. (2003), Smith et al. (2012)) have been made for a small and large diameter pipe as well as a rectangular flow.

However, there are still many difficulties in modeling the IATE. One of the challenges is to establish bubble interaction mechanisms and relationships between behavior of bubbles and turbulence. Moreover, flow characteristics in a pipe are highly dependent on size of the pipe. In a small diameter channel, as an example, stable slug bubbles can be observed, whereas it is hard for slug bubbles to maintain their shape in a large diameter channel. Eventually cap bubbles are formed since size of the bubbles is not restricted by the channel, leading to instability of the bubble surface. Due to the differences, dominant bubble interaction mechanisms can vary, and change of IAC due to the different shapes of bubbles may affect change in bubble-eddy interactions. Further, the IATE has been developed by employing area-averaging scheme and coefficients used for source and sink terms of bubble interaction mechanisms in the IATE vary with flow

conditions and geometry of the channel. Therefore, it is vital to identify applicability of the 2G IATE to CFD application and validity of numerical models developed for one-dimensional analysis and for bubbly flows in a small diameter pipe to be used for beyond bubbly flows in a large diameter pipe for the higher dimensional analysis.

Adapting population balance equation (PBE) can be a solution to reflect bubble breakup and coalescence phenomena. Diameters of particles are continuously changed due to the bubble interaction mechanisms. The evolution of bubble size distribution resulting from coalescence and breakup mechanisms can be modeled by the PBE. As explained in the previous section, the *Sγ* model was derived on the basis of the MoM approach to track growth of bubble sizes with an assumption of the log-normal particle size distribution. The basic idea behind MoM centers in the transformation of the problem into lower-order of moments of the size distribution and has many advantages in terms of computational economy which reduces the dimensionality of the problem significantly and has ability to cover a wide range of bubble sizes with reduced computational cost. This model uses only one or two moments of the size distribution and solves individual transport equations.

Even though an enthusiastic efforts (Sun et al., 2003; Krepper et al., 2009; Rzehak and Krepper, 2013; Wang and Sun, 2014; Lee et al., 2013; Sharma et al., 2017 and 2019; Parekh and Rzehak, 2018; Liao et al., 2019; Kuidjo et al., 2023) have been focused on developing and validating the constitutive equations to describe bubble interaction phenomena for the large diameter pipe flows, there are still some critical issues on validating the state-of-the-art efforts and analyzing the applicability to the different size of channels since the works covered very limited flow conditions, such as low velocity or

low void fraction, or focused on a few flow regimes, such as bubbly flows only, cap bubbly flows, or bubbly and cap bubbly flow. In this study, the 2G IATE is benchmarked with *Sγ* PBE model to evaluate the IATE model and local phase distributions for beyond bubbly flows in a large diameter channel. Two-group bubble classes are applied by using two separate *Sγ* models, implementing the 2G IATE, and introducing mass and momentum source terms for intergroup mass transfer between two-group bubble classes. The results are compared against the existing experimental data (Schlegel et al., 2012).

3.2. THREE-FIELD TWO FLUID MODEL

Two fluid models are termed Eulerian-Eulerian models because both the liquid and the gaseous phases are considered to be continuous, fully interpenetrating continua, coupled by an interaction term. The basic approach of the two-fluid model is to formulate the conservation equations of mass, momentum, and energy for a fixed control volume where both phases co-exist with the assumption of interpenetrating continua or fluids.

In the general two-fluid model, the field equations are expressed by the six conservation equations consisting of mass, momentum and energy equations for each phase. However, modified governing equations considers two bubble groups to reflect variations in bubble size and shape. Therefore it handles three field, liquid and the two gaseous phases. To apply concept of two-group bubble classification to the two-fluid model, it is necessary to make certain modifications in the two-fluid model to facilitate a mass transfer between the two groups of bubbles.

Three-field two-fluid model describes hydrodynamic phenomena of two groups of gas phases (bubbles) and one liquid phase. In the two-group formulation, bubbles can be

categorized into two groups of group-1 and group-2 bubbles in view of their different transport characteristics due to the variations in drag and lift forces and particle interaction mechanisms as shown in Figure 3.1. Group-1 bubbles include spherical and disported bubbles and exist in the range of minimum bubble diameter to critical bubble size of maximum distorted bubble diameter, $D_{d,max}$, whereas group-2 bubbles consists of cap, Taylor, and churn-turbulent bubbles and fall into the range of $D_{d,max}$ to upper limit for the maximum stable bubble size, $D_{c,max}$, due to surface instability. $D_{d,max}$ and $D_{c,max}$ are given by Kocamustafaogullari et al. (1995) and Ishii and Hibiki (2011) as:

$$D_{d,max} = 4\sqrt{\frac{\sigma}{g\Delta\rho}} \quad \text{and} \quad D_{c,max} = 40\sqrt{\frac{\sigma}{g\Delta\rho}} \tag{1}$$

where σ, g, and $\Delta\rho$ refers to the surface tension, gravity acceleration, and difference of density between liquid and gas phases, respectively.

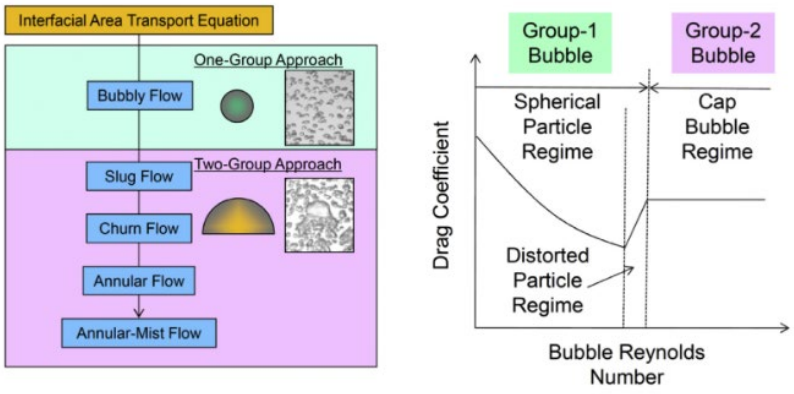

Figure 3.1. Basic Concept of Two Bubble Groups Approach (Lin and Hibiki, 2014).

By accounting for the presence of the two group bubbles, three-field two-fluid model can solve three velocity fields separately for each phase of group-1 bubbles,

group-2 bubbles, and liquid. In particular, the adiabatic three-field two-fluid model is considered in this work. Two-fluid model in the simulation is based on the two-fluid model introduced by Ishii and Kim (2004) allowing for the presence of two gas velocity field. For adiabatic condition, however, source and sink terms due to phase change are dropped off. In general, the pressure and temperature for group-1 and group-2 bubbles can be assumed to be identical. Based on this assumption, the density is the same for group-1 and group-2 bubbles. Two-group approach of bubbles requires some modification to conventional two-fluid model. Due to mass transfer between the two-group of bubbles, the continuity equation for the gaseous phase should address two equations for each group of bubbles and account for inter-group transfer of mass. Momentum equation should also include the corresponding mass transfer term between the groups. Under the limited condition, the mass and momentum conservation equation read:

3.2.1. Mass Conservation Equation.

$$\frac{\partial \alpha_k \rho_g}{\partial \mathrm{t}} + \nabla \cdot \left(\alpha_k \rho_g v_k\right) = \begin{cases} 0, & k = 0 \\ -\Delta \dot{m}_{12}, & \mathrm{k} = 1 \\ \Delta \dot{m}_{12}, & k = 2 \end{cases} \tag{2}$$

where $k = 0$ is for liquid, $k = 1$ is for group-1 bubbles, and $k = 2$ is for group-2 bubbles. $\Delta \dot{m}_{12}$ represents the net mass transfer rate from group-1 bubbles to group-2 bubbles per unit mixture volume due to the bubble interactions and expansion or compression and it is given by:

$$\Delta \dot{m}_{12} = \rho_g \left[\sum_j \eta_j + \chi \left(\frac{D_{d,max}}{D_{sm1}}\right)^3 \left(\frac{\partial \alpha_1}{\partial t} + \nabla \cdot (\alpha_1 \overrightarrow{v_1})\right)\right] \tag{3}$$

where $\sum_j \eta_{j,2}$ is the net inter-group void fraction transport and is expressed as:

$$\sum_j \eta_{j,2} = \eta_{RC,2}^{(11,2)} + \eta_{RC,2}^{(12,2)} + \eta_{WE,2}^{(11,2)} + \eta_{WE,2}^{(12,2)} + \eta_{SO,2}^{(2,12)} + \eta_{TI,2}^{(2,1)} \quad (4)$$

Each term in Equation (4) has been modeled by Smith et al. (2012) for vertical upward air-water two phase flows in a round pipe. Subscript *j* indicates bubble coalescence and breakup mechanisms including random collision (RC), wake entrainment (WE), shearing-off (SO), and turbulence impact (TI).

χ is an inter-group transfer coefficient accounting for the inter-group void transport at the group boundary due to the expansion and compression. ϕ_j is the interfacial area source/sink rate due to the bubble interactions. Sun et al. (2004) determined "χ" from the particle distribution function with respect to the bubble chord length as

$$\chi = 4.44*10^{-3} \left(\frac{D_{sm1}}{D_{d,max}}\right)^{0.36} \alpha_{g1}^{-1.35} \quad (5)$$

This value should be bounded between 0 and 2. Recently, Kumar and Brooks (2018) found the value of "χ", which improves model performance. However, this study has a purpose of investigating effect of 2G IATE, and Sun's model would be able to give appropriate results for the evaluation.

3.2.2. Momentum Conservation Equation.

$$\frac{\partial \alpha_k \rho_g v_k}{\partial t} + \nabla \cdot (\alpha_k \rho_k v_k v_k) = -\alpha_k \nabla p_k + \nabla \cdot \alpha_k (\overline{\overline{\tau_k}} + \tau_k^t) + \alpha_k \rho_k g + (-1)^k \Delta \dot{m}_{12} v_k + \overrightarrow{M_{lk}} - \nabla \alpha_k \cdot \overline{\overline{\tau_{kl}}} \quad (6)$$

Subscript *i* and l are an index of subcomponent and liquid phase. τ_k^t represents turbulent Reynolds stresses which are closed using a two-phase *k-ε* model that includes the bubble induced turbulence of the cap bubbles. $(-1)^k \Delta \dot{m}_{12} v_k$ indicates momentum

transfer term due to inter-group mass transfer in the gaseous phase. $\overrightarrow{M_{\iota k}}$ is for the interfacial forces. The last term on R.H.S. of Equation (6) describes an interfacial shear term. In this study, the interfacial shear term is not considered due to stability issue.

3.2.3. Modeling for Mass Transfer. Due to the assumption of two bubble group categorization, consideration of transfer in mass and momentum between the groups is necessary, and conventional mass and momentum conservation equations need to be modified. Breakup of large bubbles in group-2 may lead to increase of void fraction of small bubbles in group-1 that causes increase in mass of group-1 bubbles. In addition, coalescence of small bubbles in group-1 can form large bubbles, which means mass transfer from group-1 to group-2. Those mass transfer results in momentum changes of both group-1 and group-2 bubbles.

Mathematical form of the source term to be added to mass conservation equation of group-1 and group-2 bubbles is shown in equation (3). Passive scalar transport equation is used to implement the mass source term. By ignoring diffusion term and considering convection transport only, passive scalar transport equation can be simplified as shown in Equation (7).

$$\frac{\partial}{\partial t}\int_{\tilde{V}} \rho\phi_k d\tilde{V} + \oint_A \rho\phi_k\left(v - v_g\right)\cdot d\tilde{a} = \int_{\tilde{V}} S_{\phi_k} dV \tag{7}$$

Parameters of ρ, ϕ_k, v, and S_{ϕ_k} in the Equation (3-7) are density, passive scalar, velocity, and a source term for passive scalar component *k*, relatively. $d\tilde{V}$ and $d\tilde{a}$ are defined as $\alpha_k X dV$ and $\alpha_k X da$, where α_k is the volume fraction of phase *k* and X is void fraction. $\Delta\dot{m}_{12}$ in the Equation (3) is used as the source term of S_{ϕ_k}.

Solution of the Equation (7) gives a value of passive scalar, ϕ_k. Initial value of ϕ_k was set as a constant value of 1, and ϕ_k is updated every iteration of calculation based

on the source term of S_{ϕ_k}. The final form implemented into continuity equations for both group-1 and group-2 bubbles in STAR-CCM+ code is calculated as $\alpha_k(X\phi_k)$.

3.3. INTERFACIAL AREA TRANSPORT EQUATION

The use of the dynamic equation to characterize the interfacial area transport is an effective method to represent interfacial structure and flow regime transition. In view of this, two-group interfacial area transport equation (IATE) is proposed to be implemented into CFD codes to represent various transport properties as well as coalescence and breakup for each individual group.

3.3.1. Two-Group Interfacial Area Transport. Wu et al. (1998) suggested the concept of the 2G IATE, and theoretical model for the 2G IATE was established by Ishii and Kim (2004). The 2G IATE was derived from the particle transport equation by accounting for volume range of each group. The final form of the 2G IATE for adiabatic two-phase flows is formulated as:

For group-1 bubbles,

$$\frac{\partial a_{i1}}{\partial t} + \nabla \cdot (a_{i1}\overrightarrow{v_{i1}}) = \frac{2}{3}\left(\frac{a_{i1}}{\alpha_{g1}}\right)\left(\frac{\partial \alpha_{g1}}{\partial t} + \nabla \cdot \left(\alpha_{g1}\overrightarrow{v_{g1}}\right)\right) - \chi\left(\frac{D_{d,max}}{D_{sm1}}\right)^2\left(\frac{a_{i1}}{\alpha_{g1}}\right)\left(\frac{\partial \alpha_{g1}}{\partial t} + \nabla \cdot \left(\alpha_{g1}\overrightarrow{v_{g1}}\right)\right) + \sum_j \phi_{j,1} \quad (8)$$

For group-2 bubbles,

$$\frac{\partial a_{i2}}{\partial t} + \nabla \cdot (a_{i2}\overrightarrow{v_{i2}}) = \left(\frac{2}{3}\right)\left(\frac{a_{i2}}{\alpha_{g2}}\right)\left(\frac{\partial \alpha_{g2}}{\partial t} + \nabla \cdot \left(\alpha_{g2}\overrightarrow{v_{g2}}\right)\right) + \chi\left(\frac{D_{d,max}}{D_{sm1}}\right)^2\left(\frac{a_{i1}}{\alpha_{g1}}\right)\left(\frac{\partial \alpha_{g1}}{\partial t} + \nabla \cdot \left(\alpha_{g1}\overrightarrow{v_{g1}}\right)\right) + \sum_j \phi_{j,2} \quad (9)$$

The bubble interaction mechanisms for the 2G IATE are modeled as:

$$\sum_j \phi_{j,1} = \phi_{RC}^{(1)} + \phi_{RC,1}^{(12,2)} + \phi_{WE}^{(1)} + \phi_{WE,1}^{(12,2)} + \phi_{TI}^{(1)} + \phi_{TI}^{(2,1)} + \phi_{SO,1}^{(2,12)} \quad (10)$$

$$\sum_j \phi_{j,2} = \phi_{RC,2}^{(11,2)} + \phi_{RC,2}^{(12,2)} + \phi_{RC}^{(2)} + \phi_{WE,2}^{(11,2)} + \phi_{WE,2}^{(12,2)} + \phi_{WE}^{(2)} + \phi_{TI,2}^{(2)} + \phi_{SO,2}^{(2,12)} + \phi_{SI}^{(2)} \quad (11)$$

The 2G IATE is composed of three main parts. The first, second, and third terms in the right-hand side (R.H.S) of Eq. (8) and (9) are to account for volume changes due to pressure variation, volume changes caused by the inter-group mass transfer, and IAC source/sink terms of bubble interaction mechanisms, respectively. Details of the bubble coalescence and breakup mechanisms are explained in the following subsections of 3.2.2. Bubble interaction mechanisms and section 3.3. S-GAMMA (S_γ) MODEL.

3.3.2. Bubble Interaction Mechanisms. The 2G IATE with corresponding bubble interaction models have been developed and extended its applicability to beyond bubbly flows by various researchers (Wu et al., 1998; Kim, 1999; Hibiki and Ishii, 2000; Sun, 2001; Fu and Ishii, 2002, 2003; Sun et al., 2004). However, efforts of the studies are focused on flow conditions in a small diameter pipe or a narrow duct channel or consider only some of the bubble interaction mechanisms. Smith et al. (2012) developed models to describe five major bubble interaction mechanisms for large diameter pipes and suggested scalars used for the models. However, there is not a general agreement in setting values of the scalars. Since this study is primarily focus on the evaluation of 2G IATE based on MoM PBE, the effect of the scalars can be handled as a future work for further improvement. In this study Smith's bubble interaction mechanisms (Smith et al., 2012) were combined with 2G IATE. Smith model of bubble coalescence and breakup

mechanisms is the first bubble interaction model developed for large diameter channels based on the two bubble groups, small bubbles (Group-1) and large bubbles (Group-2) with a critical diameter of maximum distorted bubble for wide flow regimes including cap/slug bubble and churn-turbulent flow regimes. However, Smith's model has not be intensively evaluated for a large diameter pipe yet as well as coupling with PBE. For this reason, it would be a good starting point for the rigorous evaluation of the 2G IATE.

For coalescence mechanism in Smith's model, RC covers all collisions driven by turbulent eddies. WE describes collision due to acceleration of the following bubble in the wake region of the preceding bubble. Wake effects makes the trailing bubble move faster than the leading bubble and leads to coalescences by colliding with the leading bubble. Therefore, WE model includes relative velocity and drag coefficient terms for both group-1 and group-2 bubbles. Modeling of these coalescence mechanisms were categorized with four separate cases as to create a large group-1 bubble with interactions between two group-1 bubbles to create a larger group-1 bubble, and to create a group-2 bubble with interactions between two group-1 bubbles, between a group-1 and a group-2 bubble, and between two group-2 bubbles. The bubble breakup and coalescence modes are represented graphically in Figure 3.2.

For breakup mechanisms in Smith's model, TI presents bubble breakup due to impact of a turbulent eddy on the bubble. SO indicates small bubble production due to the liquid shear as they are sheared off from the outer rim of a large cap bubble. Surface instability (SI) describes disintegration of cap bubbles larger than the maximum stable bubble size. Furthermore, the breakup mechanisms account for trend of increase in relative velocity for group-2 bubbles because of the formation of large cap bubbles with

no wall restrictions. Several separate cases are considered in these breakup mechanisms: as breakup of a group-1 bubble to create two group-1 bubbles, breakup of a group-2 bubble to create a group-1 and a group-2 bubbles or to create group-1 bubbles and a group-2 bubble, breakup of a group-2 bubble to create two group-2 bubbles.

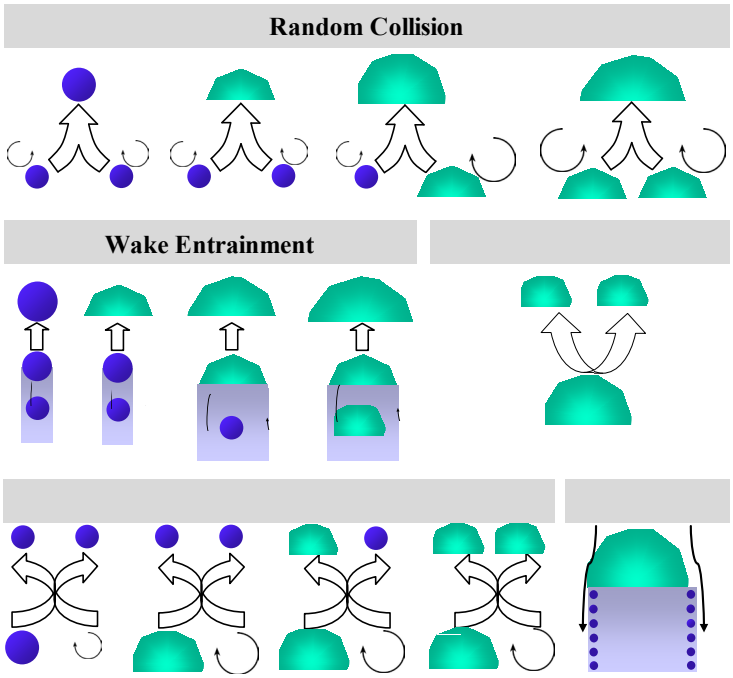

Figure 3.2. Bubble Breakup and Coalescence Modes.

3.4. S-GAMMA (S_γ) MODEL

Numerical analysis for heterogeneous bubbly flows or beyond bubbly flows requires different velocity fields with respect to the size of the bubbles. According to the studies in the past (T. Maxworthy et al., 19996; K. Ellingsen et al., 2001; A. Tomiyama et al., 2002b), bubble rising velocity is affected by bubble size, and the variation of the rising velocity changes drag on the bubbles, which result in different flow behaviors of

the bubbles. Based on the different flow characteristics corresponding to change in bubble size, the bubbles can be categorized into two groups (small and large bubbles) and the two-group approach leads to the modified two-fluid model to consider mass and momentum transfers between the two groups of bubbles. Therefore, two S_γ models for each bubble group were applied to this study, so that different velocity fields can be addressed for the two groups of bubbles.

The S_γ model basically deals with spherical monodisperse bubbles. The bubbles are assumed to remain spherical and are characterized by interaction length scale, which is defined as D_{sm}. Velocity of the bubbles is represented by mean velocity of the disperse phase. Bubble size probability distribution is assumed to follow a pre-defined log-normal distribution.

Bubble size distribution can be characterized by volumetric conserved parameter, S_γ, as:

$$S_\gamma = nM_\gamma = n\int_0^\infty d_B^\gamma P(d_B)d(d_B) \tag{12}$$

where, n is the bubble number density, M_γ is the moment of the size distribution, d_B is the bubble diameter, and $P(d)$ is the bubble size distribution.

3.4.1. S_γ Transport Equations. The $\boldsymbol{S_\gamma}$ model solves transport equations for the two moments, zeroth and second, of the particle size distribution. The zeroth-order moment, $\boldsymbol{S_0}$, represents the bubble number density, n. The second-moment, $\boldsymbol{S_2}$, is related to IAC ($\boldsymbol{a_i}$). The third-moment, $\boldsymbol{S_3}$, is related to volume fraction of the gas and liquid phases, $\boldsymbol{\alpha_g}$ **and** $\boldsymbol{\alpha_l}$. The $\boldsymbol{S_3}$ is solved by the multiphase segregated flow solver and

imported to $\boldsymbol{S_\gamma}$ model. The three parameters of *n*, $\boldsymbol{a_i}$, and $\boldsymbol{\alpha_g}$ are related to the moments as:

$$n = S_0, a_i = \pi S_2, \alpha_g = \frac{\pi S_3}{6} \tag{13}$$

d_{sm} can be obtained from the relations above as:

$$d_{sm} = d_{32} = \frac{S_3}{S_2} = \frac{6\alpha}{\pi S_2} \tag{14}$$

By adapting two S_γ models, particle size distributions of the two bubble groups can be demonstrated, and additional source terms for inter-group transfer are added to the mass and momentum conservation equations.

The transport equation for each moment of S_γ is given by:

$$\frac{\partial \rho_g^{\gamma/3} S_\gamma}{\partial \mathrm{t}} + \nabla \cdot \left(\rho_g^{\gamma/3} v_g S_\gamma\right) = \rho_g^{\gamma/3}\left(S_\gamma^{br} + S_\gamma^{cl} + Sc_\gamma\right) \tag{15}$$

S_γ^{br} and S_γ^{cl} indicate source terms for intra-group coalescence and breakup mechanisms, which are default option of the S_γ model in the STAR-CCM+ code. In this study, however, the default source terms were ignored, and new mechanical models developed by Smith et al. (2012) (Smith model) were implemented since the S_γ model only provides RC and TI for bubble coalescence and breakup, separately, that are hard to reflect actual bubble interaction phenomena in a large diameter channel. Sc_γ presents modification term and is derived based on Smith model (Smith et al., 2012) to account for mass transfers between group-1 and group-2 bubbles for the 0th order moment, S_0, and benchmark the 2G IATE for the 2nd order moment, S_2.

Detailed modeling for intra-group source terms, S_γ^{br} and S_γ^{cl}, is found from Lo and Zhang (2009). Modification term, Sc_γ , is described in the Source terms section.

Since S_γ model is basically accounts for intra-group interactions, when two groups of bubbles are considered, additional source terms should be added to the S_γ transport equations to account for inter-group interactions and other bubble interaction mechanisms that are not considered in the default options of S_γ model in STAR-CCM+. All additional terms used in this study were introduced as a user-defined field function (UDF).

3.4.2. The 0th Moment Transport. The zeroth-order moment, $\boldsymbol{S_0}$, represents the bubble number density, n. Transport equation for the 0th moment is described as:

$$\frac{\partial S_0}{\partial t} + \nabla \cdot (S_0 \boldsymbol{v}_G) = \left(S_0^{br} + S_0^{cl}\right) \tag{16}$$

where v_G is the dispersed phase velocity that is calculated by the multiphase solver.

3.4.3. The 2nd Moment Transport. The second-moment, $\boldsymbol{S_2}$, is related to interfacial area density (or IAC), $\boldsymbol{a_i}$, and the $\boldsymbol{S_2}$ transport equation is defined as:

$$\frac{\partial \rho^{\frac{2}{3}} S_2}{\partial t} + \nabla \cdot \left(\rho^{\frac{2}{3}} S_2 \boldsymbol{v}_G - \rho \alpha_g D_T \nabla \frac{S_2}{\rho^{\frac{2}{3}} \alpha_g} \right) = \left(S_{2,wb} + S_2^{br} + S_2^{cl}\right) \tag{17}$$

where turbulent diffusivity term, D_T, in the S_2 transport equation for each group-1 and group-2 bubbles, was ignored by setting a large turbulent Prandtl number, Pr_T.

3.4.4. Source Terms. There are source terms added to $\boldsymbol{S_\gamma}$ transport equations. Steady state is assumed. To reflect modified mass conservation of three field two-fluid model, source term for $\boldsymbol{S_0}$ is derived. The source and sink terms, $\boldsymbol{Sc_{0,k}}$, for $\mathbf{S_0}$ are derived by dividing the void transport source and sink terms by volume of all sizes of particles. In order to convert the 2nd moment transport equation to two group IATE, $\boldsymbol{Sc_{0,k}}$ is derived.

3.4.4.1. Transport equation for the zeroth moment (S_0). Source term for the number density transport equation was modeled to describe the exchanges between

group-1 and group-2 bubbles through coalescence and breakup interaction mechanisms (Smith model) as:

$$Sc_{0,k} = \sum(source\ terms\ for\ void\ fraction\ transport)\ /\forall_k \quad (18)$$

where the source/sink terms for void fraction transport are defined in Table 3.1 and $\forall_k$ are a sum of void fraction source/sink rate and a volume of bubble.

3.4.4.2. Transport equation for the second moment (S_2). The 2G IATE is benchmarked and implemented into S_γ model in STAR-CCM+ code. As aforementioned in the previous section, the transport equation for S_2 is related to IATE. Since, however, S_2 transport equation does not reflect two-groups of bubble categorization nor handles other major bubble interaction mechanisms, such as WE, SO, and SI, source term to accommodate the 2G IATE needs to be added to the S_2 transport equation.

Smith et al. (2012) proposed interaction mechanisms of IAC, which were implemented into S_2 transport equation as the source and sink terms. The S_2 transport equation is derived from Yao and Morel (2004)'s IATE equation, which was developed for spherical bubbles. The final form of source term added to S_2 transport equation is shown in Equation (19) and the derived source terms are addressed in Equations (20) and (21).

$$Sc_{2,k} = \sum_j \phi_{j,k} + s_{exp,\,k} \quad (19)$$

$$s_{exp,\,1} = \left[\frac{2}{3} - \chi\left(\frac{D_{d,max}}{D_{sm1}}\right)^2\right]\left(\frac{S_{2,1}}{\alpha_{gi}\rho_g}\right)(-1)\ \ \Delta\dot{m}_{12} + \chi\left(\frac{D_{d,max}}{D_{sm1}}\right)^2 S_{2,1}\left(\frac{\overrightarrow{v_{g1}}\cdot\nabla\rho}{\rho_g}\right) \quad (20)$$

$$s_{exp,\,2} = \left[\frac{2}{3}\frac{S_{2,2}}{\alpha_{g2}} - \chi\left(\frac{D_{d,max}}{D_{sm1}}\right)^2\frac{S_{2,1}}{\alpha_{g1}}\right]\left(\frac{\Delta\dot{m}_{12}}{\rho_g}\right) - \chi\left(\frac{D_{d,max}}{D_{sm1}}\right)^2 S_{2,1}\left(\frac{\overrightarrow{v_{g1}}\cdot\nabla\rho}{\rho_g}\right) \quad (21)$$

where $s_{exp,k}$ indicates volume expansion effect of each group of bubbles and the contribution of inter-group mass transfer rate to IAC. The first term of $s_{exp,k}$ is introduced from void fraction transport equation of each bubble group, which is derived from the modified continuity equation in Equation (2) and the second term presents volume expansion effect due to pressure change.

Models for bubble coalescence and breakup mechanisms implemented in the simulations are addresed in Table 3.1, and Table 3.2 shows the possible source and sink terms of intra- and inter-group interactions. In the present study, the five major mechanisms developed by Smith et al. (2012) were implemented into each S_γ transport equation.

3.5. TURBULENCE MODELING

The realizable *k*-*ε* model (Shih et al., 1994) with a two-layer all *y*+ wall approach for the near wall treatment was used for a continuous liquid phase. This model was advanced by introducing a new model equation for dissipation (*ε*) based on the dynamic equation of the mean-square vorticity fluctuation from Standard k-ε turbulence model. For the multiphase conditions, this two-equation turbulence model is scaled by volume fraction of liquid phase for the turbulent kinetic energy (*k*) and turbulent dissipation rate (*ε*) as follows:

$$\frac{\partial(\alpha_L \rho_L k_L)}{\partial t} + \nabla \cdot \left(\alpha_L \vec{v}_L k\right) = \nabla \cdot \left[\alpha_L \left(\mu_L + \frac{\mu_{L,t}}{\sigma_k}\right) \nabla k\right] + \alpha_L (P_k - \rho_L \varepsilon_L) + S_k \qquad (22)$$

Table 3.1. Summary of Models for Bubble Coalescence and Breakup Mechanisms (Smith et al., 2012).

For void fraction source term,	For group-1 IAC source/sink terms,
$\eta_{RC,2}^{(11,2)} = 3.15 C_{RC}^{(1)} \lambda_{RC}^{(1)} \frac{\varepsilon^{\frac{1}{3}} \alpha_1^2 a_{i1}^{\frac{2}{3}}}{\alpha_{1,max}^{\frac{2}{3}}} \times \left[1 - exp\left(-C_{RC1} \frac{\alpha_{1,max}^{1/3} \alpha_1^{1/3}}{\left(\alpha_{1,max}^{1/3} - \alpha_1^{1/3}\right)}\right)\right]\left(1 - \frac{2}{3} D_{c1}^*\right)$	$\phi_{RC}^{(1)} = -0.17 C_{RC}^{(1)} \lambda_{RC}^{(1)} \frac{\varepsilon^{\frac{1}{3}} \alpha_1 a_{i1}^{\frac{5}{3}}}{\alpha_{1,max}^{\frac{1}{3}}\left(\alpha_{1,max}^{\frac{1}{3}} - \alpha_1^{\frac{1}{3}}\right)} \times \left[1 - exp\left(-C_{RC1} \frac{\alpha_{1,max}^{1/3} \alpha_1^{1/3}}{\alpha_{1,max}^{1/3} - \alpha_1^{1/3}}\right)\right]$
$\eta_{RC,2}^{(12,2)} = 1.44 C_{RC}^{(12,2)} \lambda_{RC}^{(12,2)} \varepsilon^{\frac{1}{3}} \alpha_1^{\frac{5}{3}} \alpha_2^{\frac{4}{3}} a_{i2}^{\frac{2}{3}} \frac{\varepsilon^{\frac{1}{3}} \alpha_1^2 a_{i1}^{\frac{2}{3}}}{\alpha_{1,max}^{\frac{2}{3}}} \times \left[1 - exp\left(-C_{RC1} \frac{\alpha_{1,max}^{1/3} \alpha_1^{1/3}}{\left(\alpha_{1,max}^{1/3} - \alpha_1^{1/3}\right)}\right)\right]$	$\phi_{RC,1}^{(12,2)} = -1.14 C_{RC}^{(12,2)} \lambda_{RC}^{(2)} \varepsilon^{\frac{1}{3}} \alpha_1^{\frac{2}{3}} \alpha_2^{\frac{4}{3}} a_{i1} a_{i2}^{\frac{2}{3}} \times \left[1 - exp\left(-C_{RC1} \frac{\alpha_{1,max}^{1/3} \alpha_1^{1/3}}{\alpha_{1,max}^{1/3} - \alpha_1^{1/3}}\right)\right]$
$\eta_{WE,2}^{(11,2)} = 3.85 C_{WE}^{(1)} C_{D1}^{1/3} u_{r1} \alpha_1 a_{i1} \left(1 - \frac{2}{3} D_{c1}^*\right)$	$\phi_{WE}^{(1)} = -0.17 C_{WE}^{(1)} C_{D1}^{1/3} u_{r1} a_{i1}^2$
$\eta_{WE,2}^{(12,2)} = 0.33 C_{WE}^{(12,2)} \overline{u_{w12}} \alpha_1 a_{i2}$	$\phi_{WE}^{(11,2)} = 2.57 C_{WE}^{(11,2)} C_{D1}^{1/3} u_{r1} a_{i1}^2 \left(1 - \frac{2}{3} D_{c1}^*\right)$
$\eta_{TI,2}^{(2,1)} = -11.65 C_{TI}^{(2,1)} \varepsilon^{\frac{1}{3}} (1 - \alpha_{total}) \alpha_2^{\frac{1}{3}} a_{i2}^{\frac{2}{3}} exp\left(-\frac{We_{cr2}}{We_2}\right) \times \sqrt{1 - \frac{We_{cr2}}{We_2}} \left(0.15 D_{c2}^{*16/3} - 0.117 D_{c2}^{*6}\right)$	$\phi_{WE,1}^{(12,2)} = -0.33 C_{WE}^{(12,2)} \overline{u_{w12}} a_{i1} a_{i2}$
$\eta_{TI,1}^{(2,1)} = -\eta_{TI,2}^{(2,1)}$	$\phi_{WE,2}^{(12,2)} = 0.922 C_{WE}^{(12,2)} \overline{u_{w12}} \alpha_1 a_{i2}^2 / \alpha_2$
$\eta_{SO,2}^{(2,12)} = -2.33 C_{SO} \left(\frac{\sigma}{\rho_g v_{g2}}\right) \frac{a_{i2}^2}{\alpha_2} \left[1 - \left(\frac{We_{c,SO}}{We_{m,2}}\right)^4\right]$	$\phi_{TI}^{(1)} = 0.12 C_{TI}^{(1)} \varepsilon^{\frac{1}{3}} \left(\frac{a_{i1}^{\frac{5}{3}}}{a_1^{\frac{2}{3}}}\right) (1 - \alpha) \times exp\left(-\frac{We_{cr1}}{We_1}\right) \sqrt{1 - \frac{We_{cr1}}{We_1}}$
$\eta_{SO,1}^{(2,12)} = -\eta_{SO,2}^{(2,12)}$, where $D_{c1}^* = \frac{D_c}{D_{sm1}}$ and $D_{c2}^* = \frac{D_c}{D_{sm2}}$	$\phi_{TI,1}^{(2,1)} = 6.165 C_{TI}^{(2,1)} \varepsilon^{\frac{1}{3}} \left(\frac{a_{i2}^{\frac{5}{3}}}{a_2^{\frac{2}{3}}}\right) (1 - \alpha) \times exp\left(-\frac{We_{cr2}}{We_2}\right) \sqrt{1 - \frac{We_{cr2}}{We_2}} \times \left(0.212 D_{c2}^{*13/3} - 0.167 D_{c2}^{*5}\right)$
	$\phi_{SO,1}^{(2,12)} = 8.0 C_{SO} \frac{\rho_f^{3/5} v_{g2}^{1/5} \sigma^{2/5} a_{i2}^2}{\rho_g D_h^{2/5} {We_c}^{3/5} \alpha_2} \left[1 - \left(\frac{We_{c,SO}}{We_{m2}}\right)^4\right]$

Table 3.1. Summary of Models for Bubble Coalescence and Breakup Mechanisms (Smith et al., 2012) (Cont'd).

Coefficients for IATE models	For group-2 IAC source/sink terms,
Random collision (RC) $C_{RC}^{(1)} = 0.01$, $C_{RC}^{(12,2)} = 0.01$, $C_{RC}^{(2)} = 0.01$ $C_{RC1} = 3.0$, $C_{RC2} = 3.0$ $\alpha_{max,1} = 0.62$ Wake entrainment (WE) $C_{WE}^{(1)} = 0.002$, $C_{WE}^{(12,2)} = 0.01$, $C_{WE}^{(2)} = 0.06$ $We_{cr1} = 1.2$, $We_{cr2} = 1.2$ Turbulence impact (TI) $C_{TI}^{(1)} = 0.05$, $C_{TI}^{(2,1)} = 0.04$, $C_{TI}^{(2)} = 0.01$ Shearing -off (SO) $C_{SO} = 2.5 \times 10^{-6}$ $We_{c,SO} = 4000$ Surface instability (SI) $C_{RC}^{(2)} = 0.01$ $C_{RC2} = 3.0$	$\phi_{RC,2}^{(11,2)} = 4.1 C_{RC}^{(1)} \lambda_{RC}^{(1)} \frac{\varepsilon^{\frac{1}{3}} \alpha_1 a_{i1}^{\frac{5}{3}}}{\alpha_{1,max}^{\frac{1}{3}} \left(\alpha_{1,max}^{\frac{1}{3}} - \alpha_1^{\frac{1}{3}}\right)}$ $\times \left[1 - exp\left(-C_{RC1} \frac{\alpha_{1,max}^{1/3} \alpha_1^{1/3}}{\alpha_{1,max}^{1/3} - \alpha_1^{1/3}}\right)\right]\left(1 - \frac{2}{3} D_{c1}^{*}\right)$ $\phi_{RC,2}^{(12,2)} = 1.80 C_{RC}^{(12,2)} \lambda_{RC}^{(12,2)} \varepsilon^{\frac{1}{3}} \alpha_1^{\frac{2}{3}} \alpha_2^{\frac{4}{3}} a_{i1} a_{i2}^{\frac{2}{3}}$ $\times \left[1 - exp\left(-C_{RC1} \frac{\alpha_{1,max}^{1/3} \alpha_1^{1/3}}{\alpha_{1,max}^{1/3} - \alpha_1^{1/3}}\right)\right]$ $\phi_{RC}^{(2)} = -95.7 C_{RC}^{(2)} \lambda_{RC}^{(2)} \varepsilon^{1/3} \frac{\alpha_2^{7/3}}{D_h^2 a_{i2}^{1/3}} \times \left[1 - exp\left(-C_{RC2} \alpha_2^{1/2}\right)\right](1 - 0.37 D_{c2}^{*3})$ $\phi_{WE}^{(2)} = -1.02 C_{WE}^{(2)} [1 - exp(-0.7\alpha_2)] \times (1 - 0.10 D_{c2}^{*2}) \bar{u}_{rw2} a_{i2}^2 / \alpha_2$ $\phi_{WE,2}^{(11,2)} = 2.57 C_{WE}^{(11,2)} C_{D1}^{1/3} u_{r1} a_{i1}^2 \left(1 - \frac{2}{3} D_{c1}^{*}\right)$ $\phi_{WE2}^{(12,2)} = 0.922 C_{WE}^{(12,2)} \bar{u}_{w12} \alpha_1 a_{i2}^2 / \alpha_2$ $\phi_{SO,2}^{(2,12)} = -0.36 C_{SO} \frac{\sigma a_{i2}^3}{\rho_g v_{g2} \alpha_2^2} \left[1 - \left(\frac{We_{c,SO}}{We_{m2}}\right)\right]$ $\phi_{TI,2}^{(2)} = 0.378 C_{TI}^{(2)} \varepsilon^{\frac{1}{3}} \left(\frac{a_{i2}^{\frac{5}{3}}}{a_2^{\frac{2}{3}}}\right)(1 - \alpha) \times exp\left(-\frac{We_{cr2}}{We_2}\right) \sqrt{1 - \frac{We_{cr2}}{We_2}}$ $\times (1 - 0.212 D_{C2}^{*13.3})$ $\phi_{SI}^{(2)} = 2.16 \times 10^{-4} C_{RC}^{(2)} \frac{\varepsilon^{\frac{1}{3}}}{D_h^2} \alpha_2^2 \left(\frac{\sigma}{g \Delta \rho}\right)^{\frac{1}{6}} \left[1 - exp\left(-C_{RC2} \alpha_2^{\frac{1}{2}}\right)\right]$, where $P_{WE}^{(2)} = 1 - exp(-0.7\alpha_2)$

Table 3.2. Summary of Major IAEA Sources and Sinks (Smith et al., 2012).

Notation	Contribution	Effect on a_i
$R_{RC}^{(1)}$	(1) + (1) ⇒ (1)	Sink in 1
$R_{RC}^{(11,2)}$	(1) + (1) ⇒ (2)	Sink in 1; source in 2
$R_{RC}^{(12,2)}$	(1) + (2) ⇒ (2)	Sink in 1; source in 2 (no number change)
$R_{RC}^{(2)}$	(2) + (2) ⇒ (2)	Sink in 2
$R_{WE}^{(1)}$	(1) + (1) ⇒ (1)	Sink in 1
$R_{WE}^{(11,2)}$	(1) + (1) ⇒ (2)	Sink in 1; source in 2
$R_{WE}^{(12,2)}$	(1) + (2) ⇒ (2)	Sink in 1; source in 2 (no number change)
$R_{WE}^{(2)}$	(2) + (2) ⇒ (2)	Sink in 2
$R_{TI}^{(1)}$	(1) ⇒ (1) + (1)	Source in 1
$R_{TI}^{(2,11)}$	(2) ⇒ (1) + (1)	Source in 1; sink in 2
$R_{TI}^{(2,12)}$	(2) ⇒ (1) + (2)	Source in 1; sink in 2 (no number change)
$R_{TI}^{(2)}$	(2) ⇒ (2) + (2)	Source in 2
R_{SO}	(2) ⇒ (2) + n(1)	Source in 1 (multiple number); Sink in 2 (no number change)
R_{SI}	(2) ⇒ (2) + (2)	Source in 2

$$\frac{\partial(\alpha_L\rho_L\varepsilon_L)}{\partial t}+\nabla\cdot(\alpha_L v_L\varepsilon_L)=\nabla\cdot\left[\alpha_L\left(\mu_L+\frac{\mu_{L,t}}{\sigma_\varepsilon}\right)\nabla\varepsilon_L\right]+\alpha_L\left[\frac{1}{T_e}c_{\varepsilon1}P_\varepsilon-c_{\varepsilon2}f_2\rho_L\left(\frac{\varepsilon_L}{T_e}-\frac{\varepsilon_{L,0}}{T_0}\right)\right]$$

$$+S_\varepsilon \quad (23)$$

The model coefficients in Equation (22) and (23) are defined the same as those used with the single-phase equations: σ_k=1, σ_ε=1, c_μ=0.09, $c_{\varepsilon1}$=1.44, $c_{\varepsilon2}$=1.9, and $c_{\varepsilon2}$=1.9. P_k is turbulent kinetic energy production term, which is composed of productions due to gradients of mean flow velocity and buoyancy, and compressibility modification. The coefficients of T_e, T_0, f_2, and $\varepsilon_{L,0}$ are the large-eddy time scale, a

specific time scale, a damping function, the ambient turbulence value in the source terms that counteracts turbulence decay, and S_k, and S_ε are the user-specified source terms. $\mu_{L,t}$ is turbulent viscosity and was calculated as:

$$\mu_{L,t} = \rho_L c_\mu f_\mu kT \tag{24}$$

where T is the turbulent time scale ($\frac{k_L}{\varepsilon_L}$), and f_μ is a damping function. When bubble-induced turbulence (BIT) was considered, this value is composed of two components. One is shear-induced turbulence viscosity, and the other is bubble-induced turbulence viscosity, which indicates the effect of bubbles on turbulence of liquid phase. In this study, Sato model (Sato, Y. and Sekoguchi, K., 1975) for group-1 bubbles and Troshko-Hassan model (Troshko, A.A. and Hassan, Y.A., 2001) for group-2 bubbles were considered to address BIT effect. The Sato model considers the turbulence effects of the dispersed phase on the continuous phase in the form of an enhanced effective viscosity. The Troshko-Hassan model describes bubble induced turbulence effects by providing source terms to the continuous *k-ε* turbulence model.

The Boussinesq hypothesis is applied for the closure to the momentum equation with assumption that the turbulent stresses (τ_k^t) are proportional to the mean liquid velocity gradients:

$$\tau_k^t = \mu_{L,t}\left(\nabla\overline{v_L} + \nabla\bar{v}_L^t - \frac{2}{3}\nabla\cdot\overline{v_L}\boldsymbol{I}\right) \tag{25}$$

$\overline{v_L}$ and $\bar{v}_L^t$ indicate the mean velocity of liquid phase and mean turbulent velocity, respectively. $\boldsymbol{I}$ is the identity matrix

3.5.1. Sato Model. The Sato model (Sato, Y. and Sekoguchi, K., 1975) is the simplest and earliest model for particle (or bubble)-induced mixing and is a robust alternative to later source-based models for particle induced turbulence. The Sato model

considers the turbulence effects of the dispersed phase on the continuous phase in the form of an enhanced effective viscosity. It acts through enhanced effective viscosity of the continuous phase (Sharma, 2016; Sharma et al., 2017, 2019):

$$\nu_{eff} = \nu + \nu_{turb} + \nu_{Sato} \tag{26}$$

where ν, ν_{turb}, and ν_{Sato} are respectively the continuous phase kinematic viscosity, the turbulent diffusivity, and the Sato bubble-induced viscosity.

The Sato bubble-induced viscosity is given by:

$$\nu_{Sato} = k f_d f_B \alpha_g \frac{d_B}{2} v_{rel} \tag{27}$$

where k is a model calibration constant, $f_d$is the van Driest damping factor, $f_B$is a bubble diameter shape correction factor, α_g indicates the gas phase void fraction, d_B is the bubble diameter, and v_{rel} presents the relative velocity between phases.

3.5.2. Troshko-Hassan Model. The Troshko-Hassan model (Troshko, A.A. and Hassan, Y.A., 2001) describes bubble-induced turbulence effects by providing source terms to the continuous k-ε turbulence model. This model uses the Virtual Mass phase interaction model. The virtual mass coefficient, C_{VM}, is set as a default value of a spherical bubble, 0.5. The Troshko-Hassan model in the STAR-CCM+ is modified in terms of the linearized drag coefficient, A_D, to account for multi-particle effects:

$$S_k = A_D |v_{rel}|^2 \tag{28}$$

Source term for the turbulent dissipation rate uses the energy source term that decays with a characteristic time, the Bubble Pseudo-Turbulence Dissipation Relaxation (BPTDR) time, t_d, and is multiplied by a scaling constant, $C_3 = 0.45$:

$$S_\varepsilon = \frac{C_3 S_{k_C}}{t_d}, \text{ where } t_d = \frac{\rho C_{VM} \alpha_g}{2 A_D} \tag{29}$$

3.6. NUMERICAL SETUP

For the simulation, polyhedral mesh and hexagonal volume mesh were used and 5 prism layers were applied for mesh refinement. Two S_γ models were applied for the two-group of bubbles separately. Therefore it analyzed a three-field Eulerian two-fluid approach. Gas phase of air 1 and air 2 is assumed to be compressible. This is a main difference in model setup from other two-phase flow CFD work handling the gas phase as incompressible phase. And ideal gas law is applied. It assumed steady state and isothermal conditions, and there were no phase changes. Figure 3.3 shows Mesh configurations. Half section of 3D cylindrical pipe were modeled and then the geometry was converted to 2D cylindrical symmetric pipe.

Predictions of local phase profiles were compared to experimental measurements at the second and last measurement stations where *z/D* are equal to 14.1 and 28.0, respectively.

3.6.1. Geometry Configuration. Numerical simulations were performed using the STAR-CCM+ code. Pipe flows were simulated in two-dimensional (2D) plane-symmetric geometry. First, a half section of a 3D cylindrical pipe was modeled and then the geometry was converted to 2D cylindrical symmetric pipe experimental measurements of averaged profiles of velocity, void fraction, and bubble diameter at the first measurement location, and they were used for initial and inlet boundary conditions. At the inlet, fully-developed phase velocity profiles were assumed, and constant total mass flow rate boundary conditions were used for liquid and gas phases. A constant value

was set for temperature and the pressure was fixed on the outlet section. Figure 3.3 shows geometry and mesh configurations and locations for the simulation's data acquisition.

3.6.2. Boundary Conditions. Adiabatic and isothermal conditions were assumed, and mass flow inlet and pressure outlet boundary conditions were used with no slip condition at the wall. Air properties at a constant temperature were used for group-1 and group-2 bubbles based on the ideal gas law. Liquid phase was set as water with compressible fluid properties. Simulation conditions for this study are shown in Figure 3.4, including a superficial velocity map of gas and liquid phases ($j_g - j_l$), and details of flow conditions and boundary conditions are indicated in Table 3.3.

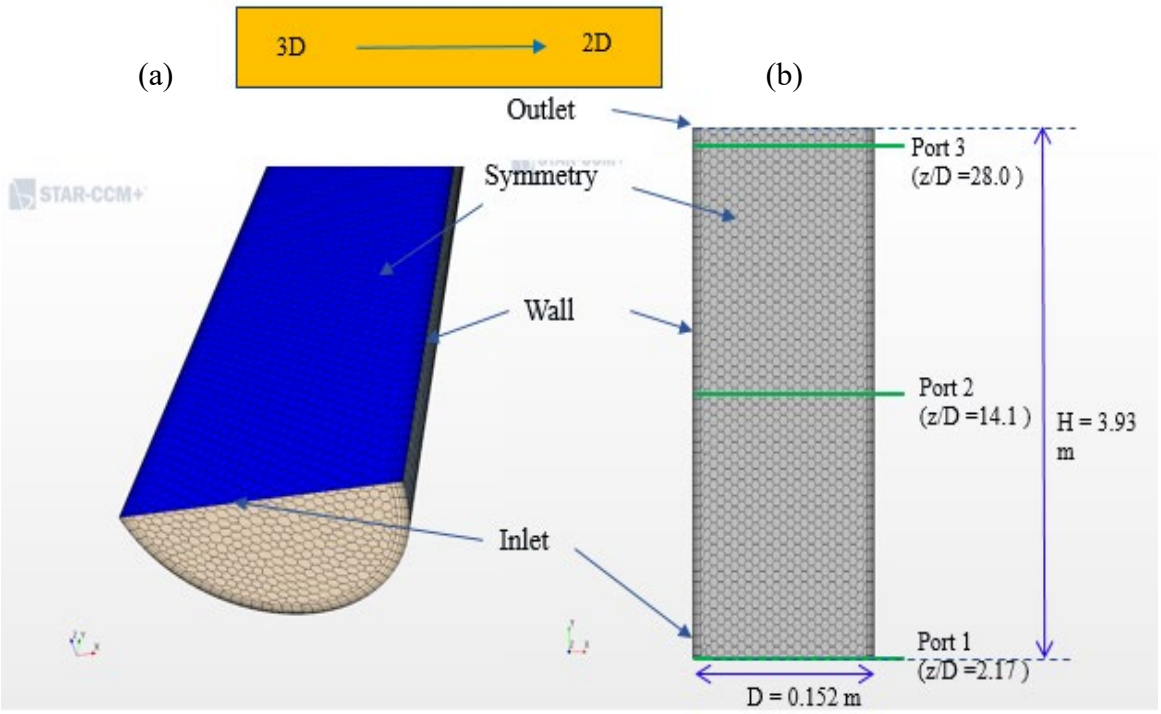

Figure 3.3. Mesh Configuration for (a) 3D and (b) 2D Geometry.

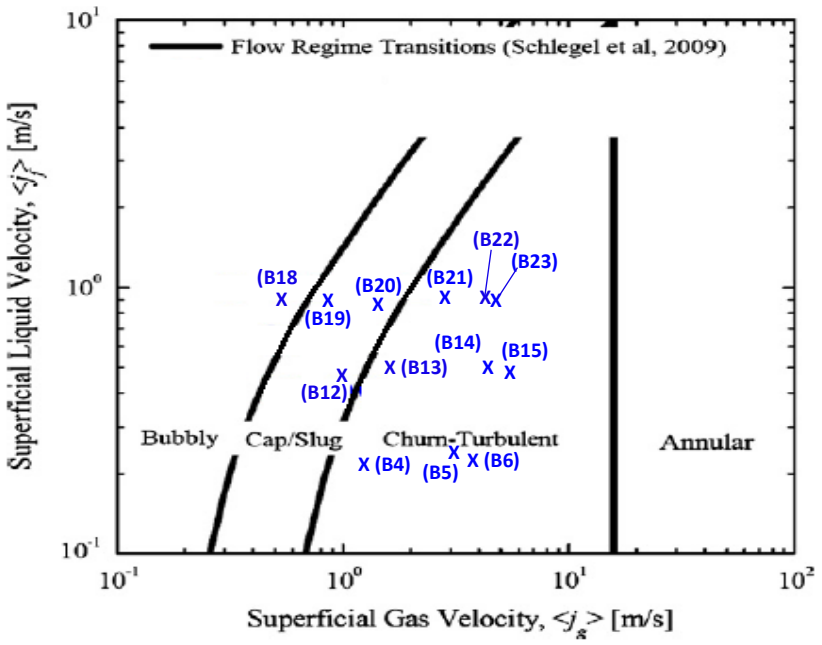

Figure 3.4. Simulation Conditions in a j_g-j_f Map (Schlegel et al., 2009).

3.6.3. Interfacial Momentum Transfer. Ranges of sizes and shapes were used for bubbles results in variation of key interfacial forces because the IAC is directly proportional to interfacial transfer terms with the two-fluid model. In this study, interfacial forces in a linear combination were for as follows:

$$\overrightarrow{M_{\iota k}} = \overrightarrow{M_{g\iota}^{D}} + \overrightarrow{M_{g\iota}^{L}} + \overrightarrow{M_{g\iota}^{TD}} + \overrightarrow{M_{g\iota}^{VM}} + \overrightarrow{M_{g\iota}^{W}} \tag{30}$$

where $\overrightarrow{M_{g\iota}^{D}}$, $\overrightarrow{M_{g\iota}^{L}}$, $\overrightarrow{M_{g\iota}^{TD}}$, $\overrightarrow{M_{g\iota}^{VM}}$, and $\overrightarrow{M_{g\iota}^{W}}$ are drag, lift, turbulent dispersion, virtual mass, and wall lubrication and the models for the interfacial momentum exchange are listed in Table 3.4.

3.6.4. Mesh Sensitivity Analysis. A mesh sensitivity study was performed for four different maximum mesh sizes (0.009, 0.01, 0.02, 0.04 m) by using default S_γ model

Table 3.3. Flow Conditions for the Evaluation of 2G IATE at Port 1 (Schlegel et. al., 2012).

Injection type*	Run (B) #	$<j_g>$ (m/s)	$<j_f>$ (m/s)	$<\alpha_1>$ (%)	$<\alpha_2>$ (%)	Pressure (MPa)	Temperature (°C)
B.	4	1.27	0.21	0.250	0.28	0.188	16
B.	5	3.1	0.23	0.209	0.358	0.173	17
C.S.	6	3.86	0.22	0.190	0.56	0.175	23
B.	12	0.95	0.46	0.240	0.214	0.192	18
B.	13	1.73	0.50	0.280	0.283	0.169	21
C.S.	14	4.05	0.51	0.317	0.394	0.173	21
C.S.	15	5.77	0.5	0.36	0.37	0.175	22
B.	18	0.52	0.93	0.167	0.068	0.191	18
B.	19	0.88	0.91	0.200	0.103	0.193	18
B.	20	1.59	0.90	0.280	0.162	0.195	19
B.	21	2.95	0.94	0.381	0.210	0.163	22
C.S.	22	4.24	0.95	0.406	0.244	0.164	23
C.S.	23	4.97	0.92	0.41	0.24	0.161	24

* B : Bubbly flow, C.S: Cap/Slug flow

options. Table 3.5 shows mesh conditions for the mesh sensitivity study. Unstructured mesh, such as polyhedral, was selected for mesh generation and mesh refinement was made in the near-wall-region with the value of $y+$ greater than 30. The realizable k-ε turbulent model was used and 'High Resolution' was selected as the advection scheme for all simulations. The convergence criterion was considered when all conservation equation residuals were lower than 1 % for both phases. There were no additional source terms implemented but the same interfacial forces were used.

Table 3.4. Summary of Coefficient Models for Interfacial Forces.

Interfacial Force	Coefficient models
Drag	Ishii and Zuber (1979) $C_{D1} = \frac{24}{N_{Re,m}}\left(1 + 0.1N_{Re,m}^{0.75}\right), \quad N_{Re,m} = 2r_d\rho_c v_{rel}/\mu_m$ * $C_{D2} = \frac{8}{3}\left(1 - \alpha_{g1} - \alpha_{g2}\right)$
Lift	Tomiyama et al. (2002a) $C_L = \begin{cases} 0.288tanh(0.121 \cdot max[Re, 7.374]) & Eo_d < 4 \\ 0.00105Eo_d^3 - 0.0159Eo_d^2 - 0.0204Eo_d + 0.474 & 4 < Eo_d \leq 10 \\ -0.27 & 10 < Eo_d \end{cases}$
Turbulent dispersion	Favre averaged drag (FAD) (Burns et al., 2004)
Virtual mass	Auton et al.(1988); $C_{VM} = 0.5$
Wall lubrication	Antal et al. (1991); $C_{w1} = -0.01, C_{w2} = 0.05$

* r_d is a radius of the dispersed phase, v_{rel} is a relative velocity between gas and liquid phases, and μ_m is a dynamic viscosity of the two-phase mixture.

Table 3.6 indicates setup for phase interactions. Radial profiles of void fraction for group-1 and group-2 bubbles at the second measurement station (port 2) were compared to B4 experimental data in terms of the different mesh sizes. The radial profiles of void fraction and D_{sm} for both bubble groups were shown in the evaluation section as a function of the normalized radial position *r/R*. Eulerian multiphase model was used for the phase setting with segregated multiphase flow solver that solves each of the mass and momentum equations, void

Table 3.5. Mesh Sensitivity Study.

Run (B) #	Base size [m]	Surface Growth rate	Prism layers	Prism growth rate	Prism h. [m]	Numb. of Cells (3D)	Numb. of Cells (2D)
4	0.009	1.1	5	1.5	0.008	110,719	12,371
	0.01	1.1	5	1.5	0.008	83,358	10,657
	0.02	1.1	5	1.5	0.008	42,162	6,238
	0.04	1.1	5	1.5	0.008	6,238	6,238

Table 3.6. Phase Interaction Setup for Mesh Sensitivity Study.

Interfacial Forces	Models
Drag force (*Sγ*)	Tomiyama et al. (2002a)
Lift force	Tomiyama et al. (2002b)
Turbulent dispersion force	Favre averaged drag (FAD) (Burns et al., 2004)
Virtual mass force	Auton et al. (1988); $C_{VM} = 0.5$
Wall lubrication force	Antal et al. (1991); C_{w1}=-0.01, C_{w2}=0.05

fraction and velocity for each phase are calculated from two-fluid model. S_γ model is used for particle number density and IAC calculation. D_{sm} is induced from the two results of two-fluid model and $\boldsymbol{S_\gamma}$ model as shown in the Figure 3.5. The system of equations and models described in the previous sections was solved using a semi-implicit numerical

scheme based on the SIMPLE (Semi-Implicit Method for Pressure Linked Equations) algorithm with pressure-velocity coupling.

Finding the solution to the governing equations is complicated due to the lack of an independent equation for pressure. The momentum and continuity conservation laws provide four independent equations which can be employed to calculate velocities in three directions and pressure. The implication of the calculation procedure is that the continuity and momentum equations are required to be solved for velocity and pressure simultaneously. Pressure-velocity coupling was solved using a multiphase extension of the SIMPLE algorithm and second-order upwind schemes were used to discretize the velocity, volume fraction, turbulent stresses, turbulence kinetic energy and dissipation rate convective terms.

3.7. EVALUATION

Two-phase flows beyond bubbly regimes in large diameter channels have an important feature of a wide range of bubble sizes and shapes. A two-bubble-group approach was adapted, and two-group interfacial area transport equation (2G IATE) coupled with *Sγ* model of population balance equation (PBE) was applied. Source terms for conservation equations and transport equations of *Sγ* model were derived to account for inter- and intra-group transfer between the two bubble groups. The effect of the 2G IATE coupled with *Sγ* model was validated against the experimental dataset obtained by Schlegel et al. (2012). The 2G IATE model with five major bubble interaction mechanisms improved prediction of void fraction and IAC distribution. Error analysis was performed and dominant mechanism of the IATE was also evaluated for a wide

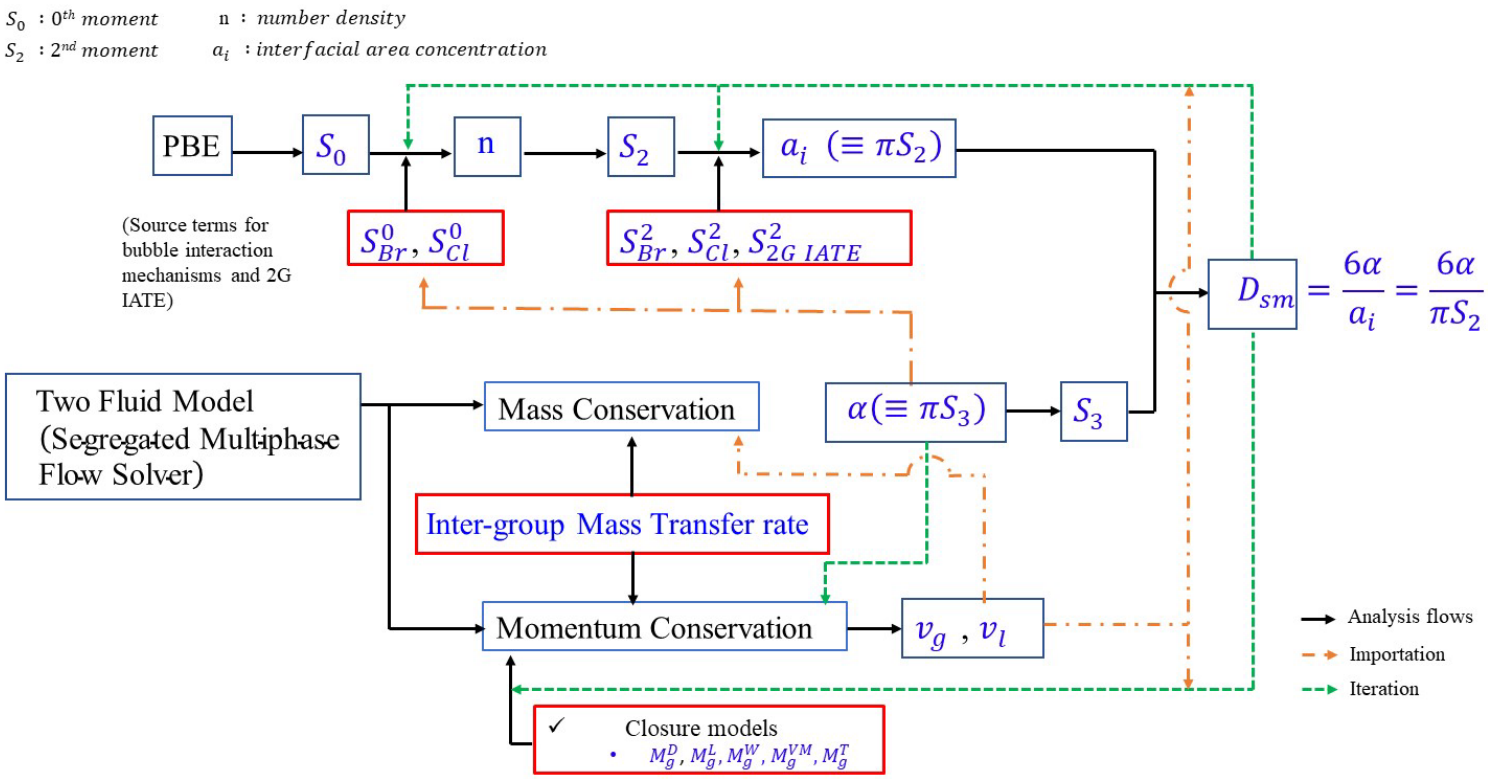

Figure 3.5. Analysis Flow for the Evaluation of 2G IATE.

range of flow regimes including bubbly flow, cap/slug flow, churn-turbulent flow, and transition between the flow regimes.

3.7.1. Mesh Sensitivity Analysis. For mesh sensitivity study, radial profiles of void fractions and Dsm for group-1 and group-2 bubbles at port 2 (*z/D*=14.1) were compared with B4 experimental data (Schlegel et al., 2012) in terms of the different mesh sizes as shown in Figure 3.6. The radial profiles are shown as a function of the normalized radial position *r/R*, which is equal to 0 at the pipe center and to 1 at the pipe wall. Through a mesh sensitivity study, the void fraction and Sauter mean diameter distributions are insensitive to mesh size and a hexahedral mesh size of 0.04 m was determined to be sufficient for 2D analysis.

3.7.2. Effect of 2G IATE. In the modified mass conservation equation, the inter-group mass transfer term ($\Delta \dot{\boldsymbol{m}}_{\boldsymbol{12}}$) is induced by void transport source and sink terms between group-1 and group-2 bubbles. Therefore, for the simulations not considering the 2G IATE, the conventional mass conservation equation for each bubble group is solved without $\Delta \dot{m}_{12}$ as well. When it comes to model implementation or simulations with the 2G IATE, it implies the simulation conditions with both the 2G IATE and inter-group mass transfer term.

For the analysis of the simulations, the results can be classified as the same with flow regimes categorization. In this point of view, simulation cases are grouped into three regimes of churn-turbulent flow case, transition from cap/slug flow to churn-turbulent flow case, and transition from bubbly flow to cap/slug flow case by varying superficial velocity of gas phase.

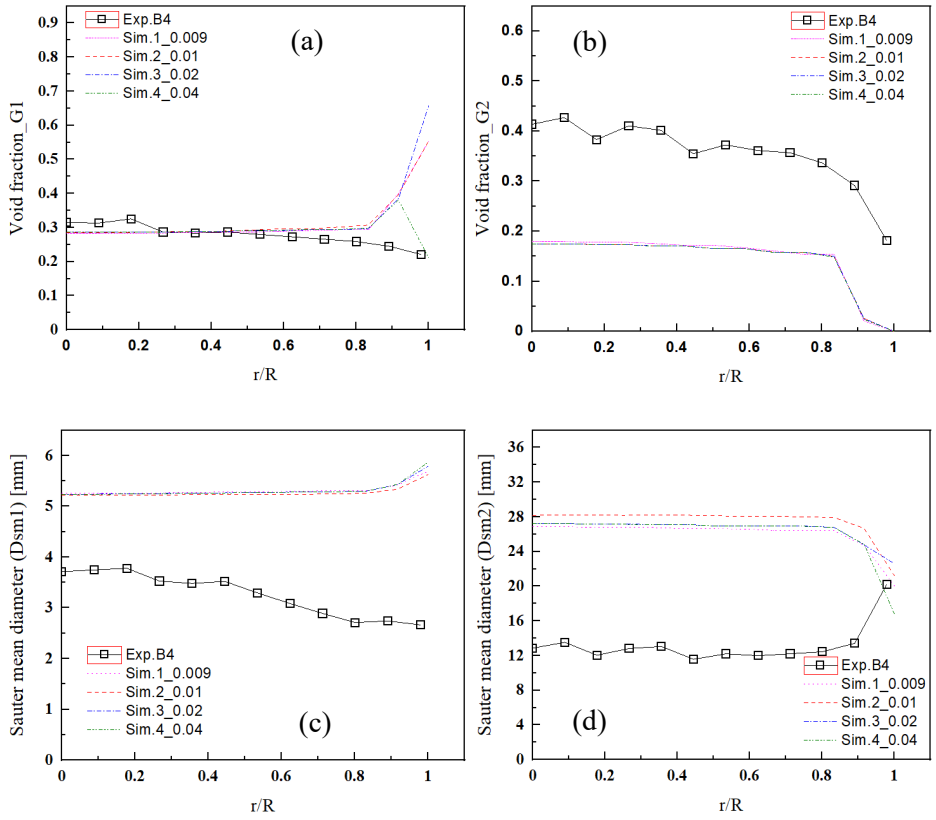

Figure 3.6. Mesh Sensitivity Study for Local Phase Distributions; Void fraction ((a) and (b)) and Sauter mean Diameter Distributions ((c) and (d)) at Port 2.

3.7.2.1. Void fraction distribution. Void fraction is fundamental characteristics of multiphase, which influences the overall performance of reactor system, affects the pressure drop, and can significantly modify the flow structure. Therefore, predicting local distribution of void fraction is pivotal to reactor systems in terms of safety, effectiveness, and performance. Figure 3.7 through Figure 3.9 show radial void fraction distributions for group-1 and group-2 bubbles in the churn-turbulent flow regime, transition area from cap/slug flow to churn-turbulent flow regimes, and transition area from bubbly flow to cap/slug flow regimes, respectively. Normalized radial position (*r/R*) represents a ratio of radial position from center to wall of the pipe to a diameter of the pipe. Solid line and

dash dot line indicates the simulation condition with the 2G IATE, and small dot line and dash line presents for the simulation without the 2G IATE. Lines in blue and in red are for data obtained at port 2 and port 3, respectively.

- **The 1st Case: Churn-turbulent flow regime at low (B4, B5, B6), middle (B14, B15), and high flow conditions (B22, and B23) in Figure 3.7**

The 2G IATE model with inter-group mass transfer improved prediction of void fraction distributions at low, middle, and high flow rate conditions.

Generally, the 2G IATE model accompanied with inter-group mass transfer term improves prediction of void fraction for each bubble group. Since void fraction is calculated by segregated multiphase flow solver, the 2G IATE model does not directly affect void fraction profile, but inter-group mass transfer term, which implements Smith' bubble interaction model, helps to differentiate overall levels of void fraction distributions at port 2 and port 3.

At low flow rate conditions (j_g =1.27, 3.1, 3.86 m/s and j_f = 0.21, 0.23, 0.22 m/s for B4, B5, and B6, respectively), the current models of the 2G IATE and inter-group mass transfer term worked better for estimating void fraction profile for group-2 bubble. Void fractions for group-1 bubbles were overestimated for B5 case but B4 and B6 cases gave relatively agreeable prediction of void fraction profile for group-1 bubbles. The overestimation of group-1 bubble void fraction of B5 case can be induced by the over-prediction of the interfacial forces due to the higher superficial liquid velocity and relative velocity leading to more turbulence-induced breakup interactions for group-2 bubbles, such as TI and SO, and evaluating the higher void fraction for group-1 bubbles by enhanced WE bubble coalescence mechanisms compared to the experimental data.

Void fractions for group-2 bubbles were estimated better compared to that for group-1 bubbles. As increasing superficial gas velocity, smaller deviation in the distributions of void fraction between at port 2 and port 3 was expected for both bubble groups. The optimization of bubble interaction mechanisms for the void fraction transport could resolve this issue.

At middle liquid flow rate conditions (j_g = 0.45, 5.77 m/s and j_f = 0.51, 0.5 m/s for B14 and B15, respectively), the models of 2G IATE and mass transfer improved the evaluation of void fractions for group-1 and grou-2 bubbles. B14 case showed good agreement of void fraction profiles for group-1 bubbles with the experimental data, and both simulation cases with and without the model implementation showed very small deviation in void fraction. The notable difference was shown at port 3. Mass transfer between the bubble groups improved the prediction. However, the bubble interaction mechanisms for group-2 bubbles were hard to differentiate void fraction profiles at port 2 and port 3. In B15 simulation, the implementation of the inter-group mass transfer term successfully separates overall level of void distribution at port 2 from the distribution at port 3. Therefore, it can be concluded that the 2G IATE and inter-group mass transfer term improved the prediction of void fractions for both group-1 and group-2 bubbles. However, the void fractions for group-1 and group-2 bubbles of B15 case were overestimated and underestimated, respectively. That indicates mass transfer from group-1 bubbles to group-2 bubbles were not correctly evaluated. It can be resulted from under-prediction of mass transfer from group-1 to group-2 bubbles, such as WE, that the small bubbles in wake region produced by the leading large bubbles were transferred to the void fraction profile of group-2 bubbles or overestimation of the bubble breakup

mechanisms of group-2, such as TI, SO, and SI, in such a way that due to the strong turbulence characteristics the turbulence-induced bubble breakup mechanisms were enhanced for group-2 bubbles. Again, this raises the need of further work for the optimization of bubble coalescence and breakup mechanisms and for the effect of bubble-induced turbulence in churn-turbulent flow conditions.

At high flow rate conditions (j_g = 4.24, 4.97 m/s and j_f = 0.95, 0.92 m/s for B22 and B23, respectively), void fractions for group-2 bubbles were well predicted with 2G IATE and inter-group mass transfer models. However, B22 case gave large discrepancies in group-1 void fraction estimation at both measurement points with the experimental data, which is the similar to the estimation of B5 case. B23 case showed different trend from the experimental data. For group-1 bubbles, void fraction at port 2 was higher than that at port 3 in the simulation and vice versa for group-2 bubbles.

From the results of simulations for the cases in churn-turbulent flow regimes, generally the 2G IATE with inter-group mass transfer models works better for the prediction of both group-1 and group-2 bubble void fractions. However, the bubble interaction model needs to be more optimized and further efforts are required for the interaction between bubbles and turbulence as well as the bubble-induced turbulence for churn-turbulent flow. It also found that the models are very sensitive to flow conditions, which determines relative velocity of the two phases.

- **The 2nd Case: Transition from cap/slug flows to churn-turbulent flow regime at middle flow and high flow conditions (B12, B13, B20, and B21) in Figure 3.8**

Run cases in the transition area can be more specifically divided into two parts by changing liquid superficial velocity from high flow to middle flow condition and by changing flow regimes from cap/slug flow regime to churn-turbulent flow regime.

At middle liquid superficial flow conditions (j_g =0.95, 1.73 m/s and j_f = 0.46, 0.5 m/s for B12 and B13 and j_g =1.59, 2.95 m/s and j_f = 0.9, 0.94 m/s for B20 and B21, respectively), the models of 2G IATE and mass transfer also improved the evaluation of the void fractions, but their effects were not significant.

Void fractions for group-1 bubbles showed good agreement with experimental data at both port 2 and port 3. However, at high liquid flow conditions, as flow regime changes from cap/slug flow regime to churn-turbulent flow regime, prediction of group-2 void fractions was well improved, whereas void fractions for group-1 bubbles were overestimated.

B12 and B20 (j_g =1.59 m/s and j_f = 0.9 m/s), which fall in the cap/slug flow regime, predicted well group-1 bubble void fractions, but overestimated void fractions for group-2 bubbles. B13 and B21 (j_g =2.95 m/s and j_f = 0.94 m/s) in the churn-turbulent flow regime with different liquid superficial velocity showed different trend of prediction. For B13 condition, group-1 void fraction was well predicted, but void fraction for group-2 bubbles was overestimated, which are the same trends of the cases in cap/slug flow regimes. For B21 condition, group-1 void fraction was overestimated, but void fraction for group-2 bubbles was well predicted.

From the results, it can be concluded that prediction of void fraction distribution is very sensitive to flow conditions. In transition area from cap/slug flow regime to churn-turbulent flow regime, the 2G IATE model with inter-group mass transfer term shows better prediction for group-1 void fraction distribution. However, as the flow condition comes close to churn-turbulent flow regime, the 2G IATE and inter-group transfer models show further improvement in evaluation of group-2 bubble void fraction distribution.

- **The 3rd Case: Transition from bubbly to cap/slug flows (B18 and B19) in Figure 3.9**

Unlike other simulation conditions in transition area and churn-turbulent flow regime, even though both B18 and B19 flow conditions (j_g =0.52, 0.88 m/s and j_f = 0.93, 0.91 m/s for B18 and B19, respectively) are in transition area, they predicted well void fraction profiles at port 2 and port 3 for both group-1 and group-2 bubbles. The 2G IATE model with inter-group mass transfer term worked very well for the cases in the bubbly to cap/slug flow transition area. It is reasonably expectable results since Smith's bubble interaction model is developed for cap/slug flows, the 2G IATE and inter-group mass transfer models based on the Smith's model can provide better predictions of void fraction for both group-1 and group-2 bubbles for cap/slug flows or bubbly flows, which have distorted spherical shape or are close to cap/slug flow regime. It seems that the 2G IATE and inter-group mass transfer models with the Smith's model are further preferable to be used for cap/slug flow conditions or regimes close to the cap/slug flow regimes.

3.7.2.2. IAC distribution. Interfacial area concentration (IAC) is defined as the sum of the interfaces per unit volume and characterizes the kinematic effect, which is strongly related to the two-phase flow structure. Figure 3.10 through Figure 3.12 show radial IAC distributions for group-1 and group-2 bubbles in the three flow regimes, respectively. The 2G IATE model and bubble interaction model directly affect IAC distribution at the different flow condition and at the different the height positions. In this section, a general change of trends in IAC distribution with flow conditions is discussed.

- **The 1st Case: Churn-turbulent flow regime at low, middle, and high flow conditions (B4, B5, B6, B14, B15, B22, and B23) in Figure 3.10**

In churn-turbulent flow regime, the effect of the 2G IATE on the local IAC distribution was significant and the implementation of the 2G IATE model improved the prediction of the IACs for group-1 and group-2 bubbles by differentiating distributions of the IAC at the different measuring positions. In the near-wall region, the IAC predictions for group-1 bubbles showed a huge discrepancy against the experimental data, whereas the predictions for group-2 bubbles captured the decreasing characteristics of the experimental data. Wall peak trend of group-1 bubbles in the predictions of IAC can be found for all simulation Run case, which is the same trend of void fraction distribution shown in Figure 3.7. There may be mainly two reasons for the wall peak trend of group-1 bubbles. First, eddy size calculated from RANS turbulence model is the one. The RANS turbulence model is based on the average field in terms of time, and it is hard to reflect actual size of eddies across the pipe, which can be grown from very small size up to the

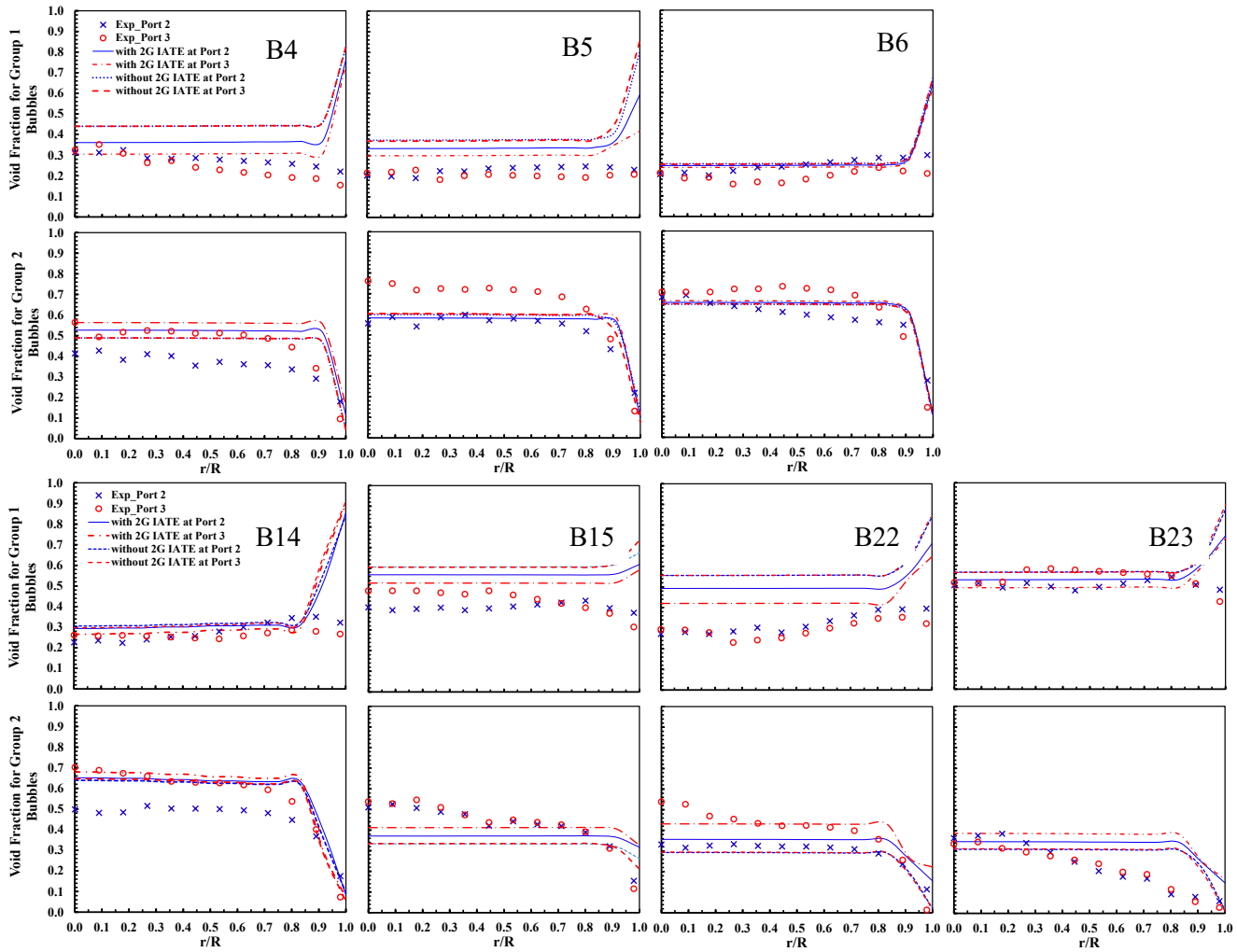

Figure 3.7. Effect of 2G IATE on Void Fraction Distribution for Group 1 and Group 2 Bubbles in Churn-Turbulent Flow Regime.

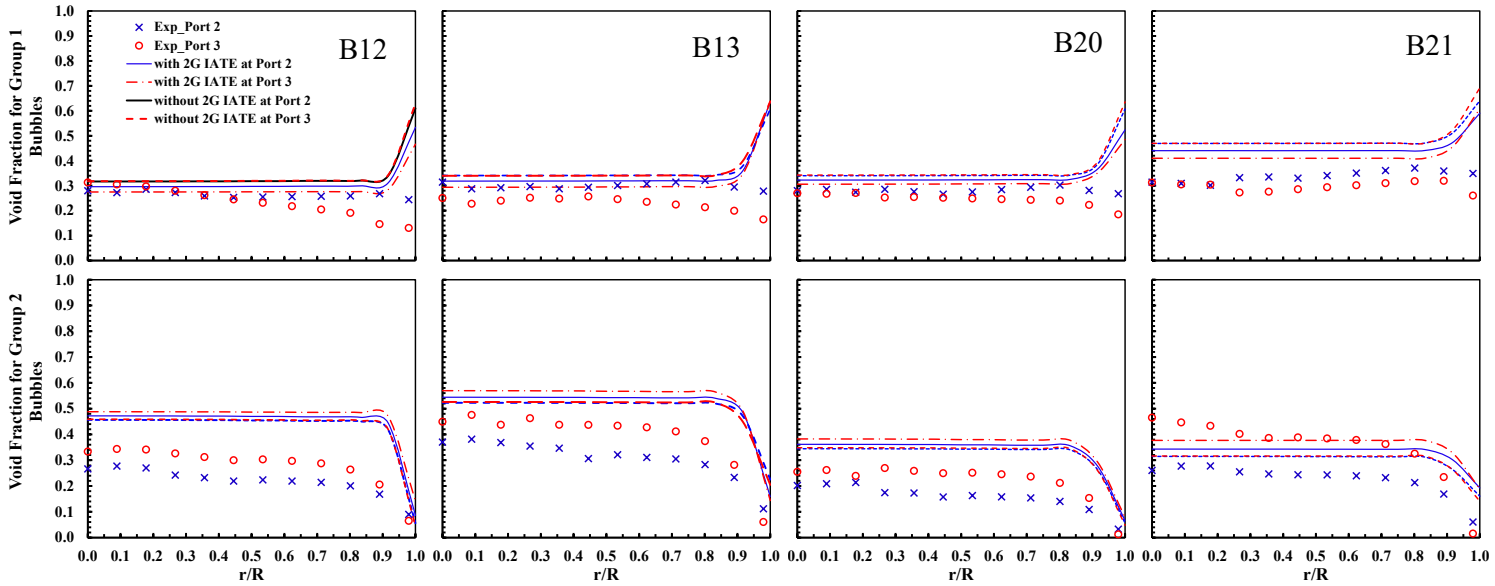

Figure 3.8. Effect of 2G IATE on Void Fraction Distribution for Group 1 and Group 2 Bubbles in Transition Area between Cap/Slug and Churn-Turbulent Flow Regime.

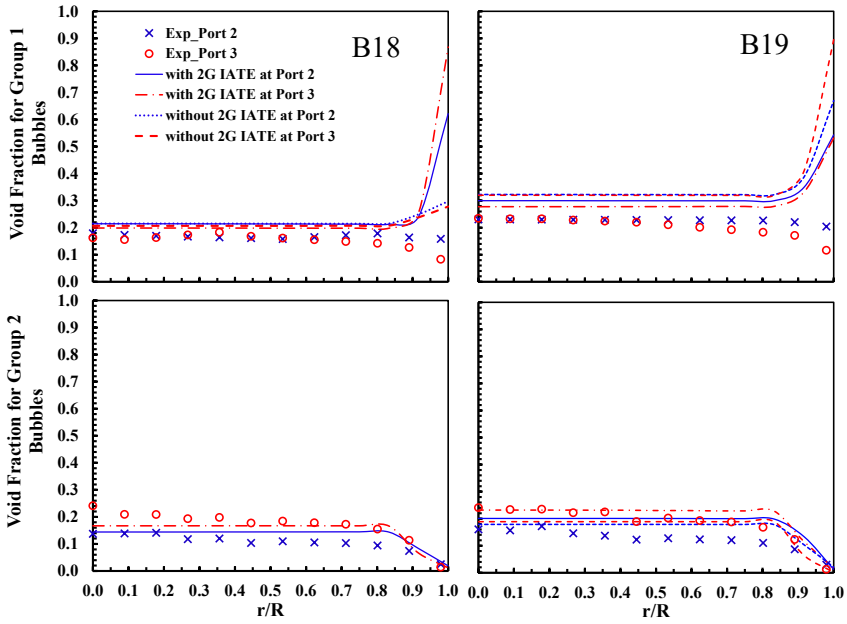

Figure 3.9. Effect of 2G IATE on Void Fraction Distribution for Group 1 and Group 2 Bubbles in Transition Area between Bubbly and Cap/Slug Flow Regime.

size of a pipe diameter. In the real situation, the presence of large bubbles in the vicinity of the wall makes flow path of fluids narrow and makes flow fast in that region. As the large bubbles move away from the region, the flow in that narrow area faces a wide open area following the large bubbles and spreads out. At this moment, larger eddies than the bubble size in the expanded area act as a carrier of the bubbles and redistribute them.

However, in the simulation, eddies with strong turbulent energy enhance bubble breakup mechanisms and accumulates small bubbles in the near-wall region and make less concentration of large bubbles in that area. Second reason can be due to interfacial force models. Lift force and wall lubrication force are the two main forces affect radial distribution of particles in the two-phase flow. However, since, with strong turbulent intensity, turbulent diffusion force can overwhelm the lift force leading to much flatter distribution and make small bubbles near the pipe wall hard to be redistributed.

Moreover, most of the interfacial force models were developed for small bubbles based on experiments in a small diameter pipe, which may not be applicable to high flow conditions in a large diameter pipe. At low flow conditions, the 2G IATE model predicted well the IAC distributions at port 2 and port 3 for group-1 bubbles. However, IAC for group-2 bubbles was underestimated for B4 and B6 cases, whereas B5 case overestimated the IAC distribution for group-2 bubbles. B4 and B6 cases successfully predicted a general trend of IAC distributions for group-2 bubbles at port 2 and port 3 but B5 case over-predicted group-2 IAC distribution at port 2 and results in a higher level of IAC at port 2 than the level at port 3. As shown in B5 case without the model implementation, IACs at port 2 and port 3 were overestimated very much for group-2 bubbles, which was caused by increasing liquid superficial velocity. By implementing the 2G IATE model, some necessary bubble interaction mechanisms, such as WE, SO, and SI, were included and TI was more optimized. The higher superficial liquid velocity caused more active breakup mechanisms of SO and TI, and bubble coalescence mechanisms of WE. However, the over-prediction of IAC at port 2 for group-2 bubbles of B5 case can be resulted from the overestimation of interfacial drag on the group-2 bubbles, which led to more production of turbulence and active interactions between group-2 bubbles and liquid turbulence, such as TI, because of the interfacial drag models developed under small diameter pipe flow conditions. These results open a room for further studies of interfacial drag models for large diameter pipes.

At middle flow conditions, the IAC predictions with the 2G IATE model showed good agreement with experimental data over the bulk area of the pipe for both group-1 and group-2 bubbles. As increasing gas superficial velocity with a slight decrease of

liquid superficial velocity for B15 case, again, a higher relative velocity enhanced breakup mechanisms, such as TI and SO, for group-2 bubbles and the bubble coalescence, such as WE, between the two bubble groups that resulted in increase in IAC for group-1 and decrease in IAC for group-2 bubbles compared to B14 case.

B14 and B15 cases with the 2G IATE model slightly underestimated the local distribution of IAC for group-2 bubbles. However, the IAC profiles for group-2 bubbles of both Run cases with the model implementation successfully followed a general trend of experimental data by giving higher level of IAC at port 2 than the level at Port 3. When it comes to the measurement error of the experimental data, the result seemed to be acceptable. Error analysis is described in the following section and can be found in the following.

At high flow conditions, B22 and B23 showed relatively large differences in values of IAC as well as a trend of general levels of the IAC distribution for group-2 bubbles at different measurement points. Both Run cases indicated good performance of the 2G IATE model at port 2 and at port 3 even though it showed a flat distribution of IAC for group-1 bubbles, which was not matching to experimental data. However, the model overestimated the IAC for group-2 bubbles of B22 case at port 3, which was supposed to be lower than the IAC at port 2. B23 case also over-predicts IAC for group-2 bubbles but captured the trend of IAC distribution of experimental data at port 2 and port 3 whereas the IACs at port 2 and port 3 were over-predicted.

- **The 2nd Case: Transition from cap/slug flows to churn-turbulent flow regime at middle flow and high flow conditions (B12, B13, B20, and B21) in Figure 3.11**

IAC distributions for group-1 and group-2 bubbles in the transition area from cap/slug flows to churn-turbulent flow increased with superficial velocities of liquid and gas phases. In the experimental data, two each middle (B12 or B13) and high flow (B20 or B21) conditions in the same flow regime showed similar characteristics of IAC distributions. In the simulation, as increasing superficial gas velocity at middle and high superficial liquid velocities, the difference in IACs for group-1 and group-2 bubbles were larger as shown from the comparison between B12 and B13 cases as well as between B20 and B21 cases.

At middle flow conditions, IAC distributions for group-1 bubbles of both Run cases in cap/slug flow regime and churn-turbulent flow regime agreed well with experimental data regardless of the 2G IATE model consideration. However, IAC for group-2 bubbles was underestimated. Different from experimental data, B12 and B20 cases in cap/slug flows regime expected lower IAC distribution at port 3 than the distribution at port 2 and it can be caused by less prediction of breakup mechanisms of group-2 bubbles, such as TI and SI, and strong evaluation of coalescence phenomena of group-2 bubbles into the same bubble group, such as WE, at port 3 that these at port 2. This can be confirmed from Figure 3.20 indicating dominant terms of the 2G IATE at port 2 and port 3. According to the Figure 3.20, the bubble interaction mechanism was the dominant term impacting on the distribution of IAC for group-2 bubbles and the dominant term at port 3 was less than the term at port 2. At high flow conditions, B21 in

churn-turbulent flow regime showed a better estimation of IAC distribution for group-2 bubbles than that for B20 in cap/slug flow regime.

- **The 3rd Case: Transition from bubbly to cap/slug flows (B18 and B19) in Figure 3.12**

B18 and B19 cases are in the transition area, and they are classified as bubbly flow and cap/slug flow, respectively. An effect of the 2G IATE was clear in prediction of IAC distribution for group-1 bubbles for both B18 and B19 cases. For group-2 bubbles, however, IAC distributions were underestimated. It can be resulted that the 2G IATE model can predict the acceptable distribution of IAC for group-1 bubbles against the experimental data, whereas the model needs further effort for optimization of the mechanistic model for the bubble interaction.

3.7.3. Error Analysis. This section shows local errors of Run cases in prediction of void fraction and IAC distributions at port 2 and port 3. For local error calculations, the differences between the predicted values and experimental data were normalized against each measured value of void fraction and IAC for each bubble group as shown in Equation. (31).

$$error_{\psi} = \frac{|\psi_{i,k,pre} - \psi_{i,k,exp}|}{\psi_{i,k,exp}} \times 100\% \tag{31}$$

where ψ, i, and k indicate void fraction or IAC, bubble group 1 or 2, and measurement location of port 2 or 3. The area-averaged value is defined as:

$$\langle \psi \rangle = \frac{\int \psi(r) dr}{A_{pipe}} \tag{32}$$

where $\langle \quad \rangle$ represents area-averaged quantity and A_{pipe} is the cross-sectional area of the flow pipe.

Due to the issue with predicting local values near-wall area, data points for the error analysis in that area were ignored.

3.7.3.1. Void fraction. Figure 3.13 through Figure 3.15 present the relative errors of the predicted void fraction against the experimental data. The local errors in prediction of void fraction for group-1 and group-2 bubbles were scaled 0% to 160%. Solid line and dash line are for the simulations with the 2G IATE model and dot line and dash dot line are for the default setup without 2G IATE model. Lines in blue and red indicate values obtained at port 2 and port 3, respectively.

- **The 1st Case: Churn-turbulent flow regime at low, middle, and high flow conditions (B4, B5, B6, B14, B15, B22, and B23) in Figure 3.13**

Figure 3.13 shows the relative prediction error of void fraction for the flow conditions in churn-turbulent flow regime. At the low flow rate conditions (B4, B5, and B6) in churn-turbulent flow regime, prediction error of void fraction for group-1 bubbles with the 2G IATE model was lower than the error without implementation of the 2G IATE model and inter-group mass transfer term associated with Smith's bubble interaction model. As increasing gas superficial velocity, the relative prediction error tended to decrease, and it was significant in the near-wall region. More specifically, B4 case showed that the 2G IATE model improved prediction of void fraction distribution for group-1 bubbles, and the error without the 2G IATE model was two times higher than the error with the model

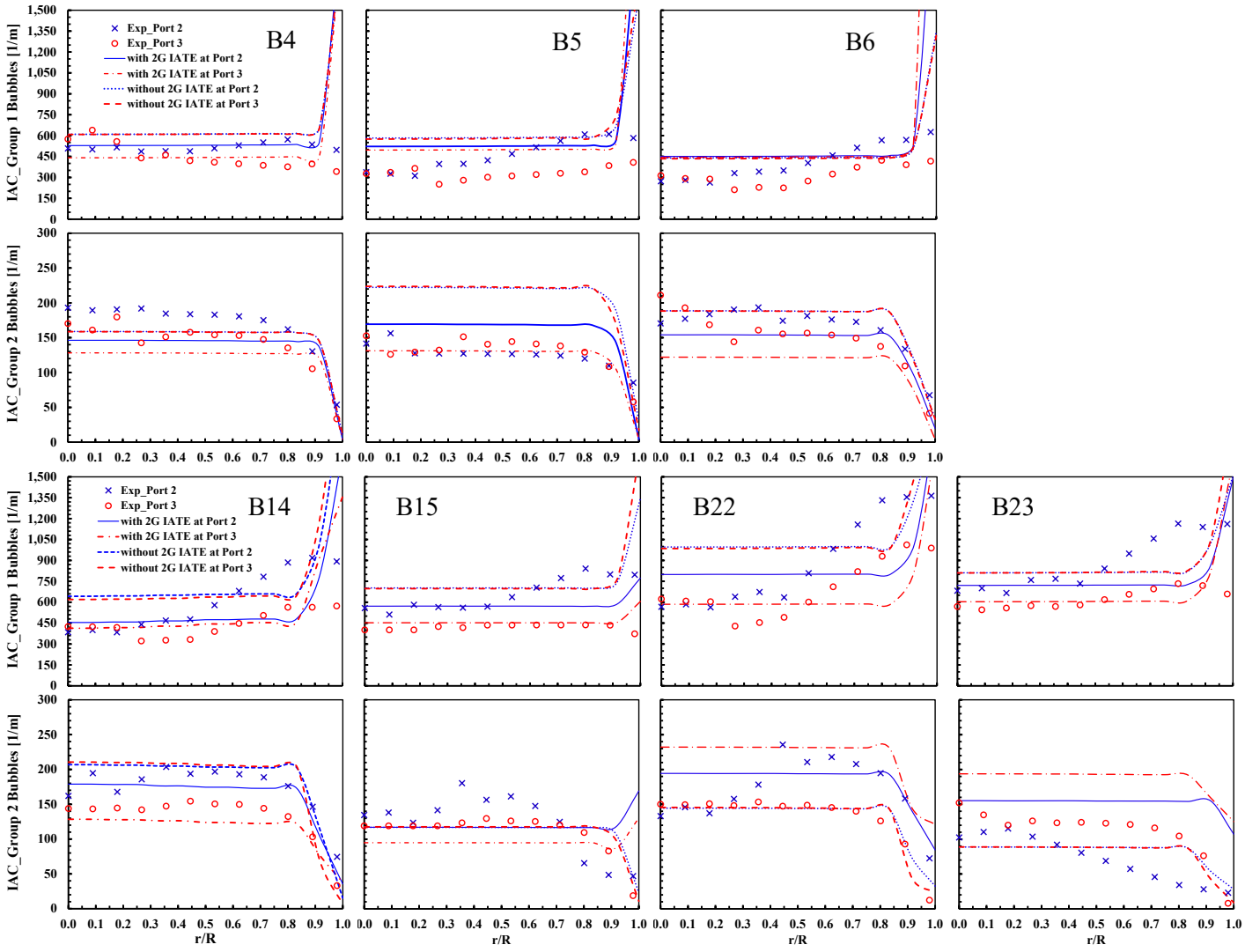

Figure 3.10. Effect of 2G IATE on IAC Distribution for Group 1 and Group 2 Bubbles in Churn-Turbulent Flow Regime.

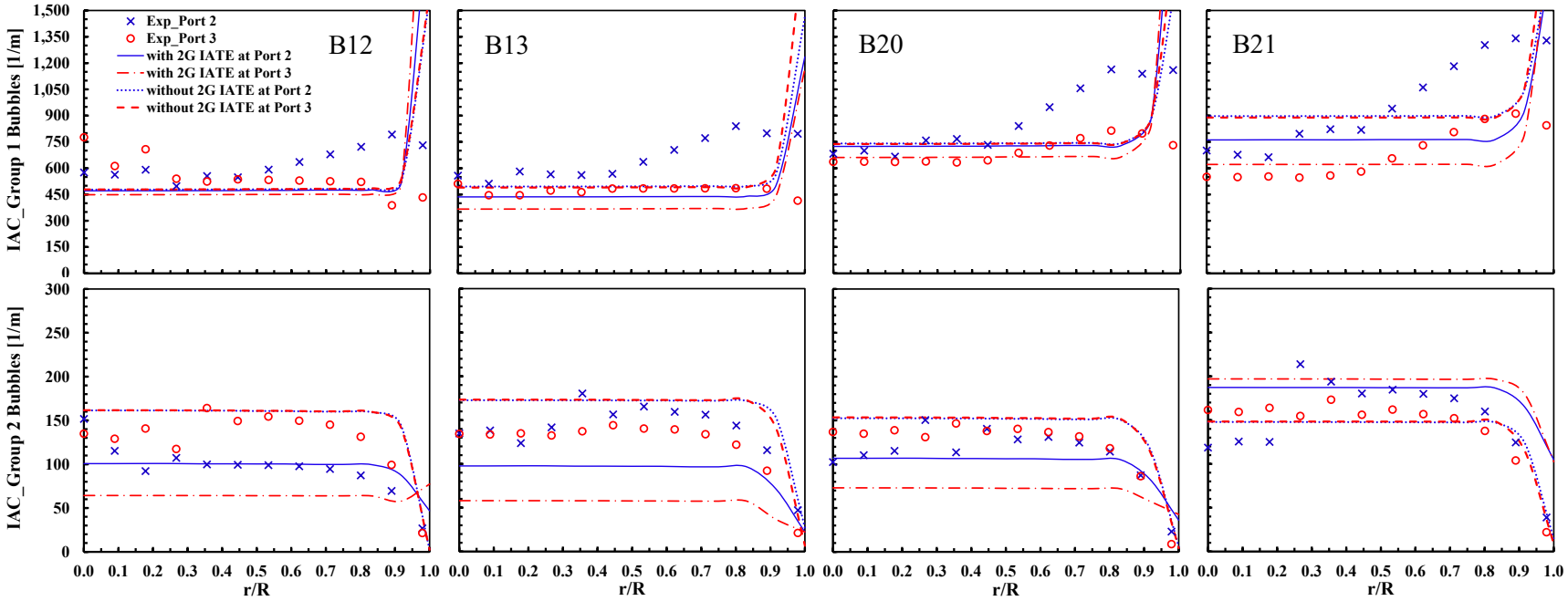

Figure 3.11. Effect of 2G IATE on IAC Distribution for Group 1 and Group 2 Bubbles in Transition Area between Cap/Slug and Churn-Turbulent Flow Regime.

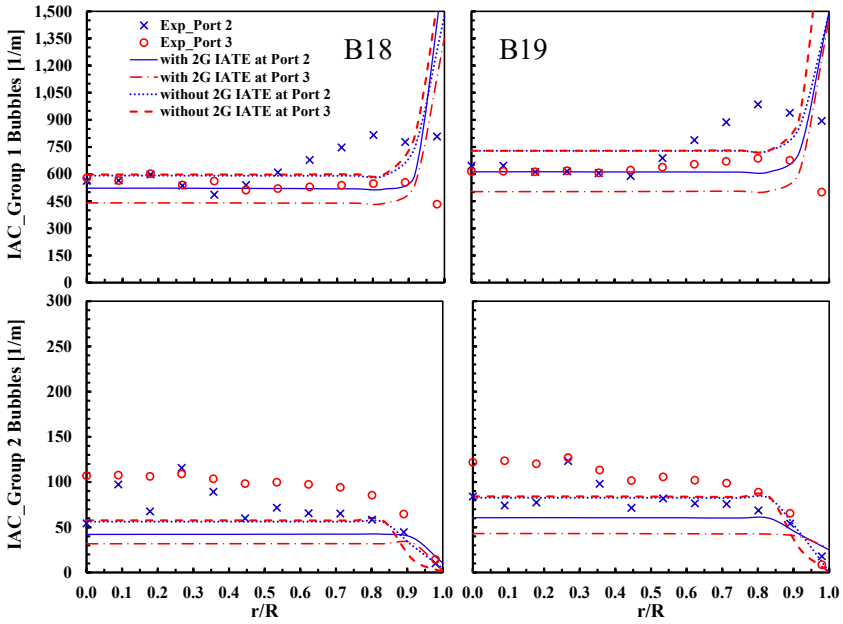

Figure 3.12. Effect of 2G IATE on IAC Distribution for Group 1 and Group 2 Bubbles in Transition Area between Bubbly and Cap/Slug Flow Regime.

implementation and the errors at port 2 and port 3 increased as a radial position moved toward the pipe wall. B5 case evaluated void fraction for group-1 bubbles with high errors over 60% at port 2 and over 40% at port 3 in the bulk area of the pipe. As the measurement point moves from center to wall of the pipe, the error at port 2 decreases but the errors at port 3 increases. B6 case showed the smallest error among the three low flow rate conditions. However, the highest error was expected in the bulk area as same as B5 case indicates. It was due to flat distribution of void fraction in the simulation, which was different from the experimental data showing small fluctuations, and small quantities of void faction that led to huge deviation. Again, this different distribution trend between the simulation and experiment revealed the issue about interfacial closure models developed for small diameter pipes.

For group-2 bubbles, the prediction error of B4 case with the model implementation was higher than the error without the 2G IATE model and inter-group interaction term. B5 and B6 cases indicated better prediction of void fraction distribution for group-2 bubbles compared to that for group-1 bubbles. However, the inter-group interaction term caused higher error at port 2 for B5 case. From the result, it can be concluded that Smith's model successfully differentiates the effect of each bubble interaction mechanism at port 2 and port 3, but less breakup mechanisms of group-2 bubbles, such as turbulent impact (TI), were expected at low flow conditions leading to overestimation of void fraction for group-2 bubbles. Since TI was the most significant bubble breakup mechanism and was strongly related with turbulent dissipation rate and its length scale (size), RANS turbulence model may have limitation to capture any eddies, which are as large as group-2 bubbles and this limitation affects intensity of the breakup mechanisms. The contribution of the eddy to bubble breakup can be scaled by adjusting critical Weber number ($\boldsymbol{We_{cr,2}}$) for group-2 bubbles. However, in this study, the same value of 1.2 for $\boldsymbol{We_{cr,2}}$ was used as described in Smith et. al. (2012).

At the middle flow conditions (B14 and B15), the 2G IATE model with Smith's model showed better prediction of void fraction distribution except for group-2 bubbles of B14 case. As gas velocity increase, void fraction varied more against radial position, this variation of void fraction resulted in larger error for B15 case.

At the high flow conditions (B22 and B23), again, as higher the phase velocity ($\langle j_f \rangle$ = 0.95 m/s and $\langle j_g \rangle$ = 4.24 m/s for B22 and $\langle j_f \rangle$ = 0.93 m/s and $\langle j_g \rangle$ = 4.97 m/s for B23) was achieved, more fluctuation of the void fraction against a local position (r/R)

was featured and higher errors in prediction of void fraction profile for group-2 bubbles were obtained.

From the results, it can be found that in the churn-turbulent flow conditions, the 2G IATE model with inter-group mass transfer term seemed to work better for group-2 bubbles and the capability of the 2G IATE model with Smith's model to evaluate the void fraction highly depended on flow conditions at very high gas velocity conditions.

- **The 2nd Case: Transition from cap/slug flows to churn-turbulent flow regime at middle flow and high flow conditions (B12, B13, B20, and B21) in Figure 3.14**

Figure 3.14 represents results of local prediction errors for Run cases at middle and high flow conditions in transition area.

B12 and B13 cases cover transition area between cap/slug flow and churn-turbulent flow regimes at the middle flow conditions. As increasing gas velocity, better prediction of void fraction profiles for both group-1 bubbles was obtained. The maximum error differences in the bulk area of the pipe between the simulations with the 2G IATE and without the 2G IATE were about 5% at port 2 and 20% at port 3. A large gradient of void fraction at port 3 in the experimental data led to higher error. In these flow conditions, turbulent diffusion comes to play and may overwhelm the lift force, which generated much flatter distribution of void fraction. The same issue can be found from void fraction distribution for group-2 bubbles. Moreover, Smith's model overestimated void fraction for group-2 bubbles.

B20 and B21 cases ranged from cap/slug to churn-turbulent flow regimes in the transition areas at the high flow conditions. The similar results with B12 and B13 cases can be found for B20 and B21 cases.

B13 and B21 case in churn-turbulent flow regime showed relatively better prediction for group-2 void fraction with the 2G IATE and inter-group mass transfer term.

The 2G IATE model was capable of provide quite a good prediction of local void fraction distribution for group-1 bubbles in the transition area between cap/slug flow and churn-turbulent flow regimes. Further, the model implementation did not impact much on void fraction distribution at middle and high flow conditions in the transition area. However, the models worked better for estimating the void fraction and IAC distribution for group-1 bubbles under the cap/slug flow conditions rather than under flow conditions in the churn-turbulent flow regime. On the other hand, the predictions for group-2 bubbles was relatively more accurate under the churn-turbulent flow conditions. Further studies of the 2G IATE model along with Smith's model seemed to be required to be used for the evaluation of void fraction profile for group-2 bubbles.

- **The 3rd Case: Transition from bubbly to cap/slug flows (B18 and B19) in Figure 3.15**

Figure 3.15 displays results for B18 and B19 case sat the high flow conditions in the transition areas between bubbly and cap/slug flow regimes. There was no significant effect of the model implementation for group-1 bubbles of B18 case in the bubbly flow regime whereas the prediction error for group-2 bubbles was higher by about 20% with the 2G IATE model and inter-group mass transfer term compared to the case without the

implementation of the models. B19 case in the cap/slug flow regime showed a clear difference in prediction error of void fraction for both group-1 and group-2 bubbles between the simulation conditions with and without the model implementation. A big improvement was captured for group-1 bubbles, but for group-2 bubbles, it showed the similar trend with B18 case. In transition area between bubbly and cap/slug flow regimes, the 2G IATE model and inter-group mass transfer model can provide better results for group-1 bubbles rather than for group-2 bubbles. Further, the models appeared to be very sensitive to flow conditions in the transition area. In the transition, as increasing gas velocity, void fractions for both group-1 and group-2 bubbles increased. A small increase in liquid velocity did not have much impact on void fraction distributions and the models barely affected void fraction prediction and both simulation conditions with and without the2G IATE showed a good agreement with experimental data.

3.7.3.2. IAC. Figure 3.16 through Figure 3.18 show the prediction error of local IAC. The local relative errors for group-1 and group-2 are also scaled from 0% to 160%. The same format of the lines and colors is used as the error analysis for the void fraction distributions does.

- **The 1st Case: Churn-turbulent flow regime at low, middle, and high flow conditions (B5, B6, B14, B15, B22, and B23) in Figure 3.16**

Figure 3.16 shows local error predictions of the implementation of the 2G IATE model and without the model implementation for the flow conditions in churn-turbulent flow regime.

For group-1 bubbles, generally, Run cases with the 2G IATE model improved the prediction of IAC distribution. However, as liquid superficial velocity increased, error in

the near-wall region increased and became higher than the simulation without the model implementation. This trend was due to the high variation of IAC in local position at higher liquid flow condition. For group-2 bubbles, at low liquid flow conditions, the implementation of the 2G IATE caused the greater local errors in prediction of IAC distribution. At middle flow conditions, the difference in prediction errors between the simulation conditions with and without the 2G IATE model was larger at port 3 than that at port 2. At high flow conditions, the deviation of error with the 2G IATE from the simulations without the model became higher than the other flow conditions and a larger error was induced by the 2G IATE model. From the results, it can be concluded that the 2G IATE model is capable of predicting IAC for group-1 bubbles in churn-turbulent flow regime. However, the model implementation does not guarantee its performance for group-2 bubbles. Moreover, the current interfacial closure models seem not applicable to flow conditions in a large diameter pipe, especially, for large (group-2) bubbles and in near-wall region.

- **The 2nd Case: Transition from cap/slug flows to churn-turbulent flow regime at middle flow and high flow conditions (B12, B13, B20, and B21) in Figure 3.17**

The local prediction error of IAC distribution for the cases in the transition area from cap/slug flow to churn-turbulent flow regime at middle flow and high flow conditions is shown in Figure 3.17. Run cases in the same flow regime, such as cap/slug flow or churn-turbulent flow regime, with different flow conditions show the similar trend of the local prediction error each other. This trend is also found in the Figure 3.20, which indicate dominance of each component of the 2G IATE model.

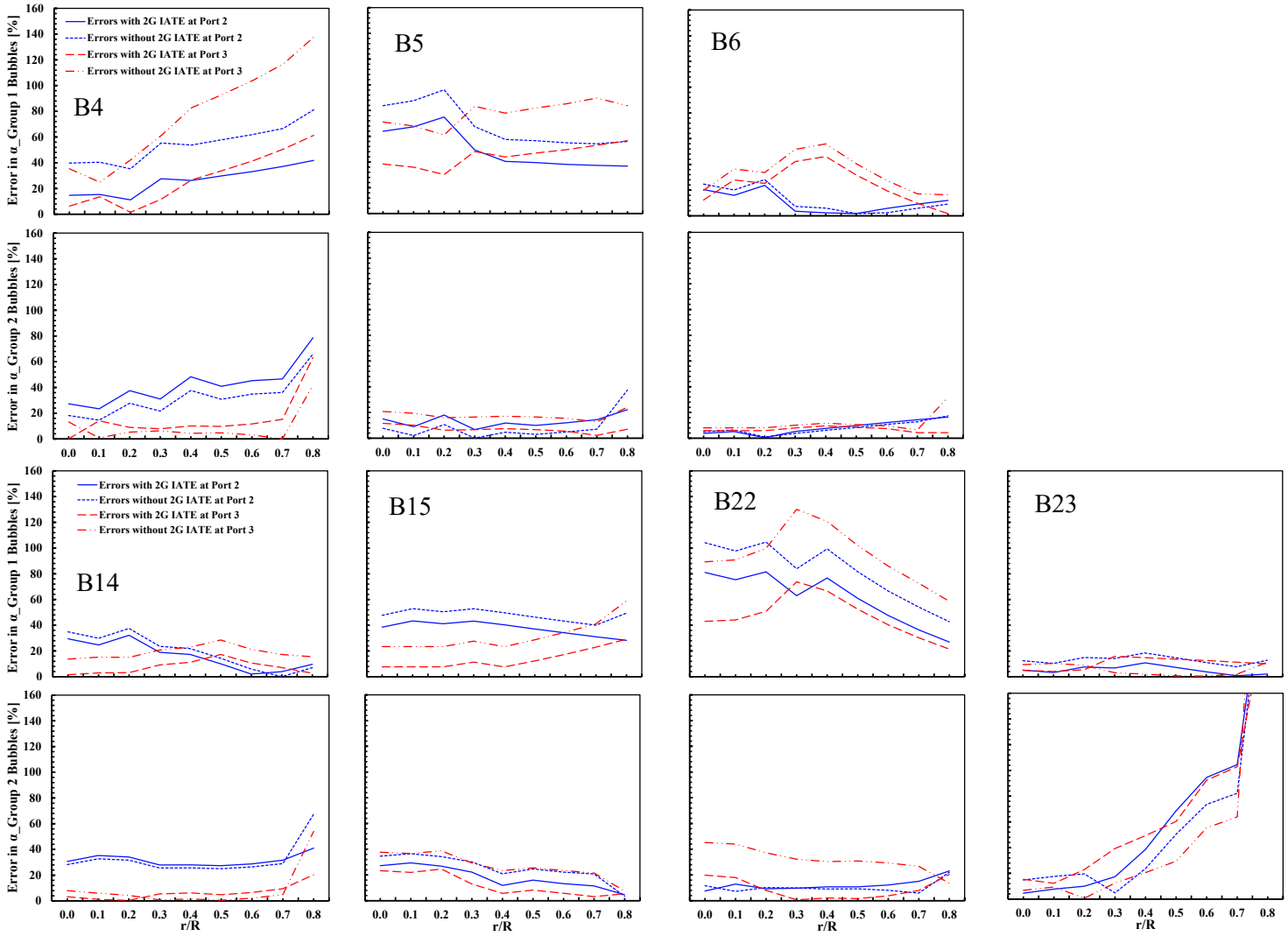

Figure 3.13. Local Error of Void Fraction at Port 2 and Port 3 in Churn-Turbulent Flow Regime.

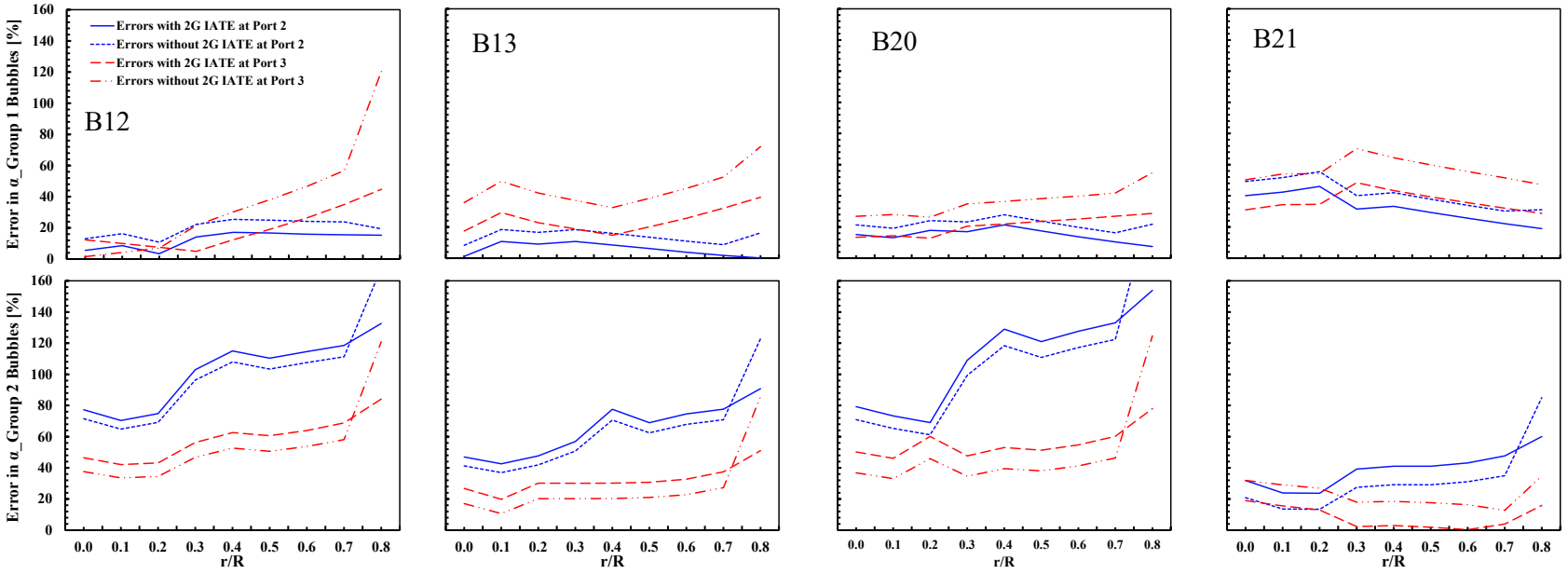

Figure 3.14. Local Error of Void Fraction at Port 2 and Port 3 in Transition Area between Cap/Slug and Churn-Turbulent Flow Regime.

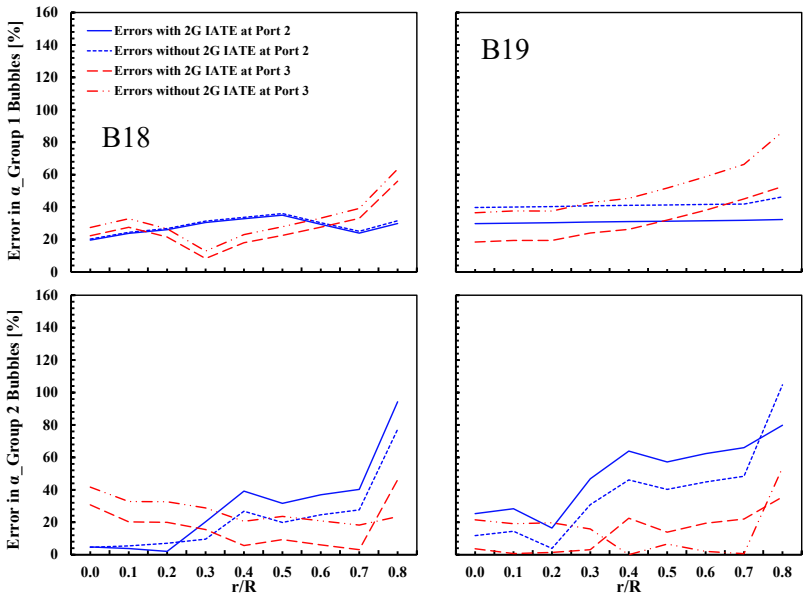

Figure 3.15. Local Error of Void Fraction at Port 2 and Port 3 in Transition Area between Bubbly and Cap/Slug Flow Regime.

- **The 2nd Case: Transition from cap/slug flows to churn-turbulent flow regime at middle flow and high flow conditions (B12, B13, B20, and B21) in Figure 3.17**

The local prediction error of IAC distribution for the cases in the transition area from cap/slug flow to churn-turbulent flow regime at middle flow and high flow conditions is shown in Figure 3.17. Run cases in the same flow regime, such as cap/slug flow or churn-turbulent flow regime, with different flow conditions show the similar trend of the local prediction error each other. This trend is also found in the Figure 3.20, which indicate dominance of each component of the 2G IATE model.

B13 has larger errors with the model implementation at port 2 and port 3. However, B21 shows that the 2G IATE improved local prediction of IAC distribution even though the model implementation increases error as the local position approaches

close to the wall. This increase of error near the wall is highly related to interfacial closure models.

For group-2 bubbles, B12 and B13 cases at middle flow conditions show higher errors compared to the errors for Run cases at high flow conditions of B20 and B21. At middle flow conditions, prediction error at port 2 for B12 is significantly decreased whereas the error at port 3 is much higher than that without the 2G IATE model. It is because IAC distributions without the model implementation have the similar values at both port 2 and port 3and they are biased to the IAC distribution at port 3, which indicate that the 2G IATE model successfully predicts IAC interaction mechanisms. However, the IAC interaction mechanisms does not guarantee IAC prediction at port 3. It can be found in Figure 3.20, which shows that the IAC interaction mechanisms are the most dominant effect on IAC distribution. Turbulence kinetic energy and turbulent dissipation rate can be one of the main causes of high prediction error at port 3.

B13 also shows the similar trend of errors except for IAC distribution at port 2. The implementation of the 2G IATE model gives higher errors at port 2. It can be concluded that the 2G IATE model is better for IAC prediction for group-1 bubbles rather than for group-2 bubbles. Moreover, the model implementation works better for the flow conditions in cap/slug flow regime compared to in churn-turbulent flow conditions.

At high flow conditions, the 2G IATE model provided very accurate prediction of IAC distributions. However, B21 case in the churn-turbulent flow regime predicts three times higher error in the center area than the prediction error of IAC without the 2G IATE model. Both B20 and B21 cases also have higher errors with the 2G IATE model at port 3.

- **The 3rd Case: Transition from bubbly to cap/slug flows (18 and B19) in Figure 3.18**

In the Figure 3.18, prediction errors of IAC distribution for group-1 bubbles for both B18 and B19 cases show similar trend with one another. As a radial position approaches to the wall, error increases regardless of the model implementation. However, the 2G IATE causes higher error. For group-2 bubbles, both Run cases with 2G IATE produces higher error.

B18 and B19 cases at high flow condition in the transition area between bubbly and cap/slug flow regimes evaluated IAC for group-1 bubbles better than the IAC for group-2 bubbles. For both Run cases, additionally, the 2G IATE model induced slightly higher errors of IAC for group-1 bubbles.

IAC prediction error for group-2 bubbles with the 2GIATE model is also higher than the error for the default model without the 2G IATE. B19 case in cap/slug flow regime relatively predicts well IAC distribution for group-2 bubbles compared to the flow condition in the bubbly flow regime.

3.7.4. Dominance of 2G IATE Terms. This section explains the effect of each term in the IATE model on IAC distribution. Interfacial in various flow regimes including transition area. The 2G IATE model can be divided into three components: IAC from bubble interaction mechanisms (IM), IAC from mass transfer between group-1 and group-2 bubbles (MT), and IAC from volume expansion (VE) due to pressure change. Absolute value of each of the three parts is divided by total IAC value and the ratio of each part to the total IAC is plotted in the Figure 3.19 through Figure 3.21. The ratio of

the three parts (IM, MT, and VE) are differentiated by colors in blue, green, and red, respectively.

- **The 1st Case: Churn-turbulent flow regime at low, middle, and high flow conditions (B4, B5, B6, B14, B15, B22, and B23) in Figure 3.19**

Figure 3.19 shows the effect of each term in IATE model on IAC distribution in churn-turbulent flow regime. As increasing liquid superficial velocity, effects of IM and MT for group-1 bubbles are increased, whereas their effects are decreased for group-2 bubbles. The effect of VE is the smallest. For B4 and B5 cases, MT shows the most dominant effect on IAC distribution and the effects become more active in the near-wall region. B6 case shows very active effects of IM and MT in the bulk area and the IM is the most dominant effect for group-1 bubbles. Dominance of the effects is gradually decreased as approaching to the wall. For group-2 bubbles, B4, B5, and B6 cases have the strongest effect of IM on IAC distribution. There is ignorable effect of VE in bulk region but its influence on IAC distribution is sharply increased in the near-wall area. At the middle and high flow conditions of liquid phase, it is commonly shown that MT and IM are the most dominant effect for group-1 bubbles and group -2 bubbles, respectively. However, B14 shows a different trend of dominance of the IATE terms for group-1 bubbles. B14 has the dominance of the effect of the IATE terms in order of MT, IM, and VE and the effect is stronger in the bulk area than that in the near-wall region. Rest of cases indicates that VE is more dominant than IM and the effects are increased as approach to the wall area, which cause high errors in the near-wall area. For group-2 bubbles, all cases in the churn-turbulent flow regime show that IM is the most dominant effect and VE is the weakest one. In the center area, the effects are more focused.

Additionally, as increase superficial velocity of gas phase, the effect of the IATE terms increases, whereas for group-1 bubbles an increase of the gas velocity does not affect dominance of the IATE terms. As increasing liquid and gas superficial velocity, mass transfer effect becomes dominant in IAC distributions.

- **The 2nd Case: Transition from cap/slug flows to churn-turbulent flow regime at middle flow and high flow conditions (B12, B13, B20, and B21) in Figure 3.20**

In the transition area, B12 and B20 fall into cap/slug flow regime and B13 and B21 are categorized as churn-turbulent flow regime, and each two cases in the same flow regime show similar trend as indicated in the Figure 3.20. For group-1 bubbles, Run cases in the bubbly flow regime have a higher influence in the near-wall area, and the effect of the IAC terms are decreased at the wall and very near wall area. For the rest two cases in the cap/slug flow regime, ratio of each IAC terms to total IAC for group-1 bubbles gradually increases as approach to the wall. MT is the most dominant term.

- **The 3rd Case: Transition from bubbly to cap/slug flows (B18 and B19) in Figure 3.21**

Both B18 and B19 cases indicates very similar dominance of each term in the 2G IATE. For group-1 bubbles, MT between the bubble groups has the strongest impact on IAC distribution and more active mass transfer happened at port 3. As the flow regime hanges from bubbly flow regime to cap/slug flow regime, VE is enhanced whereas IM is shrunk in the bulk area of the pipe.

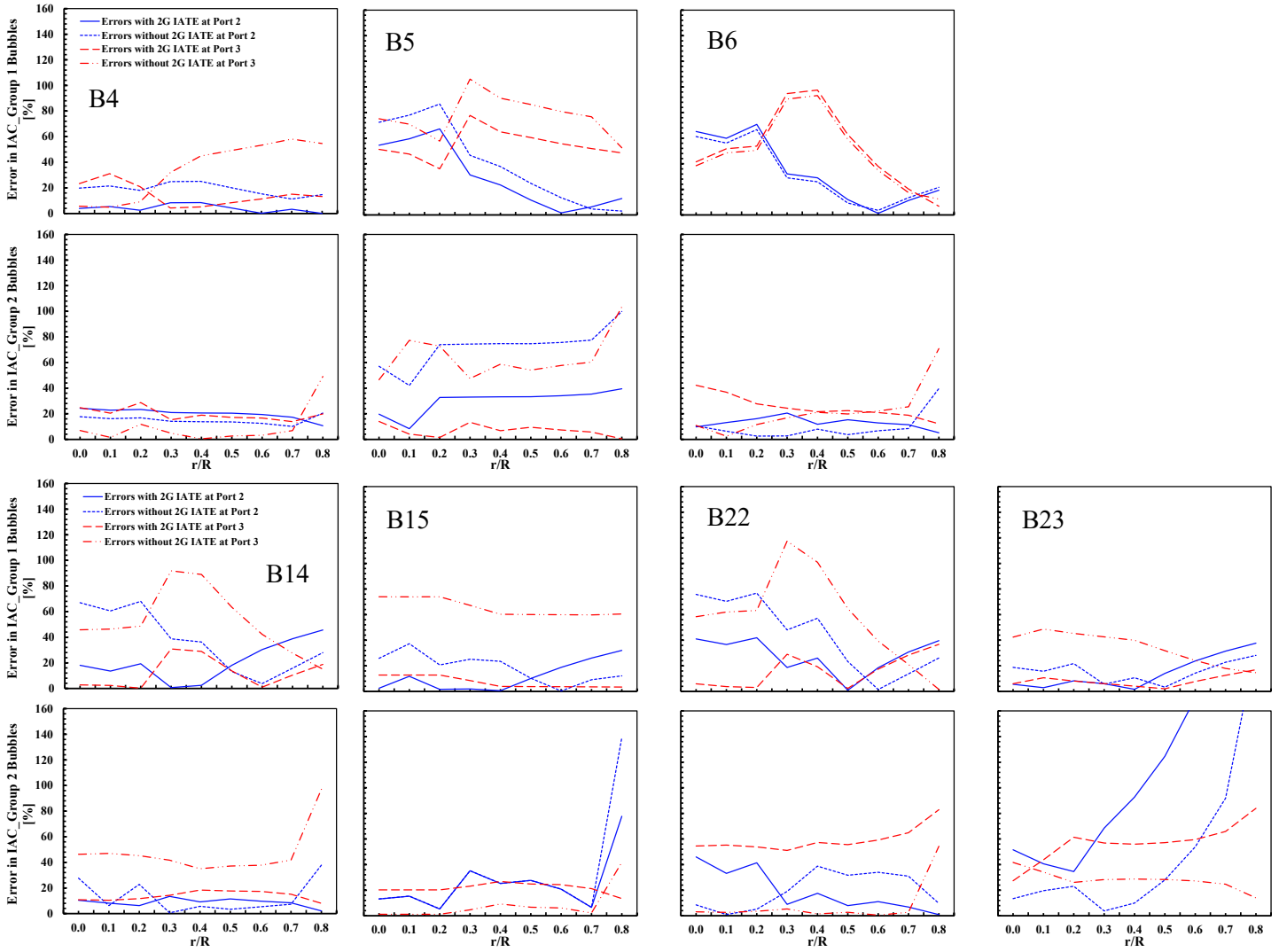

Figure 3.16. Local Error of IAC at Port 2 and Port 3 in Churn-Turbulent Flow Regime.

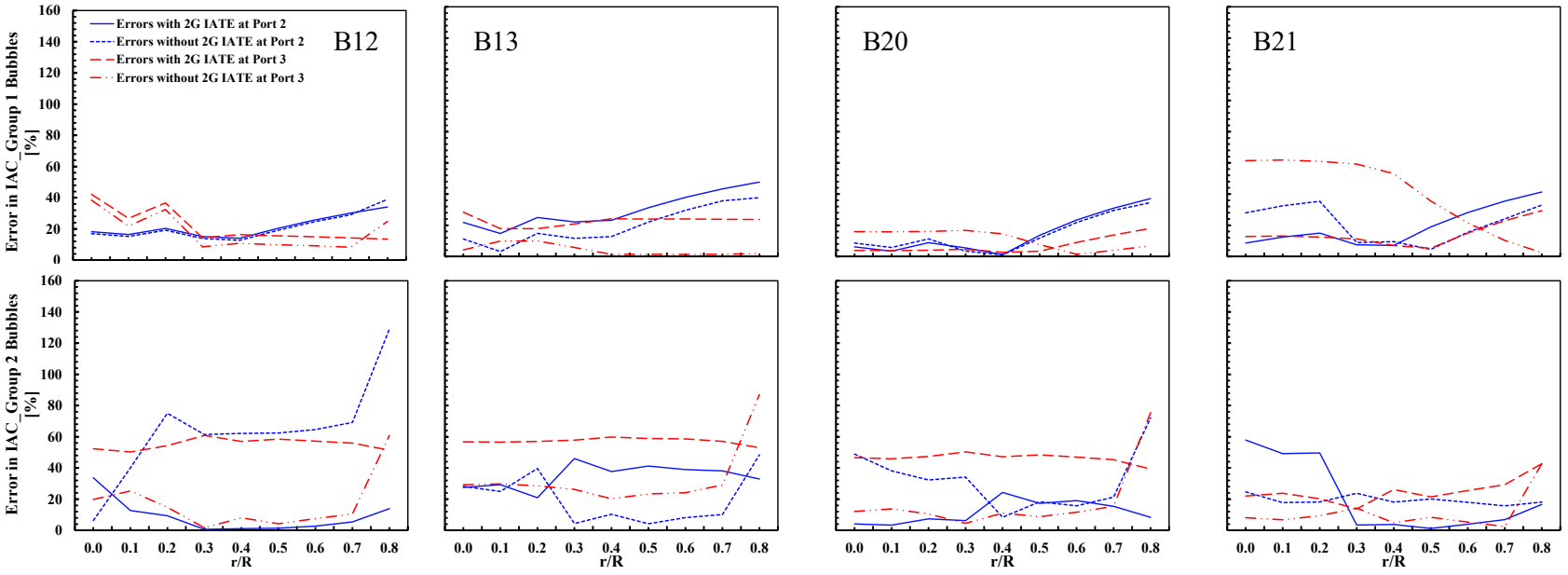

Figure 3.17. Local Error of IAC at Port 2 and Port 3 in Transition Area between Cap/Slug and Churn-Turbulent Flow Regime.

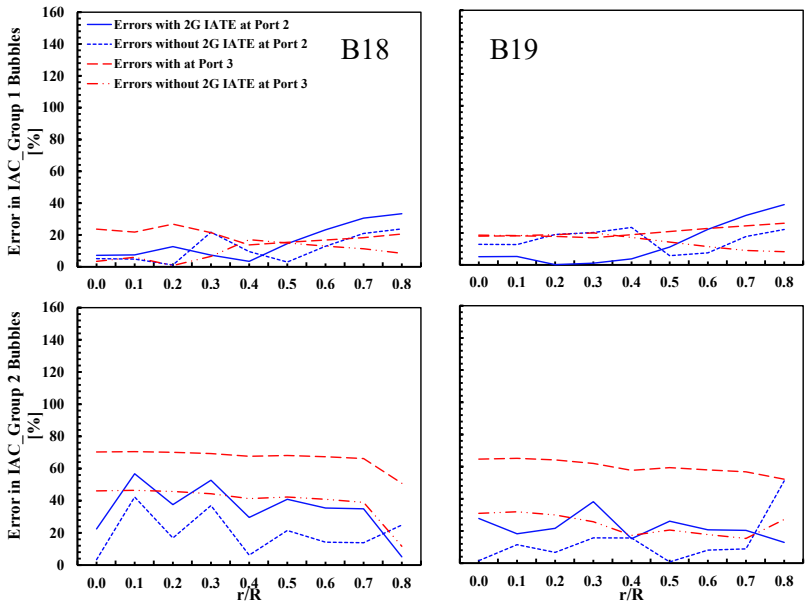

Figure 3.18. Local error of IAC at port 2 and port 3 in Transition Area between Bubbly and Cap/Slug Regime.

For group-2 bubbles, there was no change in the order of dominance. IM is the most dominant factor that affect IAC distribution and VE shows the weakest effect on the IAC prediction. It is found that IM and MT are very active in the near-wall area. However, the magnitude of the effect of IM and MT is decreased as the local point approaches to the wall. Different from the two factors, dominance of VE is sharply increased in the near-wall region.

3.8. CONCLUSIONS

A comprehensive evaluation of benchmarking the 2G IATE based on the S_γ PBE model has been conducted for beyond bubbly flows including transition region between the two flow regimes in a large diameter pipe. An approach of the two bubble group

categorization was used, and the modified two-fluid model and Smith's bubble interaction model were adopted to account for the mass transfer rate for the three-field two-fluid model. The effect of implementation of the 2G IATE model for simulation cases in the three main flow regimes of churn-turbulent flow, cap/slug flow, and bubbly flow regimes including transition area between the two flow regimes was analyzed by comparing predicted interfacial parameters of void fraction and IAC with the experimental data.

For the impact on void fraction, in the churn-turbulent flow regime at low, middle, and high flow conditions, the 2G IATE model with inter-group mass transfer improved prediction of void fraction distributions at all three flow conditions. But more work is needed to develop interfacial forces for the high flow and high void fraction flow conditions and to find optimized scaling parameters for the Smith's bubble interaction model. In the transition from cap/slug flows to churn-turbulent flow regime at middle flow and high flow conditions, the model implementation in prediction of the void fraction profiles did not show significant improvement, but the improvement relied on flow regime. Moreover, the models appeared to be very sensitive to flow conditions in the transition area from bubbly to cap/slug flows. For the IAC analysis, the 2G IATE model based on Smith's bubble interaction model improved prediction of IAC. Especially, IAC for group-1 bubbles agreed very well with experimental data. The dominance of the different types of interaction mechanisms changed depending on flow conditions and flow regimes. Generally, volume expansion effect was very small whereas interaction mechanisms and mass transfer had significant effect on IAC distributions.

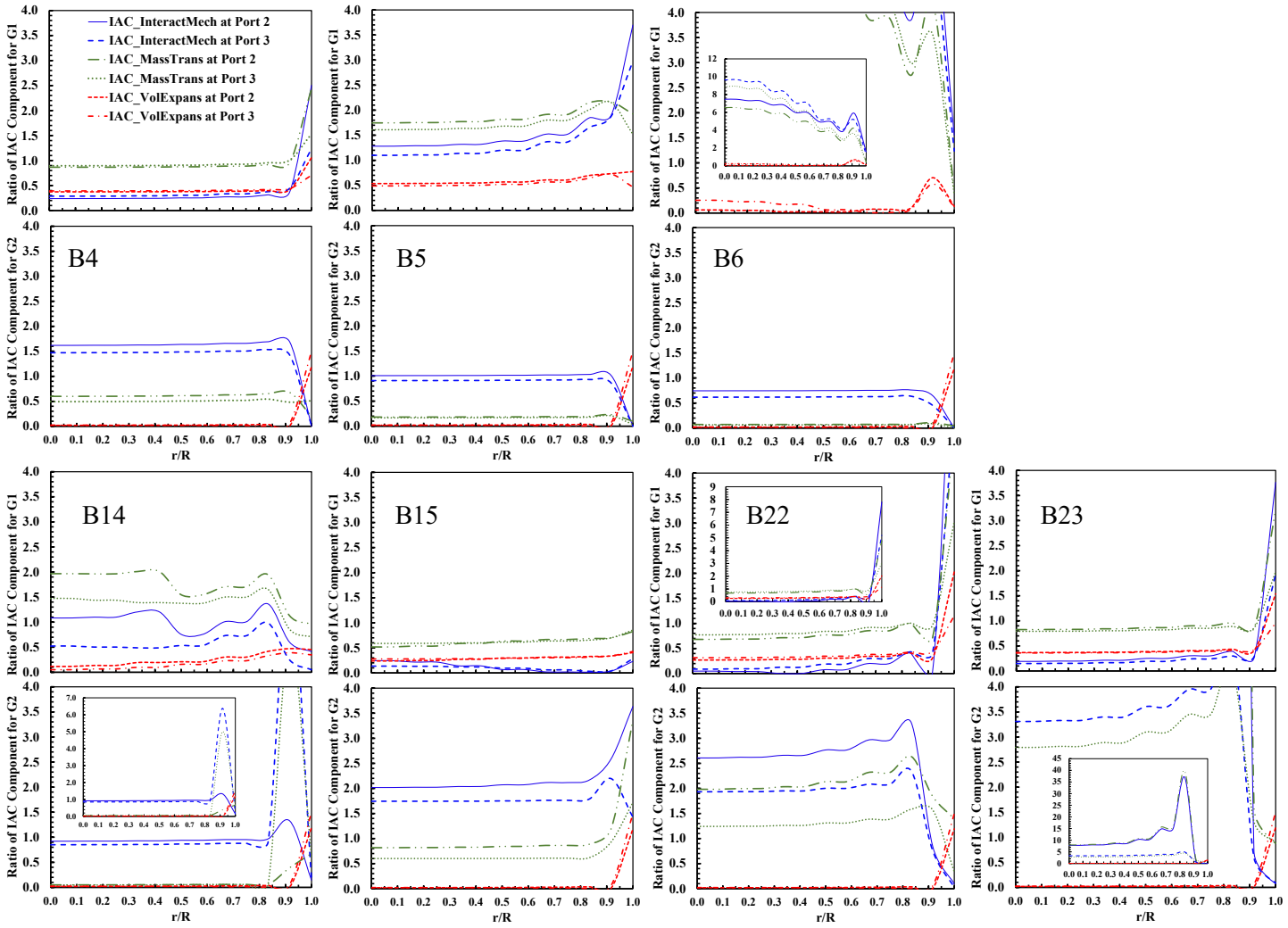

Figure 3.19. Dominance of Each Term in 2G IATE at Port 2 and Port 3 in Churn-Turbulent Flow Regime (subscription *k* indicates each contributor of IATE).

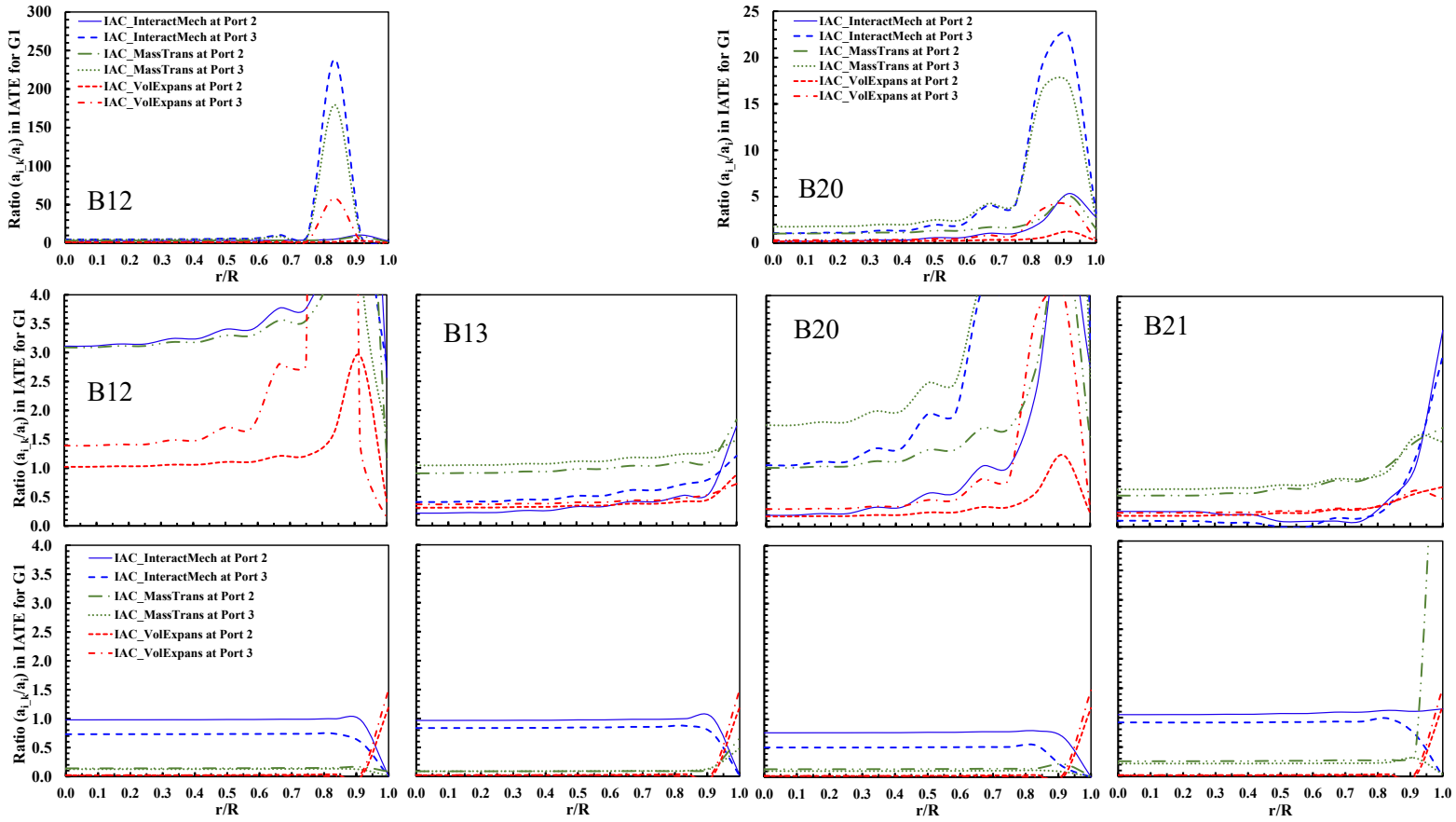

Figure 3.20. Dominance of Each Term in 2G IATE at Port 2 and Port 3 in Transition Area between Cap/Slug and Churn-Turbulent Flow Regime (subscription *k* indicates each contributor of IATE).

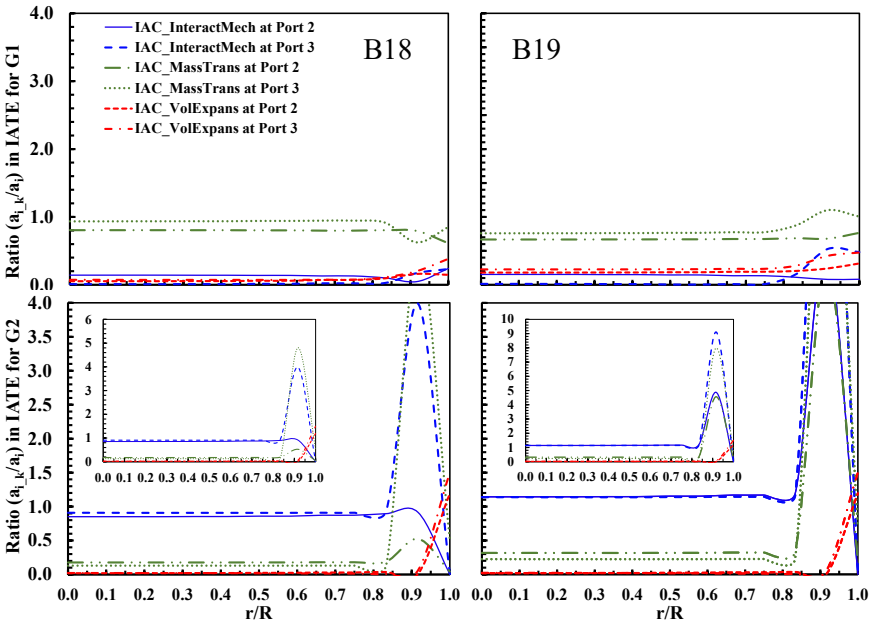

Figure 3.21. Dominance of Each Term in 2G IATE at Port 2 and Port 3 in Transition Area between Bubbly and Cap/Slug Flow Regime (subscription *k* indicates each contributor of IATE).

In churn-turbulent flow regime, the effect of the 2G IATE on the local IAC distribution was significant and the implementation of the 2G IATE model improved the prediction of IACs for group-1 and group-2 bubbles by differentiating distributions of the IAC at the different measuring positions. Bubble interaction and mass transfer were the most dominant mechanisms for IAC distributions at low and middle flow conditions. However, increasing liquid and gas superficial velocity, mass transfer effect became dominant in IAC distributions.

In transition area between cap/slug flow and churn-turbulent flow regimes, IACs for group-1 bubbles were predicted well with the 2G IATE model, but the model underestimated the IACs for group-2 bubbles. The two Run cases with different flow

conditions in the same flow regime showed the similar characteristics of the IATE effect to one another.

In transition area between bubbly flow and cap/slug flow regimes, the effect of the 2G IATE was also very clear and improved the prediction of IACs for group-1 bubble. Mass transfer effect is dominant in IAC distributions for group-1 bubbles.

4. MOMENTUM CLOSURE MODELS

A wide range of size and shape of bubbles results in variation of key interfacial forces because the IAC is linked with the two-fluid model through the interfacial momentum transfer terms with the two-fluid model. In this study, drag, lift, turbulent dispersion, virtual mass, wall lubrication, and particle (or bubble)-induced mixing (PIM or BIM) for G1 bubbles and BIT for G2 are accounted for in a linear combination as indicated in Equation (30): $\overrightarrow{M_{lk}} = \overrightarrow{M_{gl}^{D}} + \overrightarrow{M_{gl}^{L}} + \overrightarrow{M_{gl}^{TD}} + \overrightarrow{M_{gl}^{VM}} + \overrightarrow{M_{gl}^{W}}$, where $\overrightarrow{M_{gl}^{D}}$, $\overrightarrow{M_{gl}^{L}}$, $\overrightarrow{M_{gl}^{TD}}$, $\overrightarrow{M_{gl}^{VM}}$, and $\overrightarrow{M_{gl}^{W}}$ are drag, lift, turbulent dispersion, virtual mass, and wall lubrication.

As main contributors of bubble distributions and interactions of bubbles, the focus of this study is on the coefficient models for drag force and lift force. For the drag force, Schiller-Naumann model, Ishii-Zuber model, Tomiyama model, and Buffo model were chosen for the evaluation, and for the comparison analysis of the lift force models, Tomiyama model, Hibiki model, Shaver-Podowski model, and constant value of 0.01 were used. The Schiller-Naumann and Tomiyama drag models and Tomiyama lift model were available in STAR-CCM+ CFD code, and the rest models were implemented by using user-defined functions (UDFs). The models for the interfacial momentum exchange are listed in Table 4.1.

4.1. BACKGROUND

Computational fluid dynamics (CFD) has been highlighted as a tool to analyze heat and mass transfer phenomena in multi-phase flows in various industries ranging

from chemical engineering, petroleum engineering, nuclear engineering as well as bioengineering, such as cardiovascular medicine, and expending its application. The availability of a large variety of bubble sizes and shapes, and consequently various transport properties, is a crucial aspect of Two-phase flow especially beyond bubbly flow. Two-fluid model is the one of the most commonly used model to simulate two-phase flows due to its computational efficiency and applicability to a wide range of flow conditions. Basically, the two-fluid model solves the conservation equations of mass, momentum, and energy for each phase as a Eulerian-Eulerian approach, and since the conservation equations of the two-fluid model are solved based on averaged values and by assuming phases as interpenetrating continua, there is a loss of local information of hydraulic parameters. Therefore, closure relations are needed to model the effect of the local interactions between the two-phases and to close the two-fluid model by taking interfacial transfer terms into account. A proper selection of the closure models for two-phase flow analysis is vital to predict reasonably agreeable local thermal-hydraulic parameters, and it is the one systematic step of nuclear reactor safety (NRS) application to evaluate a computational models for multi-phase flows (Oberkampf and Trucano, 2002; Schwer, 2009; Bestion, 2012). The closure models are closely related with local interfacial area concentration and driving forces, referred to as constitutive models. There are some key constitutive models that include the interfacial force models, interfacial area transport models, and turbulence models for isothermal two-phase flows.

Interfacial forces in gas-liquid two-phase flows indicates interactions between gas and liquid phases and describes dynamical exchanges of momentum at the interface. The forces are incorporated in the momentum equation and affect local distributions of gas

phase as well as velocity characteristics of the phases. Generally, drag force, which is resulted from shear and form drag, is the main factor that affects residence time, terminal velocity of and relative velocity of gas phase. Lift force is the key contributor of the local phase distribution and has a great effect on flow pattern. This study focuses on the two interfacial forces and different coefficient models for drag and lift forces are compared.

The drag and lift coefficient models have been intensively developed empirically or semi- empirically by various researchers and they can be found in the recent review papers (Pourtousi et al., 2014; Chuang et al., 2017; Khan et al., 2020). Even though a great effort has been focused on the model development, most of numerical analysis and experimental work for the model development listed in the review papers and for the utilization of the models (Cheung et al., 2009; Rzehak and Krepper, 2013; Yamoah et al., 2015; Yang et al., 2015; Krepper et al., 2018; Colombo and Fairweather, 2019) focused on low void fraction flow conditions, such as bubbly flow, or restricted to small diameter channels and there are only a few studies treated beyond the limitations (Krepper et al., 2009; Lucas et al., 2010a; Lucas et al., 2010b; Kuidjo et al., 2023). In spite of the hard work of the numerical analysis with the various interfacial force models, they seem missing valid justification of the model selection or neglecting poly-dispersity of bubbles, which is known as a factor significantly impact on the prediction of the interfacial momentum transfer between dispersed and continuous phases (Zhang et al., 2006; Tabib et al., 2009) and there is no general consensus on the models to cover a wide range of two-phase flow regimes and various geometries for the numerical analysis. Again, one of the reasons of the limitation is that most of the interfacial models have been developed on the consideration of a single bubble or the experimental data in small diameter pipes. The

flow characteristics of bubbles in a large diameter channel differ from those in a small diameter channel. In terms of shape and deformity of gas phase, the large diameter channel can provide more freedom to bubbles to change its interface by growing its size without restrain of pipe wall and actively interacting with liquid. In addition, due to a large liquid space, large cap bubbles can be formed rather than slug bubbles, and small bubbles can move around the pipe. Further, in view of turbulent characteristics, since large cap bubbles have larger drag force as well as higher relative velocity than small spherical bubbles, higher turbulence is generated in the wake of large cap bubbles. This results in different interactions between bubbles and between dispersed phase and continuous phase.

Definitely, the interactions between the two phases is related with IAC, which is one of the constitutive closure model that is determined by the interfacial area transport model, referred to as the 2G IATE for the two-group bubble size approach, in this study. The IATE is a mathematical method to describe dynamical change of IAC in time and space (Kocamustafaogullari and Ishii, 1995). The two-group approach was introduced to simplify various size of bubbles in two-phase flow to two-groups as the group-1 for spherical and distorted bubble regimes and the group-2 bubbles for cap and churn-turbulent bubble regimes according to the different drag characteristics of the two bubble groups, and the 2G IATE were proposed and developed to model the temporal and spatial variation of IAC for the two groups of bubbles in a wide range of flow regimes (Ishii and Kim, 2009; Sun et al., 2003a; Sun et al., 2003b, Smith et al., 2012). However, these IATE model development makes the gap between the level of development for the interfacial force model and its applicability to numerical analysis widen. It is because of that the 2G-

IATE is capable of predicting IAC for high void fraction flow regimes and high velocity flow conditions, such as cap bubble and churn-turbulent flow regimes, in small and large diameter channels, whereas interfacial drag force model and lift force model are used for the very limited flow conditions and are not verified for the wide range of flow conditions. Therefore, the objective of this study is to evaluate the current drag and lift coefficient models for beyond bubbly flows in a large diameter pipe. In this study, four different drag and lift coefficient models respectively were evaluated to give insight of the model selection, and their effect on phase distribution and to provide the best combinations among the interfacial closure models for the two bubble group approach in a large diameter pipe.

4.2. DRAG FORCE

Drag force is a force acting on bubbles parallel to the continuous phase but opposite to relative velocity in two phase flows and can be derived from the force balance between gravity force and hydrostatic pressure under steady state condition. The drag force is given by

$$\boldsymbol{F_{Drag}} = -\frac{\boldsymbol{3}}{\boldsymbol{4d_B}}\boldsymbol{C_D\rho_L\alpha_G}|\boldsymbol{U_G} - \boldsymbol{U_L}|(\boldsymbol{U_G} - \boldsymbol{U_L}) \tag{33}$$

where d_B is diameter of bubbles, ρ is the density, α is void fraction, and U presents velocity. Subscription L and G indicate the liquid phase and the gas phase, respectively.

Accurate modeling of the drag force improves predicting void fraction. The interfacial drag force is a result of the shear and form drag of the fluid flow, which depends on the drag coefficient as well as the IAC. The coefficient of drag force indicates a dependency of drag force on hydraulic parameters and can be correlated with the

relative bubble Reynolds number Re_b=$\rho_L|U_G - U_L|d_B\mu_L^{-1}$, Eotvos number $Eo_b = (\rho_L - \rho_G)gd_B^2\sigma^{-1}$, where g is the gravitational acceleration and σ is the surface tension of the liquid, and Morton number Mo=$(\rho_L - \rho_G)\rho_L^2 g v^4 \sigma^{-3}$ (Clift et al., 1978).

4.2.1. Schiller-Naumann Model. Schiller and Naumann drag coefficient model (1975) is one of the most popular drag coefficient model for spherical rigid particles. The drag coefficient is categorized by the Reb. This model is chosen to see how the model developed for spherical bubbles affect two bubble group approach and is described as:

$$C_D = \begin{cases} \frac{24}{Re_b}(1 + 0.15Re_b^{0.687}) & Re_b \leq 10^3 \\ 0.44 & Re_b > 10^3 \end{cases} \quad (34)$$

4.2.2. Ishii-Zuber Model. Ishii and Zuber drag coefficient correlations (1979) was developed drag coefficient correlations based on a mixture viscosity model with respect to bubble flow regimes. The closure model takes account of multi-particle effect and bubble deformation for bubbles, droplets, and solid particles and is most widely used drag model for various flow regimes**:**

$$C_D = \begin{cases} \frac{24}{Re}(1 + 0.1Re^{0.75}) & Undistorted\ bubble\ regime\ (for\ group\ 1\ \ bubbles) \\ \frac{8}{3}(1 - \alpha_G)^2 & cap\ bubble\ regime\ (for\ group\ 2\ bubbles) \end{cases} \quad (35)$$

$$Re = {\rho_L|v_r|d_B}/{\mu_m} \text{ and } \frac{\mu_m}{\mu_L} = \left(1 - \frac{\alpha_G}{\alpha_{Gm}}\right)^{-2.5\alpha_{Gm}(\mu_G + 0.4\mu_L)/(\mu_G + \mu_L)} \quad (36)$$

where Re is the two-phase Reynolds number, $|v_r|$ represents magnitude of the relative velocity between gas and liquid phases, μ_m is the mixture viscosity, α_G and α_{Gm} refer to the void fraction of gas phase and maximum packing, respectively.

4.2.3. Tomiyama Model. Tomiyama et al. (1998) formulated drag coefficient models of a single bubble for spherical and non-spherical shapes of bubbles under fully developed linear shear flow for the different degree of cleanness of bubble surface. The model takes account for the effect of bubble deformation and includes bubble diameter in the calculation of the terminal velocity for non-spherical bubbles. Later, Tomiyama (2004) considered different possibilities of shapes of distorted bubbles and proposed a new set of drag coefficient models with respect to the bubble shapes based on the experimental data. The expression of the Tomiyama's drag coefficient model is:

$$C_D = \begin{cases} \boldsymbol{max\left[min\left(\frac{16}{Re_b}\left(1+0.15Re_b^{0.687}\right),\frac{48}{Re_b}\right),\frac{8Eo_b}{3(Eo_b+4)}\right]} & \boldsymbol{for\ pure\ water} \\ \boldsymbol{max\left[min\left(\frac{24}{Re_b}\left(1+0.15Re_b^{0.687}\right),\frac{72}{Re_b}\right),\frac{8Eo_b}{3(Eo_b+4)}\right]} & \boldsymbol{for\ moderate\ water} \\ \boldsymbol{max\left[\frac{24}{Re_b}\left(1+0.15Re_b^{0.687}\right),\frac{8Eo}{3(Eo_b+4)}\right]} & \boldsymbol{for\ contaminated\ water} \end{cases} \tag{37}$$

4.2.4. Buffo Model. Buffo et al. (2016) studied empirical drag closure model for poly-disperse two-phase flow in bubbly flow regime by considering swarm effect with a correction factor of a simple power-law for local polydispersity of bubbles.

$$C_D(Re_{eff}) = max\left[\frac{24}{Re_{eff}}\left(1+0.15Re_{\mathrm{eff}}^{0.687}\right),\frac{8Eo_b}{3(Eo_b+4)}\right] f(\alpha_G) \tag{38}$$

$$, Re_{eff} = {\rho_L|v_r|d_B}/{\mu_{eff}} \text{ and } \mu_{eff} = \mu_L + C_B\rho_L\frac{\kappa^2}{\varepsilon} \tag{39}$$

where μ_{eff}, C_B, κ, and ε indicate effective viscosity, a scaling constant, turbulent kinetic energy, and turbulent dissipation rate of liquid phase.

In order to account for crowding effect (swarm effect), correction factors of a simple power-law are applied as:

$$f(\alpha_G) = \begin{cases} (1-\alpha_G)^{C_A} & if\ \alpha_G \leq 0.8 \\ 1 & if\ \alpha_G > 0.8 \end{cases} \quad (40)$$

where C_A is a model parameter. All the constant parameters in the Buffo model are assumed to be the same with the values in the paper, Buffo et al. (2016), as $C_A = -1.3\ and\ C_B = 0.002$, which are found for the bubbly flows through an empirical procedure without theoretical background.

4.3. LIFT FORCE

Lift force as non-drag forces is a main contributor of lateral distribution of void fraction in gas-liquid two-phase flows. The origin of the classical lift force was to derive lateral movement of spherical bubbles in a steady flow. The perpendicular migration of the bubbles to the liquid flow direction is due to the pressure gradient on the bubble surface or the gradient of velocity in the liquid phase and is described as the cross product of the vorticity of the liquid phase and phase relative velocity as shown in Eq. (41).

$$F_{Lift} = -C_L \rho_L \alpha_G v_r \times (\nabla \times v_L) \quad (41)$$

where C_L indicates lift coefficient.

Four different lift force coefficient models were compared. As the most representative lift coefficient model, which follows an experimental approach to obtain an empirical correlation, the Tomiyama model (Tomiyama, 2002) was chosen.

4.3.1. Tomiyama Model. Tomiyama et al (1998) and Tomiyama (2002) derived one of the notable lift coefficient model based on experiments of single bubbles flowing in a well-defined shear field. From this work, it was confirmed that the sign of lift force direction is changed when bubbles are large enough in size and the bubbles are substantially deformed. Bubble deformation due to the force balance between

gravitational and surface tension forces is a key factor of the sign change, and the lift coefficient model is classified by Eo number.

$$C_L = \begin{cases} min[0.288\tanh(0.121Re_b), f(Eo_b)] & Eo_b < 4 \\ f(Eo_b) & 4 \leq Eo_b \leq 10 \\ -0.29 & 10 \leq Eo_b \end{cases} \quad (42)$$

$$f(Eo_b) = 0.00105Eo_b^3 - 0.0159Eo_b^2 - 0.0204Eo_b + 0.474 \quad (43)$$

4.3.2. Hibiki Model. The Hibiki lift coefficient model (Hibiki and Ishii, 2007) was used as the numerical approach that accounted for the bubble deformation effect on the lift force. The Hibiki and Ishii (2007) conducted extensive numerical study for modeling lift coefficient in a single particle and extended to a multiparticle systems. The Hibiki model numerically confirmed the importance of the effect of the bubble deformation, and as drag coefficient is classified by the bubble shape regime, the lift coefficient model is categorized by particle Reynolds number. The lift coefficient model describes that the model depends on the particle Reynolds number and non-dimensional shear rate at low particle Reynolds number flow conditions and that viscous number becomes important at high particle Reynolds number due to the dependency of Eo on the particle Reynolds number and viscous number.

$$C_L = \xi\sqrt{[C_L^{low\ Re}(Re, G_S)]^2 + \left[C_L^{high\ Re}(Re)\right]^2} \quad (44)$$

$$, \begin{cases} C_L^{low\ Re}(Re, G_S) = \frac{6}{\pi^2\sqrt{2ReG_S}}\frac{2.255}{\left(1+\frac{0.1Re}{G_S}\right)^{\frac{3}{2}}} \\ C_L^{high\ Re}(Re) = \frac{1}{2}\left(\frac{1+16Re^{-1}}{1+29Re^{-1}}\right) \end{cases} \quad (45)$$

$$, \xi = 2 - \exp(2.92d_b^{*2.21}) \text{ and } G_S = \left|\frac{d_d}{2v_r}\frac{dv_L}{dx}\right| \quad (46)$$

where C_L is the lift coefficient, G_S is non-dimensional shear rate in a multi-particle system, ξ is the modification factor due to deformation of bubble shapes.

4.3.3. Shaver-Podowski Model. The Shaver and Podowski (2015) proposed a new lift coefficient model, which is not dependent on bubble size but considering distance from the pipe wall. This model categorizes lift coefficient into three classes by the ratio of the distance from the wall to the diameter of the bubble. When the distance from the wall is smaller than the radius of the bubble, it forces to be 0 for the lift coefficient, and when the wall distance is greater than the diameter of the bubble, the nominal lift coefficient is used.

$$C_L = \begin{cases} 0, & \frac{y}{d_B} < 0.5 \\ C_{L0}\left[3\left(\frac{2y}{d_B}-1\right)^2 - 2\left(\frac{2y}{d_B}-1\right)^3\right], & 0.5 < \frac{y}{d_B} < 1 \\ C_{L0}, & 1 < \frac{y}{d_B} \end{cases} \quad (47)$$

$$Norminal\ lift\ coefficient,\ C_{L0} = 0.03 \quad (48)$$

4.3.4. Constant Value. Constant value of the lift coefficient was used by for small bubbles by Sharma (2016) and Sharma et al. (2017, 2019) and they confirmed that the value for small bubbles gave reasonably good predictions especially for beyond bubbly flow conditions. The constant lift coefficient of 0.01 were compared in order to overcome the limitation of the existing lift coefficient models that result in wall peaked void fraction profile for G1 bubbles in the near-wall region, which are not observed in data collected in large diameter pipes. The Shaver and Podowski model forces to decrease lift coefficient to 0 when distance between bubble and the wall is close to a certain value.

4.4. TURBULENT DISPERSION FORCE

Turbulent dispersion force acts as diffusion in dispersed flows driving gas phase away from each other when the dispersed phase is too concentrated in a certain region. Burns et al. (2004) form was used for the turbulent dispersion force. The turbulent Prandtl number for the void fraction, σ_α, was assumed equal to 0.9, which is the value typically used. This number signifies the ratio of momentum diffusivity over the void fraction diffusivity due to continuous phase velocity fluctuations.

4.5. VIRTUAL MASS FORCE

The virtual mass term in the momentum equations for dispersed two-phase flow represents the force required to accelerate the mass of the surrounding continuous phase, in the immediate vicinity of a dispersed-phase fragment, such as a bubble or droplet, when the relative velocity of the phases changes. The virtual mass force may be very small for this problem; the model is included because it stabilizes the numerical scheme. The virtual mass coefficient for a spherical particle accelerating in an unbounded fluid was set as 0.5.

4.6. WALL LUBRICATION FORCE

The wall lubrication force describes a force pushing dispersed gas phase away from wall when gas phase comes closed to the wall. The force prevents the bubbles from touching the wall since the existence of the wall causes asymmetric flow field and pressure difference around the bubbles. This is one of the important forces to be modeled in two-fluid models to recover lost information of the discrete bubble size through time

averaging process in two-fluid model. In this study, Antal model (Antal et al., 1991) was used for modeling the wall lubrication force for G1 bubbles, which has been numerically tested and most widely used. Two calibration coefficients of C_{w1} and C_{w2} in Antal model were set as -0.01 and 0.05. For G2 bubbles, the wall lubrication force was not applied since the G2 bubbles tends to move to the center of the pipe, and there are much less possibilities for the G2 bubbles to present at the wall than G1 bubbles do. Therefore, to reduce complexity of simulation, wall lubrication force for G2 bubbles is ignored. This tendency can be identified in the results of void fraction distribution of G2 bubbles in result section.

4.7. NUERICAL SETUP

4.7.1. Geometry Configuration. The same geometry configuration with the section 3 was used. The half section of 3D cylindrical pipe was converted to 2D symmetric pipe.

4.7.2. Boundary Conditions. Basically, the same boundary setup with the section 3 was applied. Table 4.2 presents inlet boundary conditions and pressure and temperature properties for the phase conditions.

4.7.3. Turbulence Model. The same turbulence model was used with the same BIT models of Sato model for group-1 bubbles and Troshko-Hassan model for group-2 bubbles.

Table 4.1. Summary of Coefficient Models for Interfacial Forces.

Interfacial Force	Coefficient models
Drag	Schiller-Naumann model
	Ishii-Zuber model
	Tomiyama model
	Buffo model
Lift	Tomiyama model
	Hibiki model
	Shaver-Podowski model
	Constant 0.01 (for group-1 bubbles)-Tomiyama (for group-2 bubbles)
Turbulent dispersion	Favre averaged drag (FAD)
Virtual mass	Auton et al.: $C_{VM} = 0.5$
Wall lubrication	Antal et al.; $C_{w1} = -0.01, C_{w2} = 0.05$

* r_d is a radius of the dispersed phase, v_{rel} is a relative velocity between gas and liquid phases, and μ_m is a dynamic viscosity of the two-phase mixture.

4.8. EVALUATION

All five major interfacial forces described in section 3 were accounted for the evaluation of interfacial force models. For the comparisons of interfacial drag force coefficient models, four different models (Ishii-Zuber model, Buffo model, Tomiyama model, and Schiller-Naumann model) were implemented. Different models only for the lift force (Tomiyama model, Hibiki model, Shaver-Podowski model, and constant value)

Table 4.2. Flow Conditions for the Evaluation of Interfacial Force Models at Port 1 (Schlegel et. al., 2012).

Injection type*	Run (B) #	$<j_g>$ (m/s)	$<j_f>$ (m/s)	$<\alpha_1>$ (%)	$<\alpha_2>$ (%)	Pressure (MPa)	Temperature (°C)
B.	5	3.1	0.23	0.209	0.358	0.173	17
C.S.	6	3.86	0.22	0.190	0.56	0.175	23
C.S.	14	4.05	0.51	0.317	0.394	0.173	21
C.S.	15	5.77	0.5	0.36	0.37	0.175	22
B.	18	0.52	0.93	0.167	0.068	0.191	18
B.	19	0.88	0.91	0.200	0.103	0.193	18
B.	20	1.59	0.90	0.280	0.162	0.195	19
B.	21	2.95	0.94	0.381	0.210	0.163	22
C.S.	22	4.24	0.95	0.406	0.244	0.164	23
C.S.	23	4.97	0.92	0.41	0.24	0.161	24

* B : Bubbly flow, C.S: Cap/Slug flow

were compared as a representative of non-drag forces contributing to a transverse distribution of bubbles.

4.8.1. Mesh Sensitivity Analysis. For mesh sensitivity study, radial profiles of void fraction and IAC for group-1 and group-2 bubbles at port 2 and port 3 (*z/D*=14.1 and 28.0) were compared to the experimental data of B4 case (Schlegel et al., 2012) in terms of the different sizes of mesh as shown in Figure 4.1. All source terms needed to model 2G IATE and five major bubble interaction mechanisms were implemented, and the five interfacial forces of drag, lift, turbulent dispersion, virtual mass, and wall lubrication

force were considered that are the same setup with the interfacial forces to be used for the comparison analysis in this study.

The radial profiles are shown as a function of the normalized radial position *r/R*, which is equal to 0 at the pipe center and to 1 at the pipe wall. Through a mesh sensitivity study, it was confirmed that the void fraction and IAC distributions were not sensitive to mesh size in bulk area of the pipe whereas small variations were expected in the near-wall region, and a hexahedral mesh size of 0.04 m was used for 2D analysis.

4.8.2. Drag Force Coefficient Model Comparison. Figure 4.2 through Figure 4.3 present the effects of the different drag coefficient models on distributions of void fraction and IAC for group-1 and group-2 bubbles at various flow conditions.

4.8.2.1. Void fraction distribution. Figure 4.2 shows void fraction distributions of group-1 and group-2 bubbles at low, middle, and high superficial liquid velocities in the churn-turbulent flow regime.

All drag coefficient models predicted very similar distributions of void fraction for both group-1 and group-2 bubbles. The distributions were all flat in the bulk region of the pipe, while the void fraction distributions varied with the different drag models near the wall region.

At low flow conditions (B5 and B6 cases), Ishii-Zuber model predicted higher void fraction distributions for group-1 bubbles of B5 case at both port 2 and port 3compared to the other drag models, but the Schiller-Naumann model captured the best prediction of void fraction profile for both bubble groups. For B6 case, the Tomiyama model provided a better prediction of void fraction distributions for both group-1 and group-2 bubbles among other models.

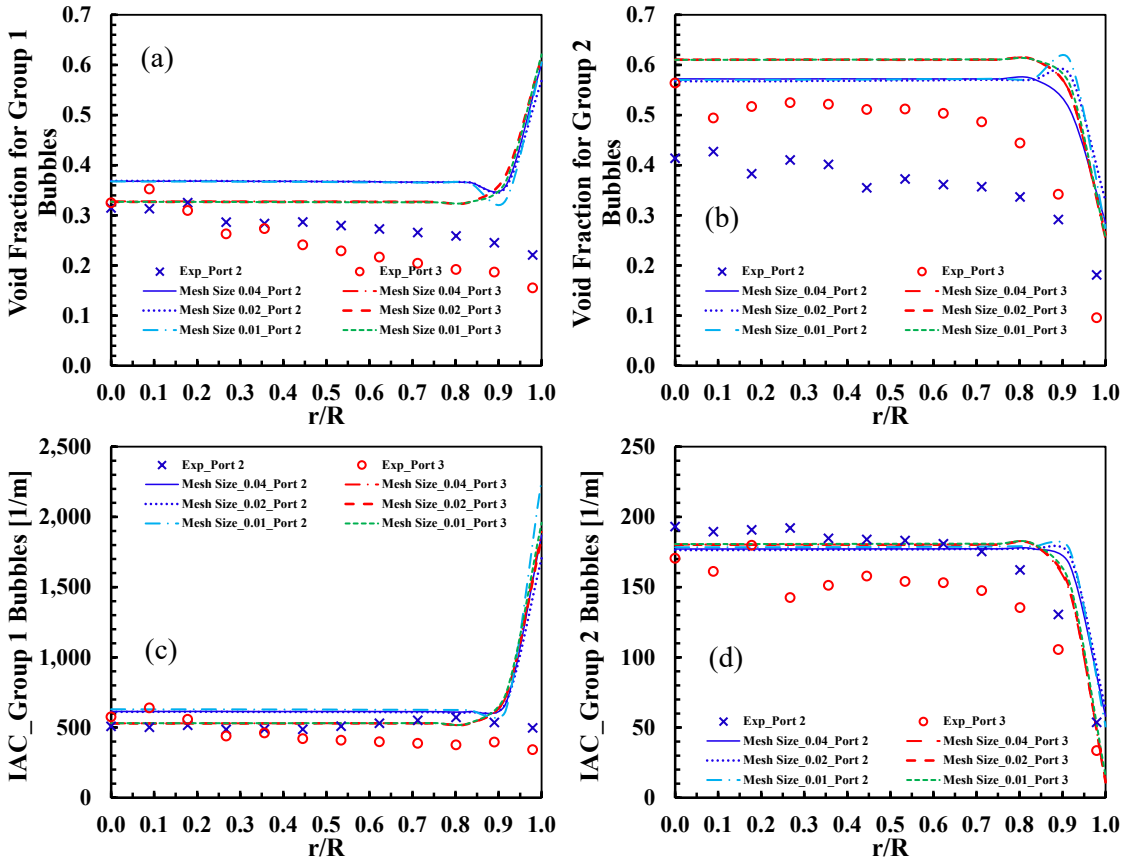

Figure 4.1. Mesh Sensitivity Study for Local Phase Distributions; Void fraction ((a) and (b)) and IAC ((c) and (d)) at Port 2 and at Port 3.

At middle flow conditions (B14 and B15 cases), there were no big differences in void fraction distributions found among the drag models. The void fraction distributions at port 2 and port 3 were overlapped and it was hard to separate from another. Although all drag models predicted the same wall peak trend of the void fraction distributions, the increasing shape of the wall peak distribution near the wall differs with the drag models. For B14 case, Tomiyama model and Schiller-Naumann model were the best options for group-1 and group-2 bubbles, respectively, and Schiller-Naumann model gave a good prediction for both bubble groups of B15 case.

At high flow conditions (B22 and B23 cases), all drag coefficient models overestimated void fraction profile for group-1 bubbles of B22 case, but Ishii-Zuber model calculated the most agreeable distribution of void fraction among the drag models. It seems that the result from Ishii-Zuber model was the most accurate for group-2 bubbles. However, when it comes to the combined error of the void fraction distributions at port 2 and port 3, Tomiyama drag model was the best option.

Figure 4.3 shows void fraction distributions of the flow conditions in transition areas between bubbly and cap/slug bubble regimes (B18 and B19) and between cap/slug bubble and churn-turbulent flow regimes (B20 and B21). All drag models estimated void profiles very well for both group-1 and group-2 bubbles that falls into the transition region between bubbly and cap/slug bubble regimes. It is noted that Tomiyama model and Schiller-Nauman model estimated the best void profiles for group-1 and group-2 bubbles, respectively, for all simulation cases.

4.8.2.2. IAC distribution. The effects of the drag models on the IAC distribution in different flow regimes are shown in Figure 4.4 and Figure 4.5. The IAC profiles varied with the drag models and the impact of the different drag models was much stronger for group-2 bubbles than that for group-1 bubbles.

Figure 4.4 presents the comparison results of the flow conditions in the churn-turbulent flow regimes. B5 and B6 cases at low flow conditions show that Ishii-Zuber model estimated the highest error of the IAC distributions for group-1 bubbles. The rest three models excepted for Ishii-Zuber model predicted very similar profiles of the IAC for group-1 bubbles at port 2 to another, and Tomiyama model provided the best matched IAC profile for group-1 bubbles to the experimental data among the four models for B5

and B6 cases. However, for group-2 bubbles, the Schiller-Naumann model was better estimated than the rest of the drag coefficient models for predicting the IAC distribution for B5 case, and Ishii-Zuber model was better for B6 case.

A similar trend of the IAC profile for the case at low flow rate conditions was found for the case at middle flow conditions. Small variations were found in the IAC profiles of group-1 bubbles with the all drag models for both B14 and B15 cases. The IAC distributions of group-1 bubbles were well captured by all drag models, but the estimate of group-1 IAC profiles was slightly better with the Schiller-Naumann model. However, the distribution of the IAC for group-2 bubbles significantly depended on the drag models. Surprisingly, Schiller-Naumann model better predicted the IAC profiles for group-2 bubbles compared to the estimates from other models that take into account the effects of bubble deformation and multi-particle environment.

At high flow conditions, the case of B22 exhibits a different IAC distribution trend from B23, as do the other cases at low and middle flow conditions. The drag models affected the radial profiles of the IAC for both group-1 and group-2 bubbles in the B22 case. The Ishii-Zuber and Schiller-Naumann model predicted the IAC profiles for group-1 bubbles, while the Schiller-Naumann model worked better for the group-2 IAC distributions. For B23 case, the Tomiyama and Schiller-Naumann models predicted well the distribution of the IAC for group-1 and group-2 bubbles, respectively. Figure 4.5 shows the IAC profiles of the flow conditions in the transition areas. B18 and B19 cases can be categorized as bubbly flow and cap/slug flow regimes in the transition area between the two flow regimes. As shown in the results of B14, B15, B22 and B23 cases, as the superficial velocity of the liquid phase increased, all drag models predicted similar

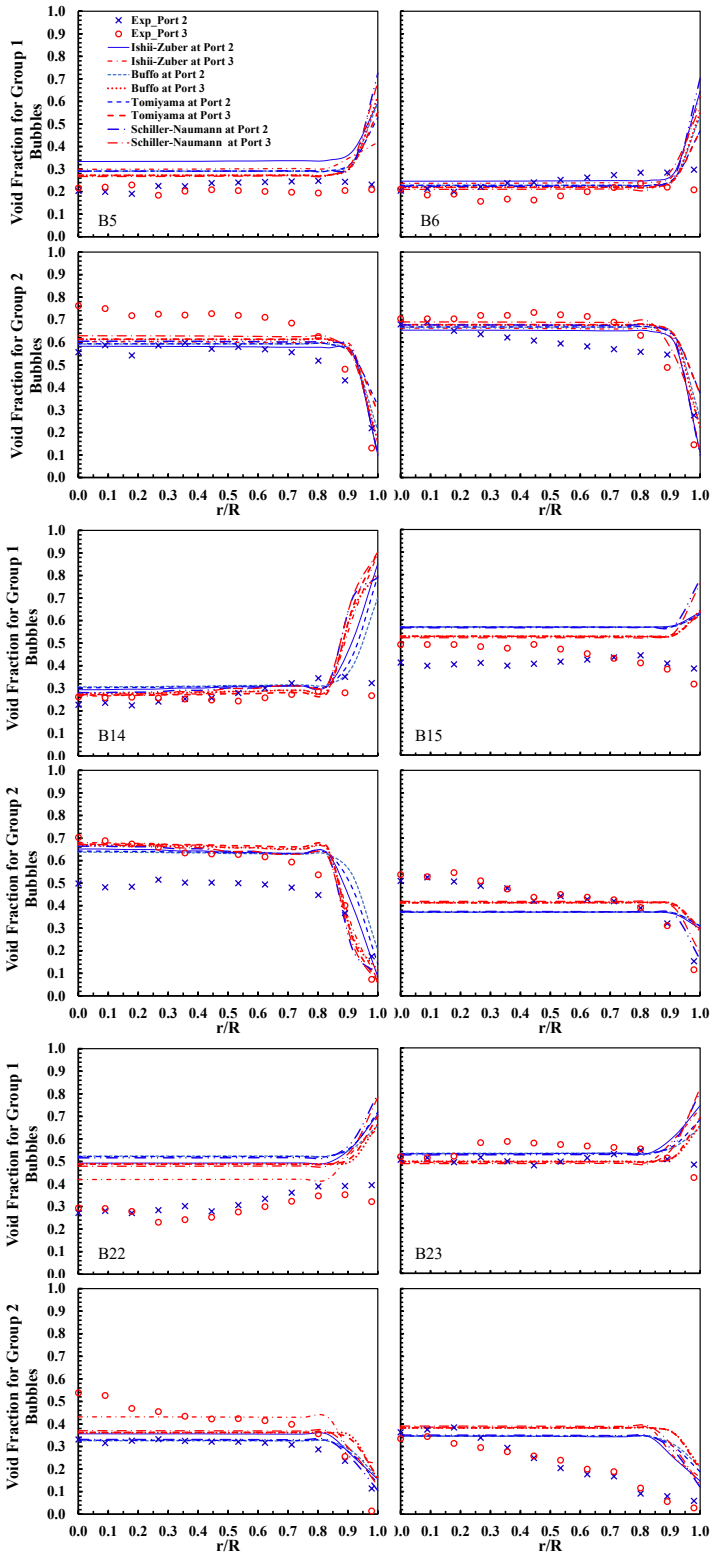

Figure 4.2. Effect of Drag Coefficient Models on Local Void Fraction Distributions for Group-1 and Group-2 Bubbles in Churn-Turbulent Flow Regime at Port 2 and at Port 3.

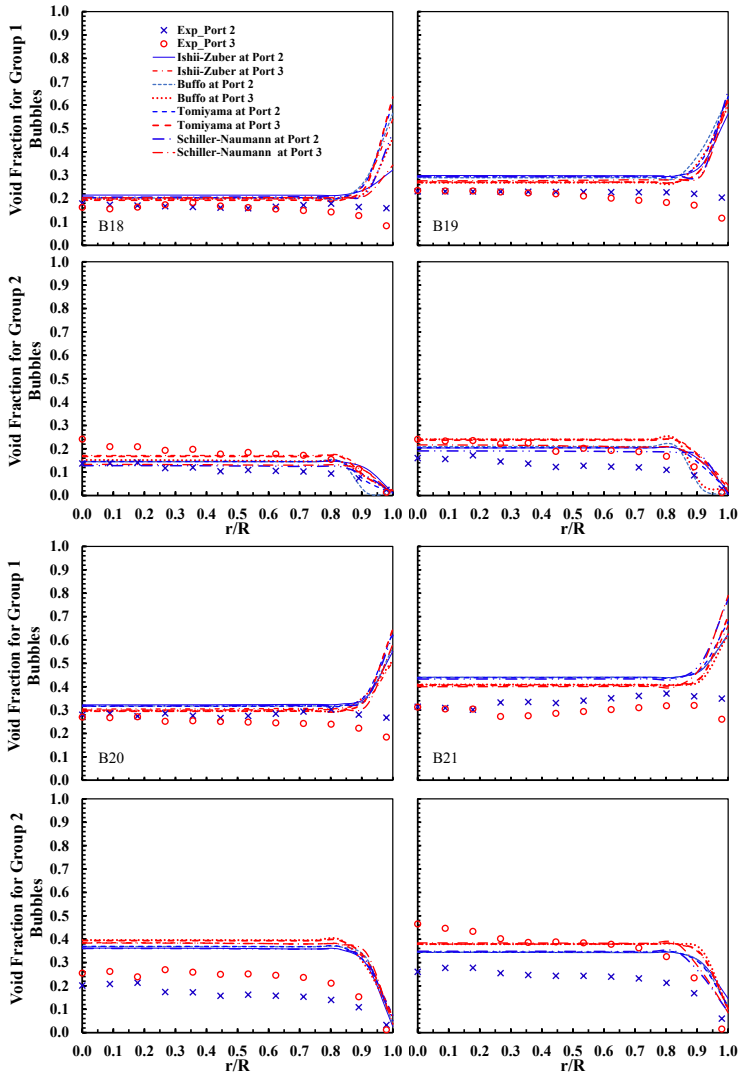

Figure 4.3. Effect of Drag Coefficient Models on Local Void Fraction Distributions for Group-1 and Group-2 Bubbles in Transition Areas between Bubbly and Cap/Slug Bubble Regimes (B18 and B19) and between Cap/Slug Bubbly and Churn-Turbulent Flow Regimes (B20 and B21).

IAC distributions and the differences in the prediction of the IAC profile for group-1 bubbles among the drag models were very small and ignorable.

However, it is noteworthy that the IAC profiles for the group-2 bubbles of the B18 case in bubbly flow regime and the B19 case in cap/slug flow regime were well captured by Ishii-Zuber and Schiller-Naumann models, respectively, in contrast to the

IAC predictions for group-1 bubbles. Other drag models underestimate the IAC profiles. For the B20 and B21 cases, both Ishii-Zuber model and Schiller-Naumann model predicted well the group-1 IAC profiles that belongs to cap/slug flow and churn-turbulent flow regimes at the transition between the two regimes. However, for the B18 case, only Ishii-Zuber model correctly estimated the distribution of the IAC for group-2 bubbles, and the Schiller-Naumann model showed a better prediction of group-2 IAC distributions for the B19, B20, and B21 cases than the other models.

From the results above, it can be found that:

1) At low flow conditions, bubble swarm effect is important for small bubbles (group-1 bubbles). Ishii-Zuber's drag coefficient model for spherical bubbles (group-1 bubbles) was empirically developed based on the area-averaged void fraction, assuming similarity with the approach to describe the drag coefficient in the viscous flow regime and considering the concept of the mixture viscosity in the multiparticle flow conditions. The concept of the area-averaged void fraction and the mixture viscous approach based on the area-averaged void fraction may cause higher errors in the prediction of the IAC profile for group-1 bubbles.
2) As increasing flow conditions, the swarm effect becomes less important for the prediction of the IAC profile for group-1 bubbles.
3) At high flow conditions, the drag models seem to work in the similar way to the lower flow conditions. However, the swarm effect is ignorable for group-1 bubbles, and Ishii-Zuber model comes to play again for the estimation of the IAC distribution for group-1 bubbles. In the case of group 2 bubbles, it is preferable to use the Schiller-Naumann model, unlike the low and medium flow conditions.

Especially, with faster superficial gas velocity, Schiller-Naumann model provides better prediction for group-2 bubble. It seems that at high flow conditions area-averaged approach does not capture the feature of group-2 bubbles. However, more research is required to develop a drag model for churn-turbulent flow regime.

4.8.3. Lift force Coefficient Model Comparison. Four different lift coefficient models are compared to investigate the effect on distributions of void fraction and IAC for group-1 and group-2 bubbles in a various flow regimes. As same with the analysis of the drag coefficient models, a wide range of gas flow conditions in the churn-turbulent flow regime are mainly investigated and the evaluation is focused on the flow conditions at a level of the high superficial liquid velocity conditions with increase in the superficial velocity of gas phase.

4.8.3.1. Void fraction distribution. Figure 4.6 and Figure 4.7 present results of the comparisons for the void fraction distributions. The effect on the radial distribution of void fraction in the churn-turbulent flow regime is shown in Figure 4.6. In general, the difference in void fraction predictions for the same level of liquid superficial velocity conditions became more dependent on the lift coefficient model as the superficial velocity of the gas phase increases. It should be noted that lift force coefficient model was more sensitive to change in the superficial gas velocity than to change in superficial liquid velocity. These characteristics can be seen by comparing the cases of B5, B14 and B22 with those of the cases of B6, B15 and B23. The void fraction profiles on the left side of the Figure 4.6 that are for lower superficial gas velocity differed depending on the lift coefficient model, but the distributions of the void fraction on the right side of the

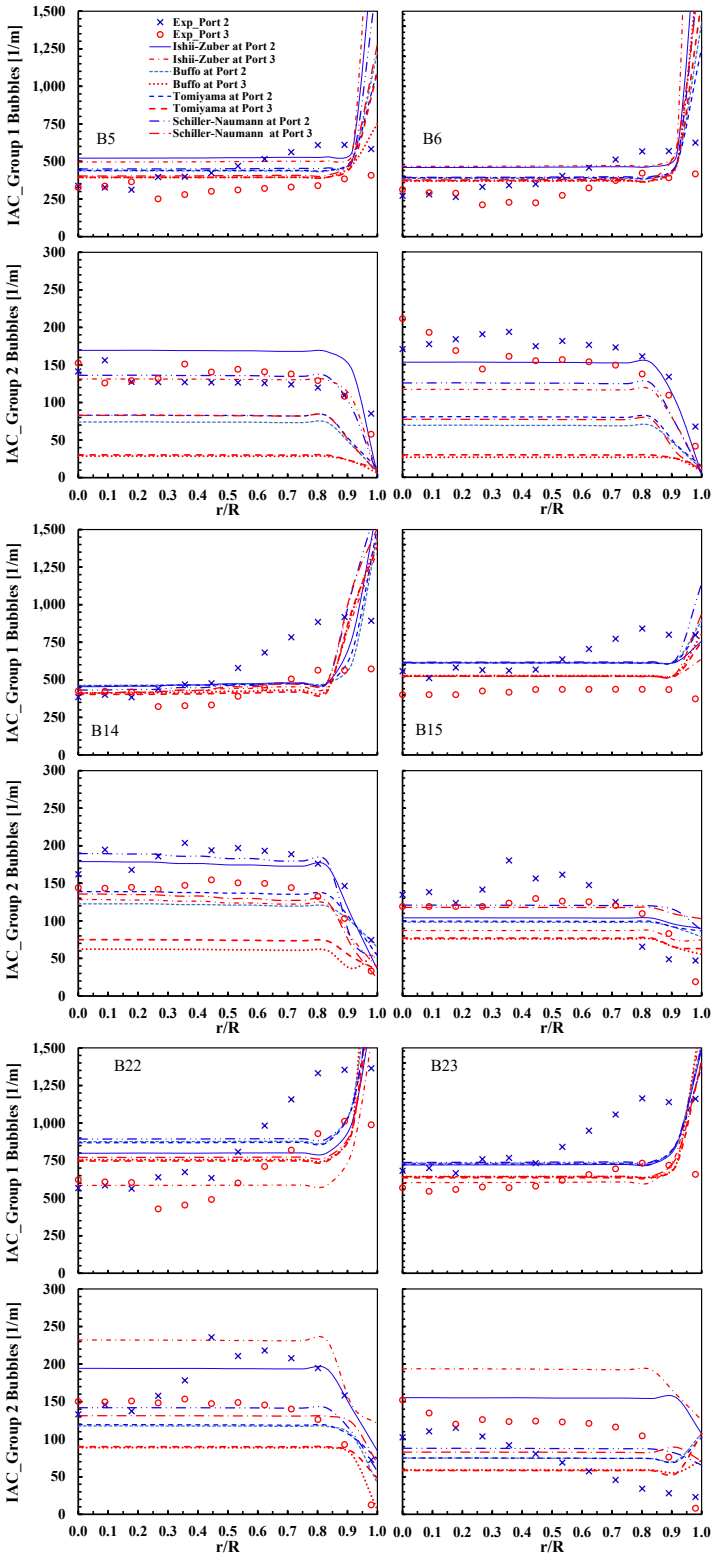

Figure 4.4. Effect of Drag Coefficient Models on Local IAC Distributions for Group-1 and Group-2 Bubbles in Churn-Turbulent Flow Regime at Port 2 and at Port 3.

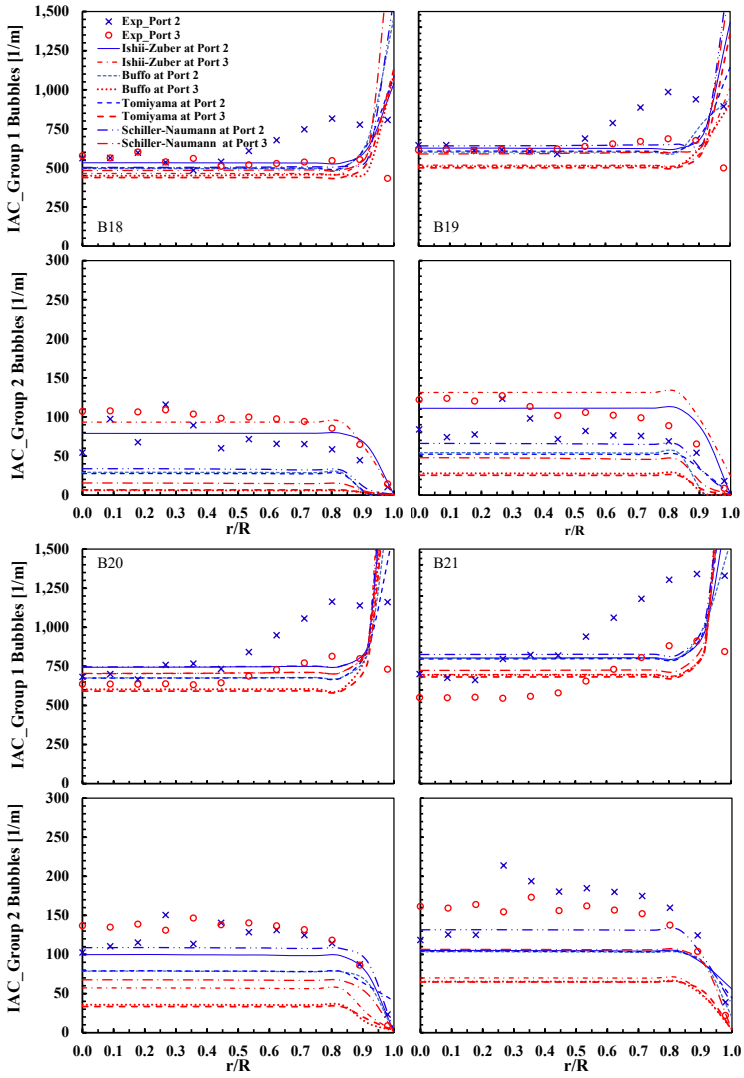

Figure 4.5. Effect of Drag Coefficient Models on Local IAC Distributions for Group-1 and Group-2 Bubbles in Transition Areas between Bubbly and Cap/Slug Bubble Regimes (B18 and B19) and between Cap/Slug Bubble and Churn-Turbulent Flow Regimes (B20 and B21) at Por2 and at Port 3.

Figure 4.6, which are for higher superficial gas velocity, were not sensitive to the lift coefficient models making it difficult to distinguish by the coefficient models. However, changes in the superficial liquid velocity affected changes in the near-wall void fraction profile. Therefore, the following comparison focuses on the case of the slower velocity conditions.

Under low flow conditions, Hibiki model estimated the most accurate void fraction profiles of group-1 and group-2 bubbles at port 2 and port 3 among other models in the bulk area of the pipe of the B5 case. For B6 case, the Hibiki and Shaver-Podowski models worked better for the predictions of the void fraction of group-1 and group-2 bubbles, respectively. In predicting the void fraction profile in the near-wall region, Shaver-Podowski model made the lift coefficient zero when the distance between the bubble center and the wall was less than the bubble radius, so it did not represent the wall peak distribution of the void fraction for group-1 bubbles. However, this model overestimated the void fraction for group-2 bubbles near the wall because the number density of group-2 bubbles near the wall was low.

The distributions of the void fraction in the middle flow conditions were similar to that in the low flow conditions and showed changes according to the lift coefficient models. However, the change in the void fraction profile near the wall region was enhanced by an increase in the liquid superficial velocity for both group-1 and group-2 bubbles. The results for the B14 case showed that the constant value of 0.01 predicted the distribution of the void fraction well for group-1 bubbles and that the Hibiki and Tomiyama models predicted the distributions of the void fraction better for group-2 bubbles than the other models, even though the estimates by all lift coefficient models were biased to the void fraction distribution at port 3 of the experiment data.

B22 and B23 cases at high superficial liquid velocity conditions showed the similar distributions of the void fraction among the lift coefficient models except for Tomiyama model for B22 case. It can be said that only Tomiyama model estimated a proper void fraction profiles at port 2 and port 3 for B22 case, while the other models

predicted nearly identical distributions of the void fraction for both B22 and B23 cases. Further, Shaver-Podowski model also showed wall peak void fraction distribution for group-1 bubbles for both B22 and B23 cases as the other models did, which means more research effort is needed to correctly estimate void fraction by considering the effect of wall lubrication force in the near-wall region.

Figure 4.7 shows the void fraction distributions in the transition areas. The results also presented very similar trend to that in churn-turbulent flow regime. B18 and B19 cases, which fall into bubbly flow and cap/slug flow regimes in the transition area, showed a significant changes in the prediction of the void fraction with the different lift coefficient models, especially for group-2 bubbles, and the significance was enhanced by increasing superficial gas velocity. For B18 case, when the locations near the wall were excluded, Hibiki model worked the best for group-1 bubbles in the bulk area of the pipe. However, the Shaver-Podowski model for group-1 bubbles captured good agreement with experimental data in the near-wall region. For large bubbles, Shaver-Podowski model failed to predict void fraction near the wall, but Hibiki model can predict well the distribution of the group-2 void fraction. B19 case showed the similar results with B18 case, but large variations were found for group-2 bubbles. Tomiyama and Shaver-Podowski model estimated better void fraction distributions for group-1 and group-2 bubble, respectively, for B19 case. B20 and B21 cases categorized as cap/slug bubble and churn-turbulent flow regimes in the transition area did not show differences in the void fraction prediction with the different lift coefficient models.

4.8.3.2. IAC distribution. The effect of the lift coefficient models on the IAC distributions is shown in Figure 4.8 and Figure 4.9, which are respectively for churn-

turbulent flow regime and transition area ranging from bubbly flow to churn-turbulent flow regimes. Since *Sγ* model was used to obtain IAC distribution, which was different from the calculation of the void fraction, the best option of the lift coefficient model for the accurate prediction of the IAC distribution may be different from that for the void fraction prediction.

Figure 4.8 shows that the distribution of the IAC did not change much depending on the lift coefficient models at low flow conditions. However, the impact of the lift coefficient model became larger as increasing liquid superficial velocity. B5 case was less sensitive to the coefficient models while B14 and B22 were more subject to the models. Moreover, as the same with the results of the void fraction distribution, the IAC profile was more likely to change with the lift coefficient models at slower superficial gas velocity conditions.

At low flow conditions, the noticeable change in the IAC profile was found only near-wall region for both bubble groups while there was a variation in the distribution of the IAC in both bulk and near-wall regions at middle and high flow conditions. Even though Shaver-Podowski model and the constant value of 0.01 lift force coefficient were intended for group-2 bubbles to make lift force being none or very small near the wall, a wall peak tendency was obtained. It is because of less recirculation in the simulation resulting in more accumulation of small bubbles in the near wall region as shown in void fraction distributions. This trend was commonly captured in all simulation cases.

At middle flow conditions, B14 case shows that Tomiyama model predicts well the IAC profiles for group-1 bubbles at port 2 and port 3 and for group-2 bubbles both

Tomiyama model and Shaver-Podowski model provided good agreement with experimental data.

At high flow conditions, only Tomiyama model estimated reasonable distributions of the IAC for both bubble groups at port 2 and port 3 of B22 case. For B23 case, there is no big difference among the results from the four lift coefficient models, but constant value of 0.01 for group-1 bubbles provided the smallest combined error of 15.7% between the results at port 2 and port 3. For group-2 bubbles of B23 case, Hibiki model showed good agreement with the experimental data. The Hibiki model treats lift coefficient as a combined lift coefficients derived for each case of low and high Reynolds number flow conditions with a special consideration of bubble deformation as a function of bubble diameter. Tomiyama model overestimated the IAC profile.

Figure 4.9 presents the effect of the lift coefficient models on the local radial distribution of the IAC for the simulation cases in the regime transition area. In general, again, the similar trend appeared with the results for the void fraction distribution. Group-2 bubbles reacted more sensitively to the different model of the lift coefficient for B18 and B19 cases at middle flow conditions. Only Tomiyam model predicted the correct trend of the IAC distributions for group-2 bubbles of B18 and B19 cases, and the other models underestimated the group-2 IAC profiles. However, as increasing superficial velocity of liquid phase at high flow conditions in the transition between cap/bubbly and churn-turbulent flow regimes, it was hard to see the differences in the IAC distributions among all four coefficient models.

4.8.4. Error Analysis. This section shows local errors of Run cases in prediction of void fraction and IAC distributions at port 2 and port 3. For local error calculations,

the differences between the predicted values and experimental data are normalized against each measured value of void fraction and IAC for each bubble group as shown in Equation (49).

$$\boldsymbol{error_{\psi}} = \frac{|\boldsymbol{\psi_{i,k,pre}} - \boldsymbol{\psi_{i,k,exp}}|}{\boldsymbol{\psi_{i,k,exp}}} \times \mathbf{100}\% \tag{49}$$

where ψ, i, and k indicate void fraction or IAC, bubble group 1 or 2, and measurement location of port 2 or 3. The area-averaged value is defined as:

$$\langle \boldsymbol{\psi} \rangle = \frac{\int \boldsymbol{\psi}(\boldsymbol{r}) \boldsymbol{dr}}{\boldsymbol{A_{pipe}}} \tag{50}$$

where $\langle \quad \rangle$ represents area-averaged quantity and A_{pipe} is the cross-sectional area of the flow pipe. Due to the issue with predicting local values near-wall area, data points for the error analysis in that area are ignored.

The root-mean-square (RMS) error combining both void fraction and IAC at port 2 and port 3 for each group is obtained by Equation (51).

$$RMS_i = \sqrt{\frac{\sum_{k=2}^{3} \left\{ \left[\left(\langle \alpha \rangle_{pred,i,k} - \langle \alpha \rangle_{exp,i,k} \right) / \langle \alpha \rangle_{exp,i,k} \right]^2 + \left[\left(\langle a_i \rangle_{pred,i,k} - \langle a_i \rangle_{exp,i,k} \right) / \langle a_i \rangle_{exp,i,k} \right]^2 \right\}}{4}} \times 100\% \tag{51}$$

The effect The RMS error represents the total combined error based on the area-averaged distributions of void fraction and IAC for each bubble group, and each error term of the void fraction and IAC is weighted equally.

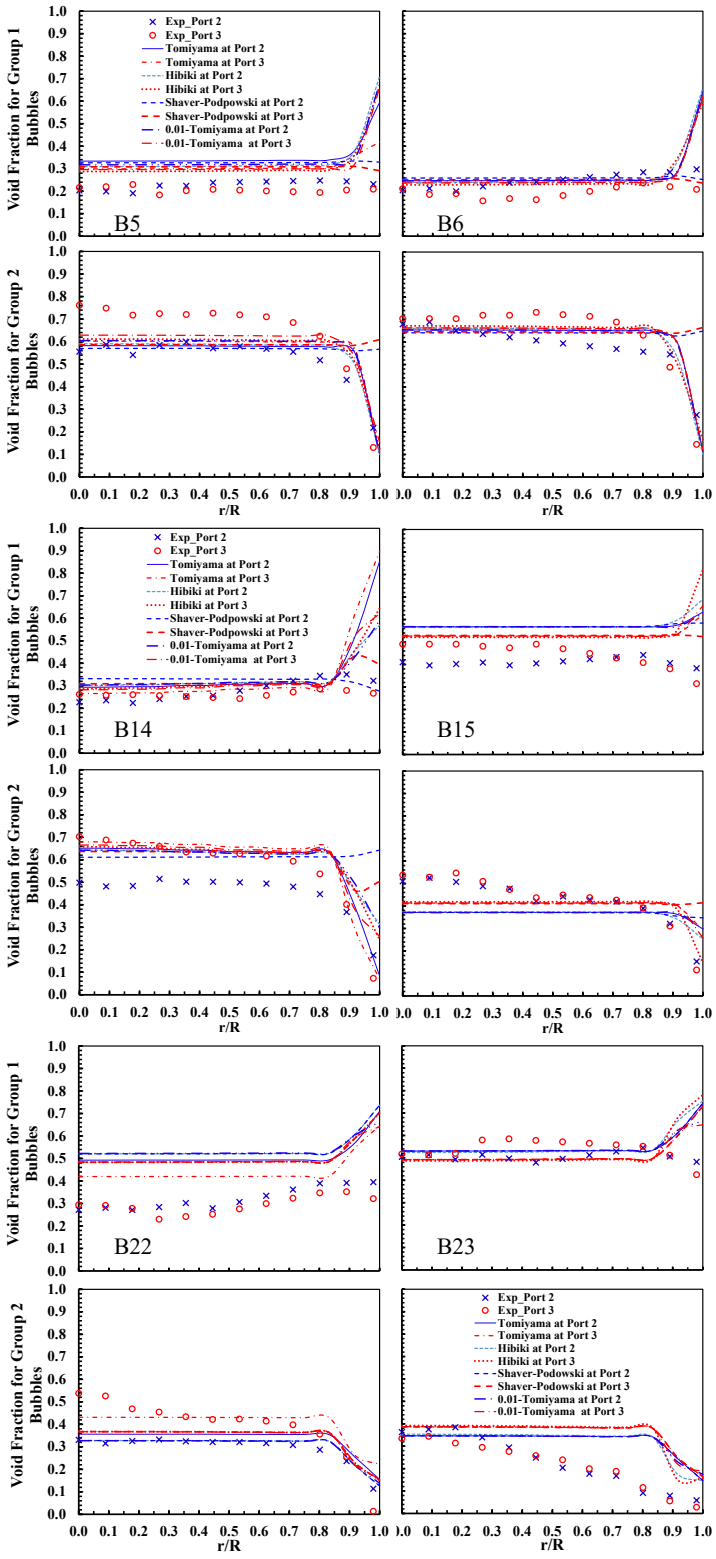

Figure 4.6. Effect of Lift Coefficient Models on Local Void Fraction Distributions for Group-1 and Group-2 Bubbles in Churn-Turbulent Flow Regime at Port 2 and at Port 3.

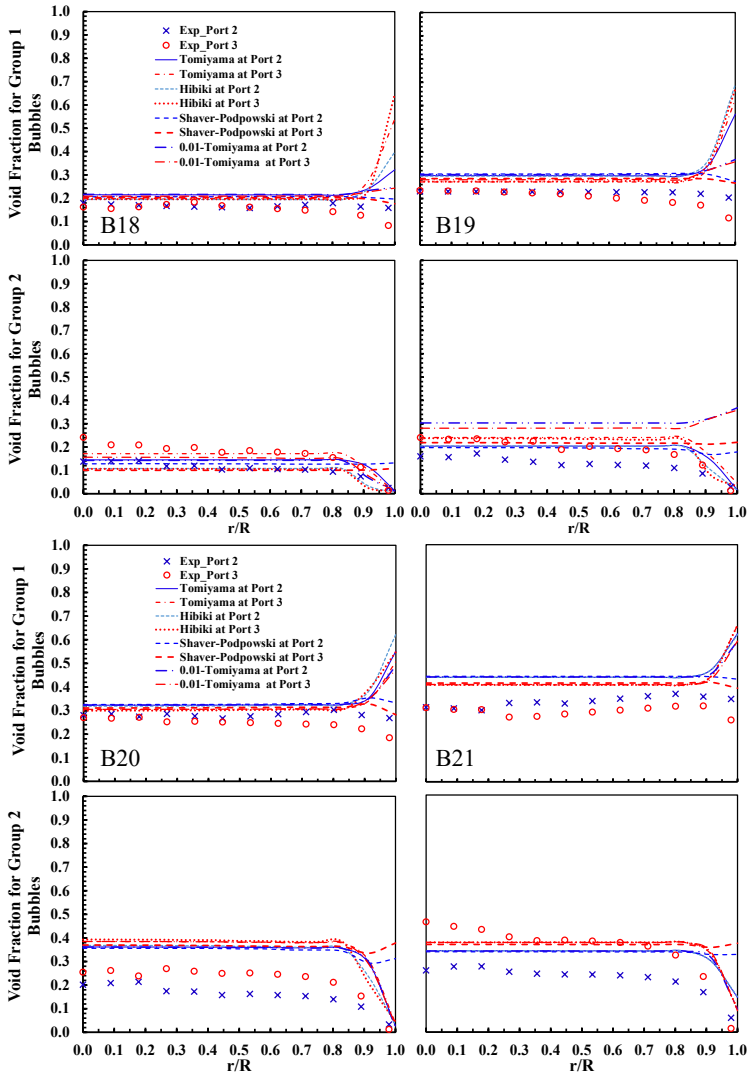

Figure 4.7. Effect of Lift Coefficient Models on Local Void Fraction Distributions for Group-1 and Group-2 Bubbles Transition Areas between Bubbly and Cap/Slug Bubble Regimes (B18 and B19) and between Cap/Slug Bubble and Churn-Turbulent Flow Regimes (B20 and B21) at Por2 and at Port 3.

Therefore, the models which can be proposed as the best option to be used for the CFD two-phase flow analysis for beyond bubbly flow regime, can be different from the individual results described in the previous sections.

4.8.4.1. RMS error of drag coefficient models. Figure 4.10 indicates the RMS error for drag coefficient models. At low flow conditions (B5 and B6), Ishii-Zuber drag

coefficient model predicted the highest error of about 40% and about 25% for B5 and B6 cases, respectively, while the other three models (Tomiyama et al., Buffo et al., and Schller-Naumann) estimated well for group-1 bubbles by giving about 27% and 13% of errors for each B4 and B5 case. This points out that the bubble swarm effect was important for the flows with low superficial liquid velocity in churn-turbulent flow regime. However, for group-2 bubbles, Schiller-Naumann model and Ishii-Zuber model respectively worked better than other models for B5 and B6 cases. At middle flow conditions (B14 and B15) in the churn-turbulent flow regime, Ishii-Zuber model showed a good prediction for both bubble groups. The RMS errors by Ishii-Zumber model were about 17.8% and 25% for group-1 bubbles of B14 and B15 cases and around 22.8% and 11.3% for group-2 bubbles, respectively.

At high flow conditions (B22 and B23), Ishii-Zuber model was expected to guarantee better results for both bubble groups of B22 case, but Schiller-Naumann model for group-1 bubbles and Buffo model for group-2 bubbles estimated a good prediction for B23 case. In the transition area, B18 with Tomiyama model for group-1 bubbles and Ishii-Zuber model for group-2 bubbles resulted in the smallest error, about 26.2% for group-1 bubbles and 27.2% for group-2 bubbles, compared to the errors from the other models. B19, B20, and B21 cases in beyond bubble flow regime showed better performance with Schiller-Nauman drag coefficient model than the prediction with other models by having the errors of 28.9%, 18.7%, and 23.6% for group-1 bubbles and 41.8%, 85%, and 34% of each simulation case, respectively. However, the errors were still high for group-2 bubbles. Therefore, it needs more research to develop interfacial drag model for the flow conditions in the regime transition area.

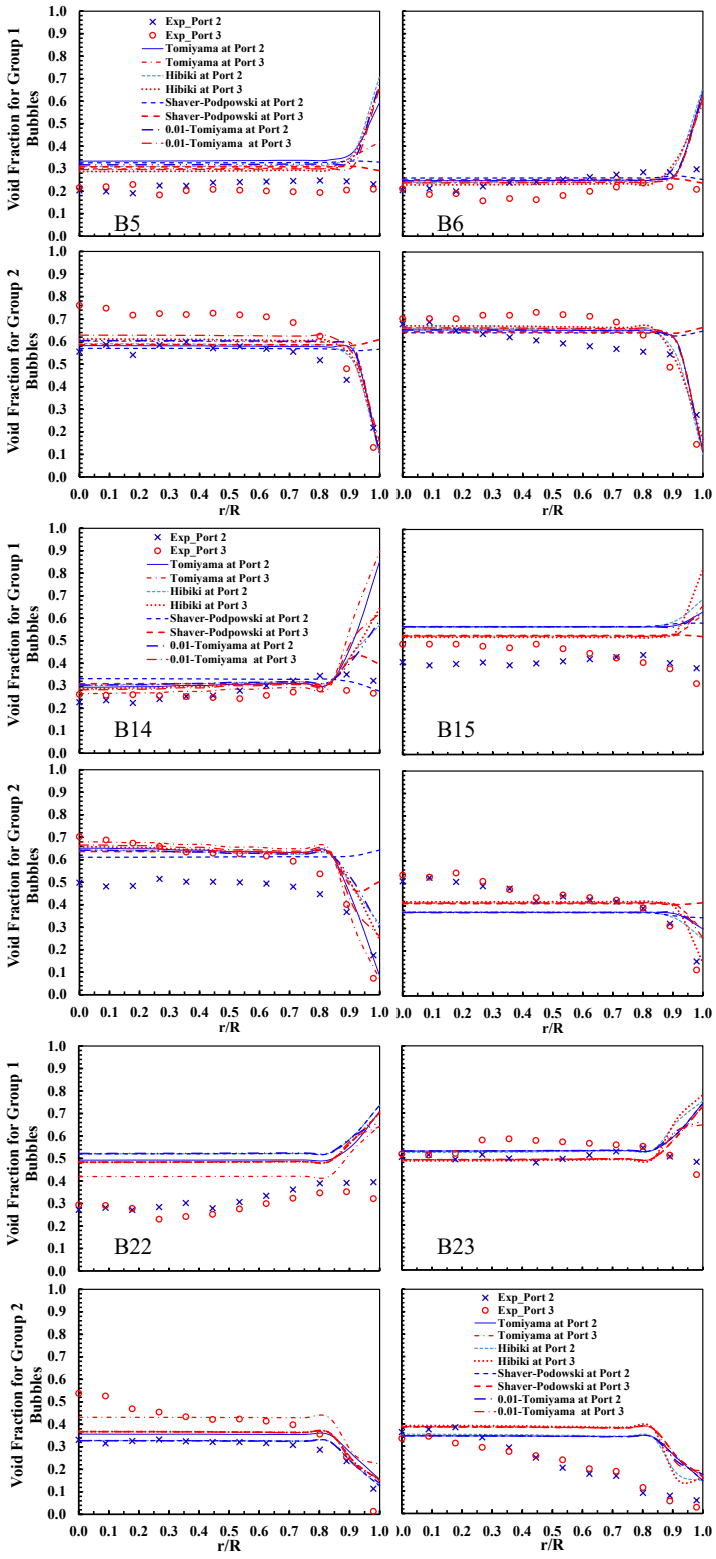

Figure 4.8. Effect of Lift Coefficient Models on Local IAC Distributions for Group-1 and Group-2 Bubbles in Churn-Turbulent Flow Regime at Port 2 and at Port 3.

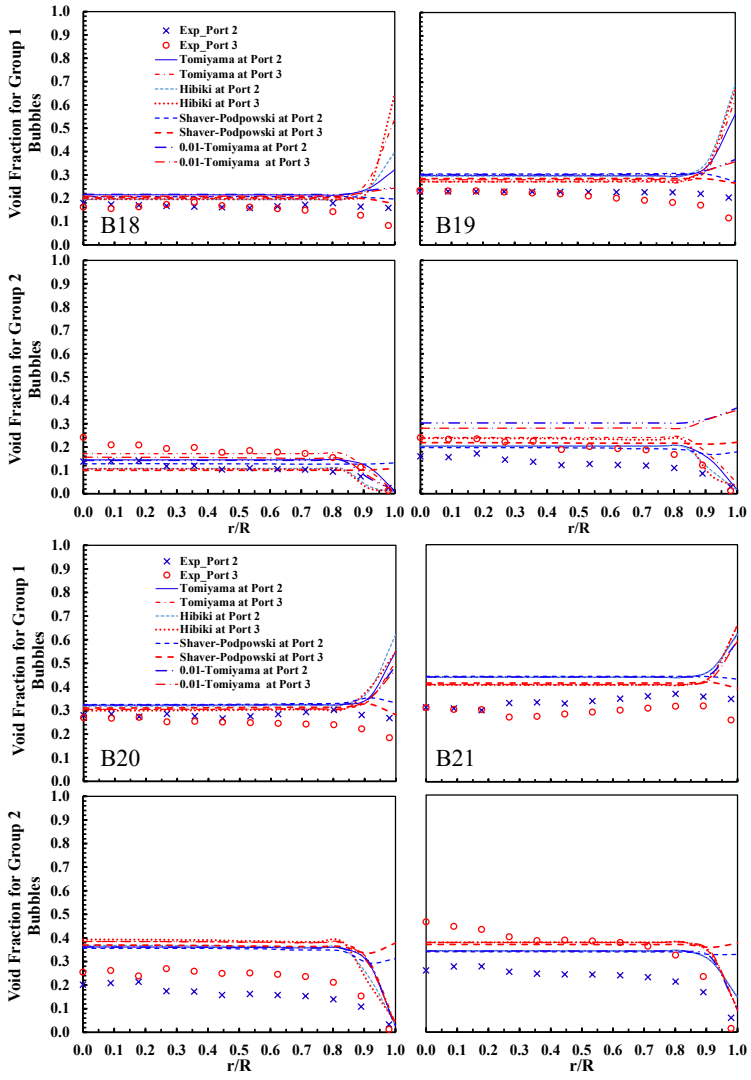

Figure 4.9. Effect of Lift Coefficient Models on Local IAC Distributions for Group-1 and Group-2 Bubbles in Transition Areas between Bubbly and Cap/Slug Bubble Regimes (B18 and B19) and between Cap/Slug Bubble and Churn-Turbulent Flow Regimes (B20 and B21) at Port 2 and at Port 3.

4.8.4.2. RMS error of lift coefficient models. Figure 4.11 shows the comparison of RMS errors of the different lift coefficient models. Generally, RMS errors for group-1 bubbles did not change much with the lift coefficient models for all simulation cases. However, the total combined errors for group-2 bubbles showed a big variation depending on the coefficient model and the flow conditions. At low flow conditions (B5

and B6) in churn-turbulent flow regime, Hibiki model was preferable to be used for group-1 bubbles, but there were no big differences in the total error with all lift coefficient models. The smallest errors for B5 and B6 cases were about 38.3% and 20.2% for group-1 bubbles, respectively, and 20.9% and 11.2% for group-2 bubbles of each simulation case. At middle flow conditions (B14 and B15), the total errors of all four models were very close to another for both bubble groups by having the errors of around 17.5% and 25% for group-1 bubbles and about 22% and 11.1% for group-2 bubbles, respectively for B14 and B15 cases. At high flow conditions (B22 and B23), it was found that Tomiyama model for both bubble groups provided the most acceptable results among the other models.

For the flows in the transition area, Hibiki model and Tomiyama model predicted well for group-1 and group-2 bubbles, respectively, of both B18 and B19 cases. For B20 and B21 cases, which had higher superficial gas velocities than B18 and B19 cases, there were not a noticeable differences in the total RMS error among the lift coefficient models for group-1 bubbles while Shaver-Podowski model worked better than other models for group-2 bubbles of B20 case and the rest three models except for Shaver-Podwski model provided relatively better estimation for group-2 bubbles of B21 case. However, the total errors for group-2 bubbles in transition area were huge against the experimental data.

4.9. CONCLUSIONS

Drag force is a major factor that directly affects bubble interaction mechanisms as well as turbulence transport with turbulent dissipation rate and lift force is one of main contributors related to transverse bubble distribution. The forces are affected by bubble

diameter and deformation of the bubbles. On the two-fluid model framework, the interfacial closure models is a key for accurate predictions of local two-phase flow profiles. However, the closure models have been adopted without any validation process. In that sense, four popularly used drag and lift coefficient models were evaluated for the concurrent upward air-water two-phase flows in large diameter channels for beyond bubbly flow regimes due to the different flow characteristics in large diameter pipes from the flows in small diameter pipes. The best interfacial force closure models selected based on the combined total error may differ from the model selection based on the local error comparison result.

There are some specific findings of this work including:

1) The drag models did not impact much on void fraction distributions for both group-1 and group-2 bubbles, while IAC distributions varied with the different drag models because the drag coefficient was directly implemented into the bubble interaction mechanisms to reflected the effect of the drag force on momentum changes of the bubbles.
2) The correlations or the empirical models developed in small diameter channels or derived from averaging approaches were hard to capture the unique flow characteristics in large diameter channels, such as secondary recirculation produced in the wake region following the leading large bubbles that acted as a source of turbulence production and resulted in an enhancement of turbulence diffusion, because these changes in the flow characteristics in large diameter channels generally occur in local area.

3) The bubble swarming effect decreased as flow conditions increase. Moreover, the IAC profiles of group-2 bubbles was more sensitively to the drag coefficient models than the distributions of the IAC for group-1 bubbles. This indicates that most of the interfacial force closure models developed or derived for small bubbles under very limited flow conditions should be verified to be used for the flows in large diameter channels and for a wide range of flow regimes.
4) The number density distribution can be a factor for modeling lift force model near the wall and the effects of the recirculation and a large size of eddies need to be handled for the correct prediction of the void fraction near the wall area. More research efforts are needed to correctly estimate void fraction by considering the effect of wall lubrication force in the near-wall region
5) In transition between flow regimes at low superficial gas velocities, the effect of bubble deformation was a key factor for the prediction of the IAC profile for group-2 bubbles, such as Tomiyama model.

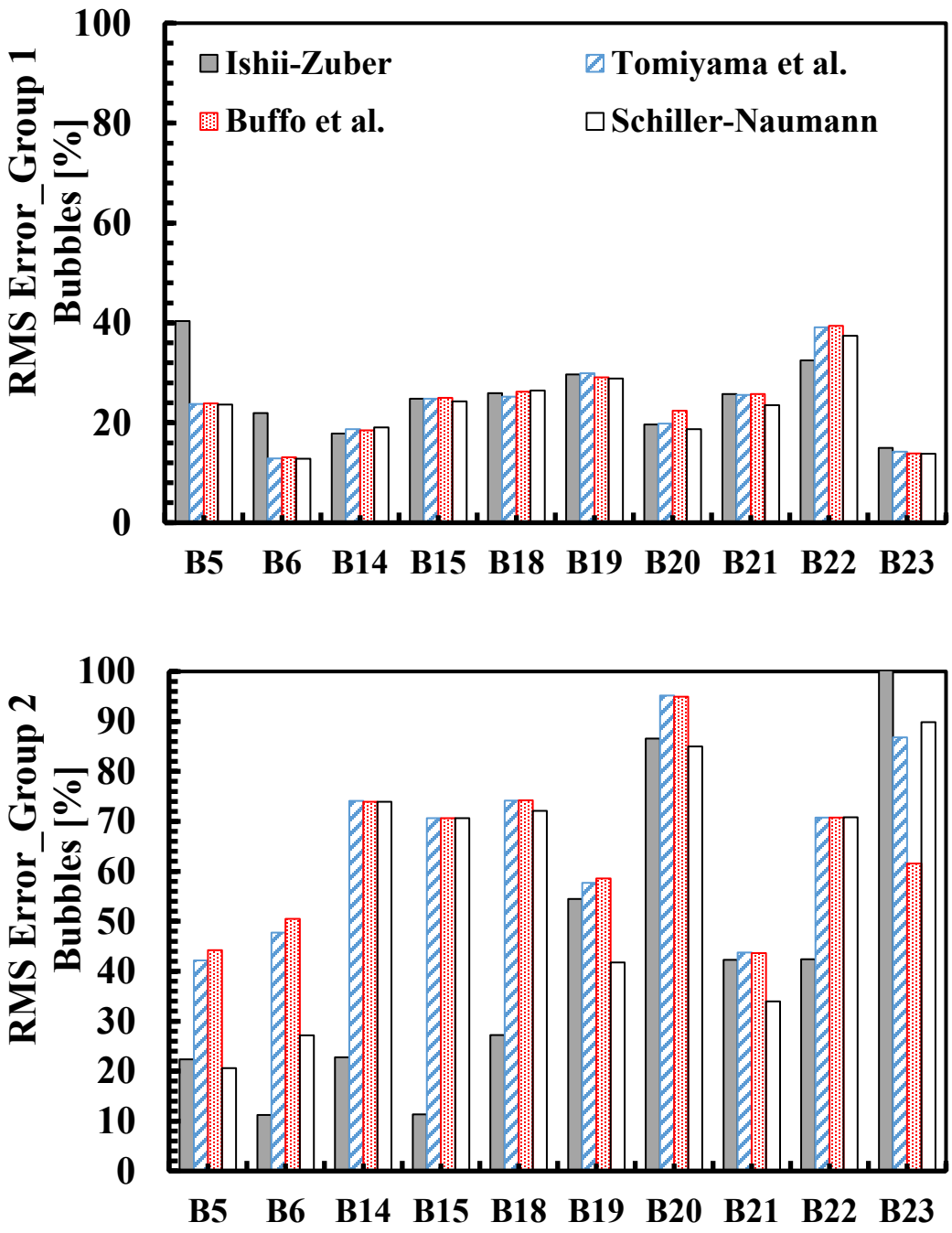

Figure 4.10. RMS Error of Drag Coefficient Models for Group 1and Group 2 Bubbles.

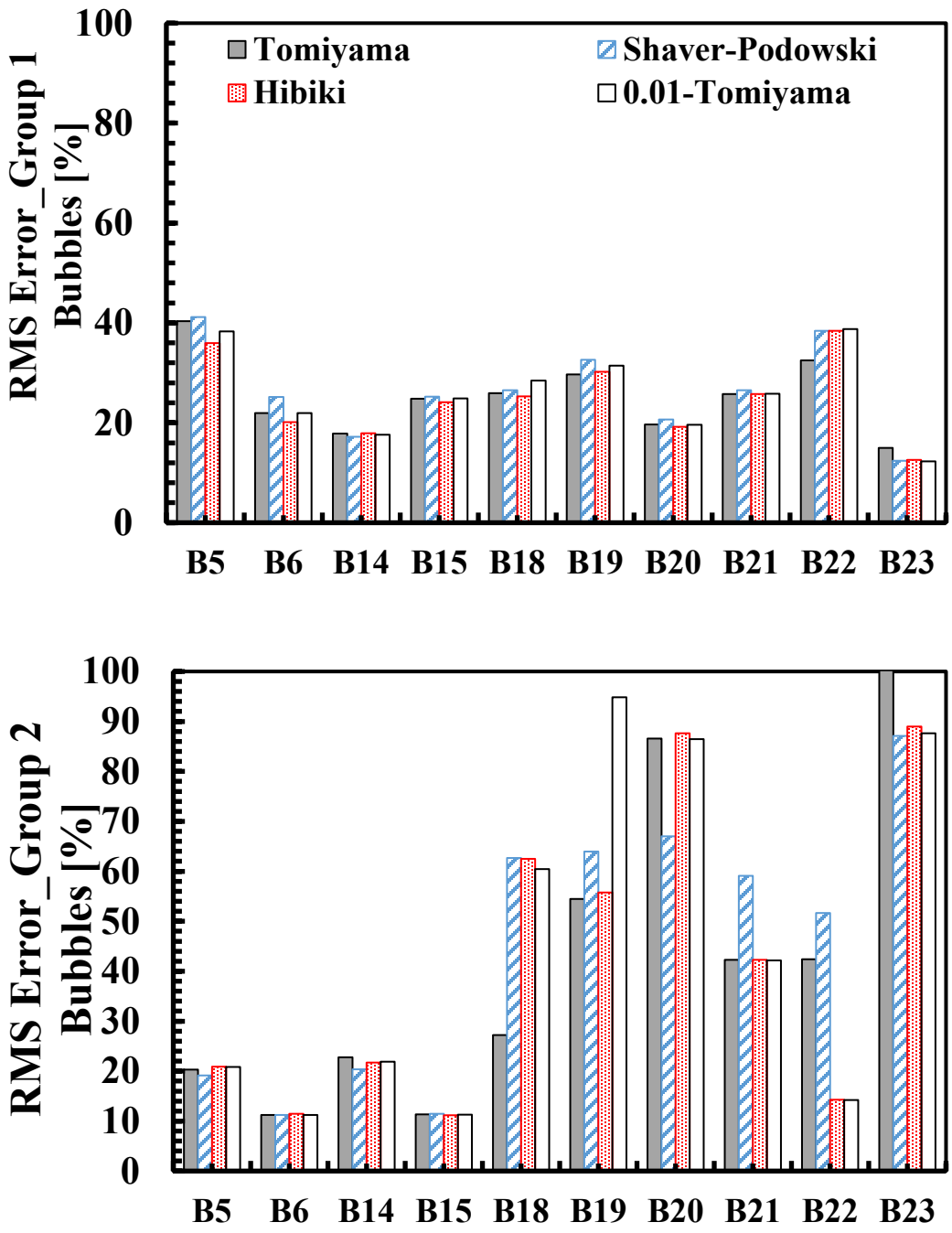

Figure 4.11. RMS Error of Lift Coefficient Models for Group-1 and Group 2 Bubbles. (B18 and B19) and between Cap/Slug Bubbly and Churn-Turbulent Flow Regimes (B20 and B21) at Port 2 and at Port 3.

5. BUBBLE-INDUCED TURBULENCE

5.1. BACKGROUND

Two-phase flows have been highlighted in various industries due to their efficient mass and energy transfer characteristics. However, the characteristics of two-phase flows are different depending on the size of channels, and it is hard to expect accurate flow regimes. Especially, understanding characteristics of the highly turbulent gas-liquid two-phase flows with high void fraction of gas phase in large diameter channels as for example the churn-turbulent flows is crucial for the efficient operation and safety of reactor in various fields, including pharmaceuticals, petrochemical engineering, and nuclear power industry.

Bubblers used in the melter, which is the key equipment to improve the heating and melting steps of the vitrification process. The bubblers were installed to achieve faster waste processing throughout the SRS liquid waste facilities. The bubblers agitate the molten glass pool by deploying bubbles near the bottom of the melter using argon gas. The rising bubbles effectively agitate the melt pool. This agitation creates more convection and mixing within the melt pool, increasing the heat transfer to the melt pool cold cap. The cold cap is the layer of unmelted feed floating on top of the melt pool, similar to ice floating on top of water. This rise in heat transfer increases melter throughput, allowing it to pour more canisters of vitrified waste more frequently.

In large diameter channels, flows are different from flows in a small diameter channel (Schlegel et al., 2014). Therefore, the differences need to be accounted for bubble interaction mechanisms to reflect flow features of a large diameter channel. In terms of physical changes, stable slug bubbles are not able to form or to maintain their

shape due to Rayleigh-Taylor and Kelvin-Helmholtz instabilities on the upper surface resulting in replacement of ‘slug flow’ regime to ‘cap-turbulent’ transition. In another perspective of flow characteristics, its size of a large diameter channel drives a different behavior of turbulence. A key difference is length scale of turbulence in a large diameter channel. The larger length scale of turbulence can cause carrying groups of bubbles or enhance turbulent mixing. Therefore, turbulence is a key parameter that should be handled in bubble interaction mechanisms, for example, turbulent eddies. The increase in strength of the turbulent eddies leads to more energy transfer to bubble interface, and results in the breakup of the bubble into small bubbles due to sufficient deformation of bubble interface.

Two-phase flows are characterized by the surface area of the dispersed phase. In dispersed multiphase flows, the interaction between dispersed and continuous phases results in dynamical change in interfaces, which is closely related to efficiency of energy or mass transfer in the two-phase flows. Moreover, the prevalence of particle-particle interactions of coalescence and breakup can lead to change in overall performance of system by altering particle distribution that affects interfacial area or void fraction of the particle and by changing the IAC (or a_i) that is directly proportional to interfacial transfer terms and is available for mass transfer between the phases.

Since accurate prediction of local phase distribution, such as void fraction and bubble diameter (D_{sm}), directly affects interaction area changes, prediction of particle distribution in terms of various particle sizes using an advanced mechanistic bubble size model is essential and modeling interfacial transfer terms is vital in dispersed multiphase flow hydrodynamics.

Interfacial forces are strongly related to the IAC and to the local transfer mechanisms. For the two-phase turbulent flows, in particular, turbulence can be modified by bubble depending on the size of bubbles. The variations of turbulence production and dissipation lead to changes in interfacial forces, and the effect of the turbulence feeds back to the variations of local phase distribution which relies on flow regimes. In view of the effect of the turbulence for the two-phase turbulent flows, particle (or bubble)-induced turbulence (PIT or BIT) has been studied by many researchers for theoretical improvement as well as for their application to numerical analysis (Sato and Sekoguchi, 1975; Morel, 1997; Pan et al., 1999; Troshoko and Hassan, 2001; Deen et al., 2001; Bove et al., 2004; Lucas et al., 2007; Krepper et al., 2009; Liao and Lucas, 2012; Rabha et al., 2013; Scott et al., 2014; Liao et al., 2019). Recently, extensive efforts on BIT model analysis for application to CFD code have been made. Liao and Lucas (2012) investigated effect of four different BIT models (Morel, 1997; Troshko and Hassan, 2001; Pfleger and Becker, 2001; Rzehak and Krepper, 2013) by comparing with four experiment databases (Hosokawa et al., 2009; Kibiki et al., 2001; Liu, 1998; Shawkat et al., 2008) for small and large diameter channels. Results of the study showed that turbulence parameters of turbulent kinetic energy and eddy viscosity were underestimated without BIT models and different BIT models led to noticeable deviation in predicting local profiles of turbulence parameters and liquid velocity. However, further research may be needed to evaluate BIT models for beyond bubbly flows. Rzehak and Krepper (2013a) compared various BIT models (Sato and Sekoguchi, 1975; Morel, 1997; Troshko and Hassan, 2001; Politano et al., 2003) and showed radial profiles of void fraction of gas, liquid velocity, effective turbulent viscosity of liquid phase, turbulent kinetic energy.

This study addressed that wall peak of void fraction was too high, and gradient of liquid velocity was overestimated near the wall. These comparison results are only compared with dataset (Liu, 1998) developed under small diameter pipe and applicable only for bubbly flows and low void fraction of gas cases. Rzehak and Krepper (2013b) also described BIT model comparisons with dataset in a small diameter pipe as well as with databases of large diameter pipe. However, this research is also limited to mono dispersed flow conditions with low void fraction of gaseous phase. Moreover, averaged constant bubble diameters were considered, so that modeling for bubble coalescence and breakup mechanisms were ignored. Liao et al. (Liao et al., 2019) validated a new BIT model proposed by Ma et al. (2017) against various datasets for small and large diameter channels. However, this work is also limited in a range of 1 to 22% of a void fraction and 3 to 8 mm of a bubble size, and only for bubbly flows.

In view of bubble flow characteristics in large diameter channels, turbulent characteristics induced by bubbles are different compared to that in small diameter channels. Since large cap bubbles have larger drag force as well as higher relative velocity than small spherical bubbles, higher turbulence is generated in the wake of large cap bubbles. This results in different interactions between bubbles and between dispersed phase and continuous phase. In large diameter channels, large cap bubbles are generated by collapse of slug bubbles as well as coalescence of smaller bubbles, and the quantity of the large cap bubbles are much greater than the number of slug bubbles in small diameter channels. Moreover, while slug bubbles in small diameter channels are bounded in size by the channel wall, which leads to high concentration of small bubbles near the wall region and a small production of bubble induced turbulence, large cap bubbles in large

diameter channels are smaller than the slug bubbles and more numerous and are distributed in the whole area of the flow channel. In addition, the large cap bubbles increase in the interfacial surface area of the dispersed phase due to its numbers. This dominance of large cap bubbles results in a larger contribution to production of turbulence. This effect was observed by Ohnuki and Akimoto (2000).

In this study, the effect of BIT source terms on local distribution of void fraction and IAC as well as the effect on three terms in 2G IATE were analyzed for beyond bubbly flows. Two-bubble-group (2G) method is applied by implementing 2G IATE based on $S\gamma$ population balance equation (PBE) model. The distributions of void fraction and IAC were compared against the experimental data developed by Schlegel et al. (2012).

5.2. MODELING BUBBLE-INDUCED TURBULENCE

Particle (or bubble)-induced mixing (PIM or BIM) model contributes to the effective viscosity of the continuous phase, whereas particle (or bubble)-induced turbulence (PIT or BIT) accounts for the influence of the dispersed phase on the turbulence of the continuous phase and this influence enters the modified turbulence transport equations in the form of source terms. Those two concepts of BIM and BIT basically indicate the same effect in view of changing turbulence parameters and affect mixing. The terminologies of BIM and BIT, however, are used to clearly separate between the two different approaches modifying turbulence parameters according to STAR-CCM+ user-manual (CD-ADAPCO, User Guide). Sato's BIM model (Sato and Sekoguhi, 1975) was applied for group-1 bubbles, and confirmed to give good agreement

for spherical bubbles in monodisperse flows, and the BIT model, Troshko-Hassan model (Troshko and Hassan, 2001) was tested for G2 bubbles.

5.2.1. Approaches to BIT Modeling. Turbulence models for gas phases of group-1 and group-2 bubbles are not directly applied. Instead, turbulence response model for each bubble group is accounted by means of response coefficient ($\boldsymbol{C_t}$) of unity. It was identified that the $\boldsymbol{C_t}$ is strongly related to the void fraction of the gas phase and the value of unity is acceptable when gas phase void fraction is over 6% by Behzadi et al. (2004).

For BIT, turbulence modified by bubbles is considered with different BIT models. There are two approaches to reflect effect of bubbles on turbulence of liquid. One approach is an indirect way by modifying $\mu_{L,t}$, which is used in two-equation turbulence model. Adding source terms directly to the two-equation turbulence model is the other approach. $\mu_{L,t}$ is a parameter that affects two equation turbulence model via varying the value of $\mu_{L,t}$ itself through superposition of turbulent and bubble-induced viscosities and impacts momentum equation through changing turbulent stresses. In addition, adding source terms to turbulence model changes solutions of k-ε turbulence transport equation. Since shear-induced turbulence viscosity ($\mu_{L,t}^{SI}$) is directly affected by the calculated values of k and ε, when turbulent source terms are relatively significant the effect of bubble-induced turbulent viscosity ($\mu_{L,t}^{BI}$) could be unnoticeable or ignorable. Details of BIT models evaluated are discussed in following section 5.2.2. The two approaches to the effect of CFD models were described in Figure 5.1.

5.2.2. Sato Model. The Sato model is described in Equations (26) and (27). The same concept is applied for the viscosity source term. The equations are re-addressed here:

$$\nu_{eff} = \nu + \nu_{turb} + \nu_{Sato} \tag{26}$$

where ν, ν_{turb}, and ν_{Sato} are respectively the continuous phase kinematic viscosity, the turbulent diffusivity, and the Sato bubble-induced viscosity.

The Sato bubble-induced viscosity is given by:

$$\nu_{Sato} = k f_d f_B \alpha_g \frac{d_B}{2} v_{rel} \tag{27}$$

where *k* is a model calibration constant, f_d is the van Driest damping factor, f_B is a bubble diameter shape correction factor, α_g indicates the gas phase void fraction, d_B is the bubble diameter, and v_{rel} presents the relative velocity between phases.

5.2.3. Troshko-Hassan Model. The Troshko-Hassan model is also addressed in Equations (28) and (29). However, the equations are presented here again to help understanding of and remind the effect of the two different approach of modeling BIT. The Troshko-Hassan model in STAR-CCM+ is modified in terms of the linearized drag coefficient, $\boldsymbol{A_D}$, to account for multi-particle effects:

$$S_k = A_D |v_{rel}|^2 \tag{28}$$

The dissipation term uses the energy source term that decays with a characteristic time, the Bubble Pseudo-Turbulence Dissipation Relaxation (BPTDR) time, t_d, and is scaled with a calibration constant, $C_3 = 0.45$:

$$S_\varepsilon = \frac{C_3 S_{k_C}}{t_d}, \text{ where } t_d = \frac{\rho C_{VM} \alpha_g}{2 A_D} \tag{29}$$

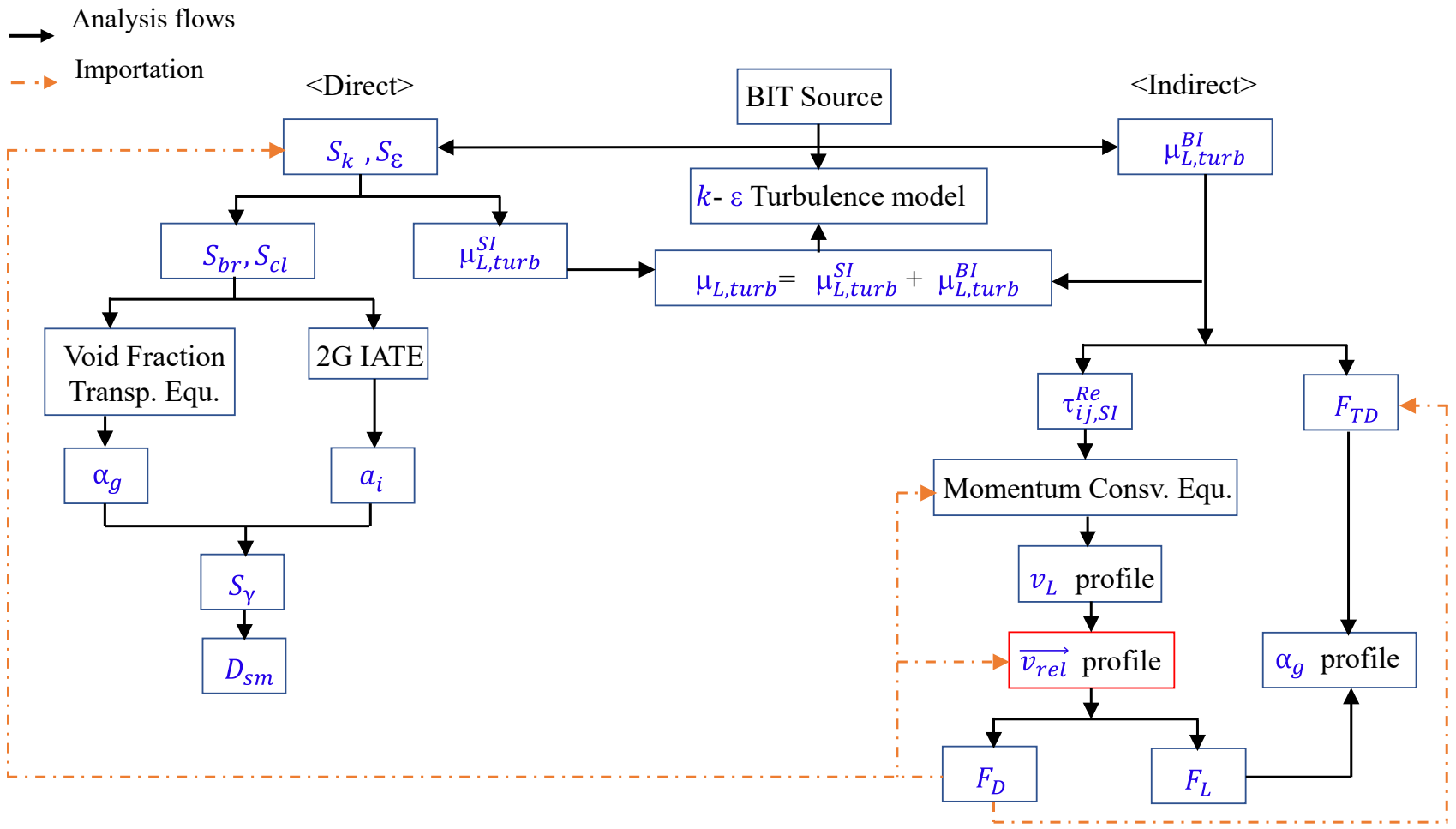

Figure 5.1. Effect of Different Approach of Source Terms for Bubble-Induced Turbulence on CFD Model.

5.2.4. Tchen Model. The Tchen Particle Induced Turbulence (PIT) model (Chen et al., 2009) adds source terms to the continuous turbulent kinetic energy equation due to the interaction with particles, based on Tchen's theory, which was finally developed by Hinze (1975). The Hinze-Tchen model considers particle fluctuation tracking a turbulent eddy, and the model assumes that fluid fluctuation is stronger than the particle fluctuation. Therefore, the influence of particle fluctuation becomes smaller as the size of the particle grows, and larger particles slowly diffuse compared to smaller particles.

Reynolds averaging of continuous-phase velocity fluctuation times the drag source term from the fluctuating part of the continuous-phase momentum equation results in the following source term for the continuous-phase turbulent kinetic energy:

$$S_{k_C} = C_0 A_D (q_{cd} - 2q_c^2 - V_{TD} \cdot V_{rel}) \tag{52}$$

Include paragraph how the terms are calculated in the STAR-CCM+, where C_0 is a scale factor, A_D is a generalized drag coefficient and $A_D(V_{TD} \cdot V_{rel})$ represents the work that is done by the turbulent dispersion force against mean slip velocity. q_{cd} and $q_c$indicate the dispersed-phase average of the product of dispersed and continuous phase velocity fluctuations and half the dispersed-phase average of the product of continuous and continuous phase velocity fluctuations, respectively. Detail definitions of the terms in Equation (52) can be found in the STAR-CCM+ user manual (CD-ADAPCO, User Guide).

5.3. NUMERICAL SETUP

The same mesh and physics settings as discussed in the section 3 and section 4 were applied. Constant density for the liquid phase and the ideal gas law for the two air

phases were assumed. Inlet and system boundary conditions for both liquid and gas phases can be found in the Table 3.3. Regarding the interfacial force setup, the same closure models as in the section 3 were used. For the evaluation of the effect of the BIT, Sato model for group-1 bubbles and Troshko-Hassan model for group-2 bubbles were used as the reference, and additionally Tchen model was added for the comparison to the reference model for group-2 bubbles. All source terms were implemented as addressed in the section 3, and the same solver scheme was used.

5.4. EVALUATION

This section discusses the effect of the BIT models. First, the results of the simulation with BIT models for both group-1 and group-2 bubbles were compared to that without BIT models for both bubble groups. Second, the two ways of modeling BIT were evaluated.

5.4.1. Effect of BIT Model. Turbulence parameters, such as turbulence kinetic energy and turbulence dissipation rate of liquid phase, local transverse distributions of void fraction and IAC, and dominance of each term in the 2G IATE for churn-turbulent flow regime and transition area between cap/slug flow regime and churn-turbulent flow regime were evaluated by comparing both with BIT models and without BIT models for group-1 and group-2 bubbles.

5.4.1.1. Turbulent kinetic energy (KE or *k*). Figure 5.2 shows local distribution of turbulence kinetic energy for the churn-turbulent flows. Turbulence kinetic energy is affected by both source terms of direct and indirect approaches, and the variation of turbulence kinetic energy changes in turbulence intensity that is closely related to

interactions between bubbles and between bubble and liquid phases. The turbulent kinetic energy varied more with higher superficial gas velocity as shown in the comparison of B5, B13, and B22 cases with B6, B15, and B23 cases, respectively. B6 case at the low superficial liquid velocity showed the largest differences in the calculation of turbulent kinetic energy at both port 2 and port 3 measurement points. Without the BIT source terms, generally, higher turbulent kinetic energy was predicted near the wall than that in the pipe center region while the radial distribution of the turbulent kinetic energy got much flatter or showed core peak with the BIT source terms. Unexpectedly, B15 case predicted opposite trend to the other cases by showing core peak distribution without the BIT source terms and wall peak near the wall with the source terms.

Figure 5.3 shows the turbulent kinetic energy profiles for the flows in the transient region between cap/slug flow and churn-turbulent flow regimes. Both B18 and B19 cases calculated relatively small variations in the turbulent kinetic energy distribution. Therefore, the cases are separated as in a full scale (a) and in a zoomed-in scale (b) in the Figure 3. In the transition area, the profile of the turbulent kinetic energy showed different trend from the distributions of the flows in the churn-turbulent flow regime. Wall peak distributions were predicted with and without the BIT sources, and greater turbulent kinetic energy was calculated without the BIT source terms. B18 case, which falls into cap/slug flow regime in the transition area, expected higher turbulent kinetic energy in the bulk area from the center of the pipe without the BIT source terms. B19 case categorized as churn-turbulent flow regime in the transition area calculated lower and higher turbulent kinetic energy in the pipe center and near the pipe wall without the BIT source terms.

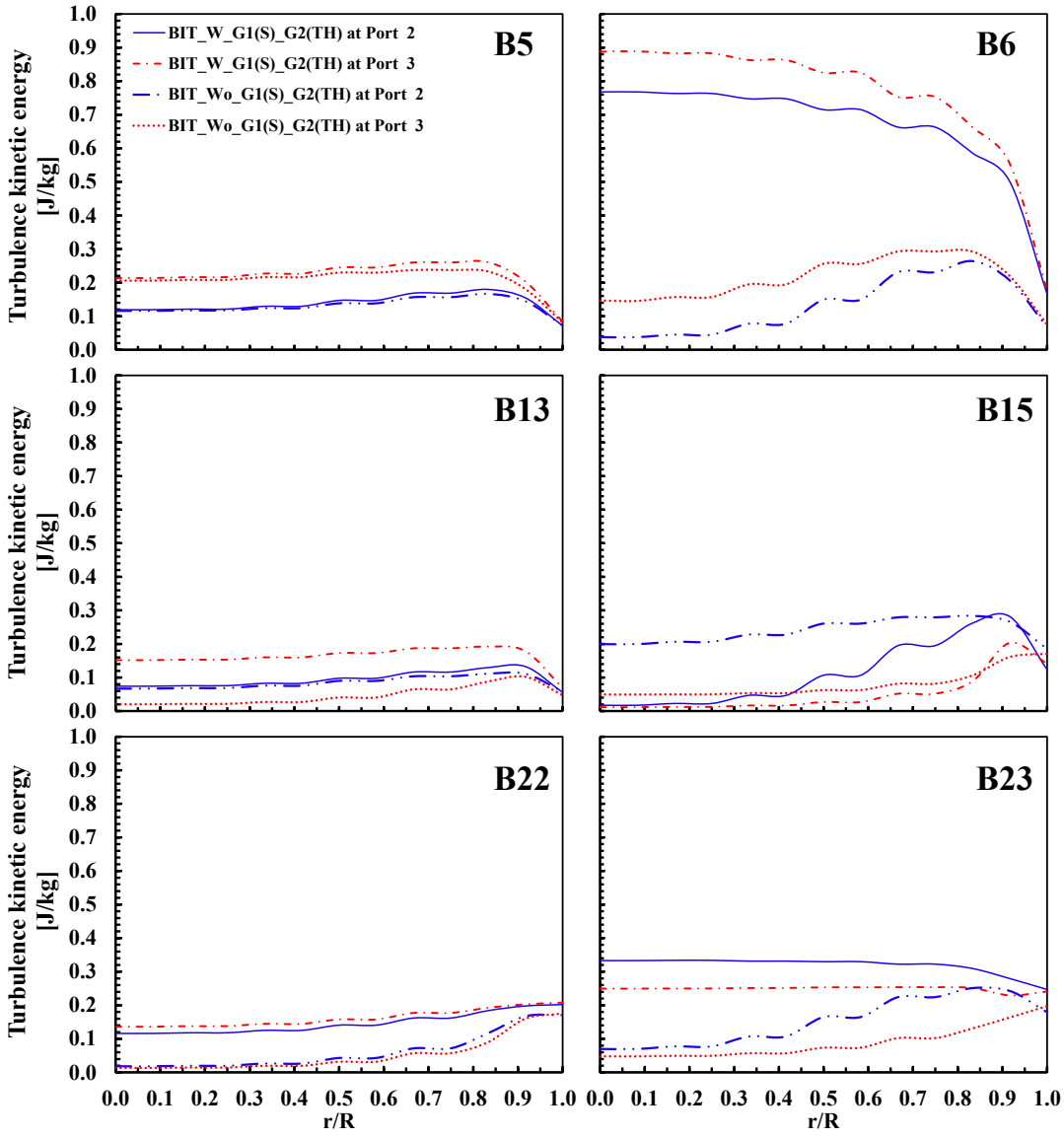

Figure 5.2. Effect of BIT on Turbulence Kinetic Energy Distribution for Flows in Churn-Turbulent Regime.

5.4.1.2. Turbulent dissipation rate (ε). Figure 5.4 shows the local turbulent dissipation rate profiles at low, middle, and high superficial liquid velocity conditions in the churn-turbulent flow regime. Similar to the distributions of the turbulent kinetic energy, the turbulent dissipation rate was increased by the BIT source terms and the gap between the conditions with and without BIT source terms was widen as the flow velocity increased.

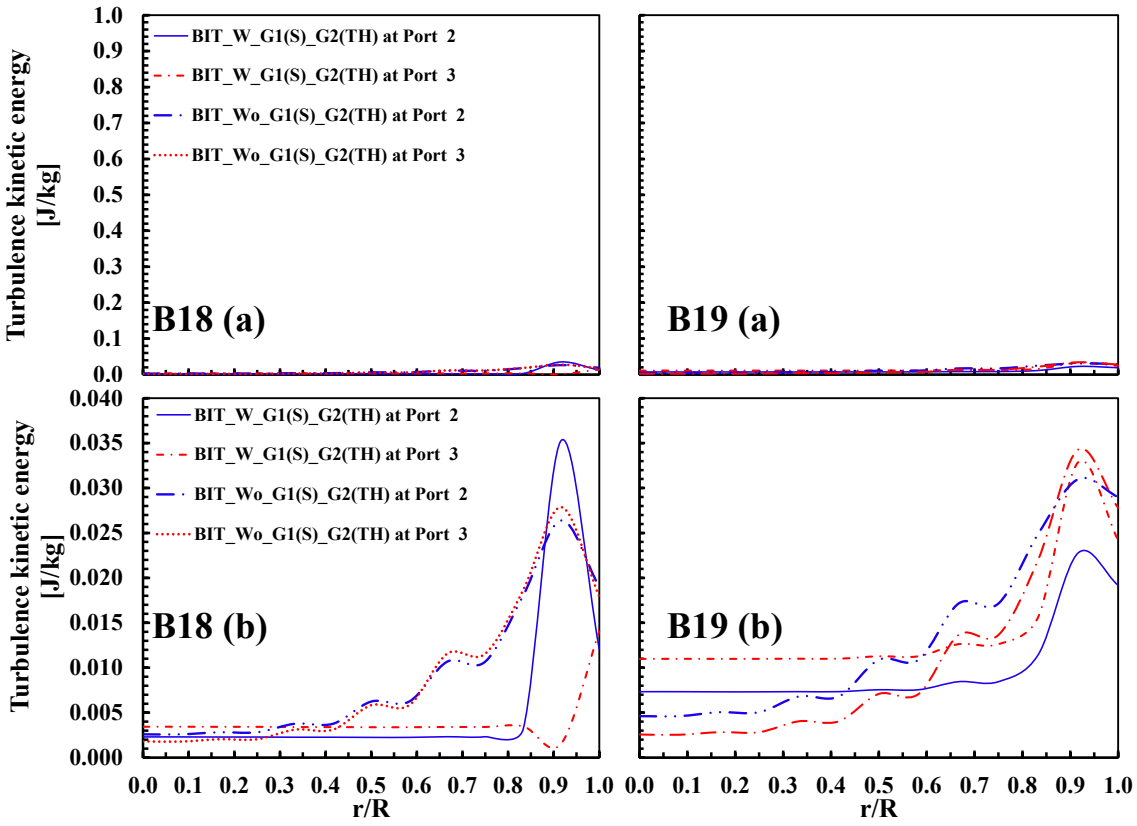

Figure 5.3. Effect of BIT on Turbulence Kinetic Energy Distribution for Flows in Transition Flow Regime: (a) is in a full scale, (b) is zoomed in scale.

B6 case showed the most remarkable increase in the turbulent dissipation rate. However, different from the turbulent kinetic energy distribution, the turbulent dissipation rate increased as close to the pipe wall and exponentially increased near the wall.

Figure 5.5 indicates the distribution of the turbulent dissipation rate profile for the transition area. With the BIT source terms, flatter distributions and higher values of turbulent dissipation rate were predicted in the bulk area of the pipe than these without the source terms.

5.4.1.3. Void fraction. The effect of the BIT source terms on the void fraction distribution for the churn-turbulent flow regime is shown in Figure 5.6. At lower and middle values of liquid flux, no remarkable changes in void fraction distribution were found with and without the BIT source terms. However, B22 case at high flow condition, the BIT source terms provided a good agreement with the experimental data.

B18 and B19 cases in the transition area also showed not a big differences between the two simulation cases with and without the BIT source terms as shown in Figure 5.7.

5.4.1.4. IAC. Comparison of the IAC distributions in churn-turbulent flow regime are shown in Figure 5.8. As described in the Figure 1, the direct approach of BIT model (TH model) directly affects source terms of 2G IATE bubble interaction mechanisms for IAC distribution. At low superficial liquid velocity conditions, IAC profiles for group-1 and group-2 bubbles were not affected by the BIT source terms. However, B6 case was reacted by the BIT source terms although the difference between the two considerations with the BIT source terms and without them at both port 2 and port 3. At middle flow conditions, it starts to show the effect of the BIT source terms on IAC distribution of group-1 bubbles. The variation of turbulent dissipation rate in Figure 4 caused the changes in the group-1 IAC distribution, and it seems that group-1 bubbles react more sensitively to change in the turbulent dissipation rate than group-2 bubbles. At high superficial liquid velocity conditions, IAC distributions of both group-1 and group-2 bubbles were affected by the BIT source terms.

It can be found that the larger discrepancy in turbulent dissipation rate between the simulation cases with the BIT source terms and without the source terms induced the

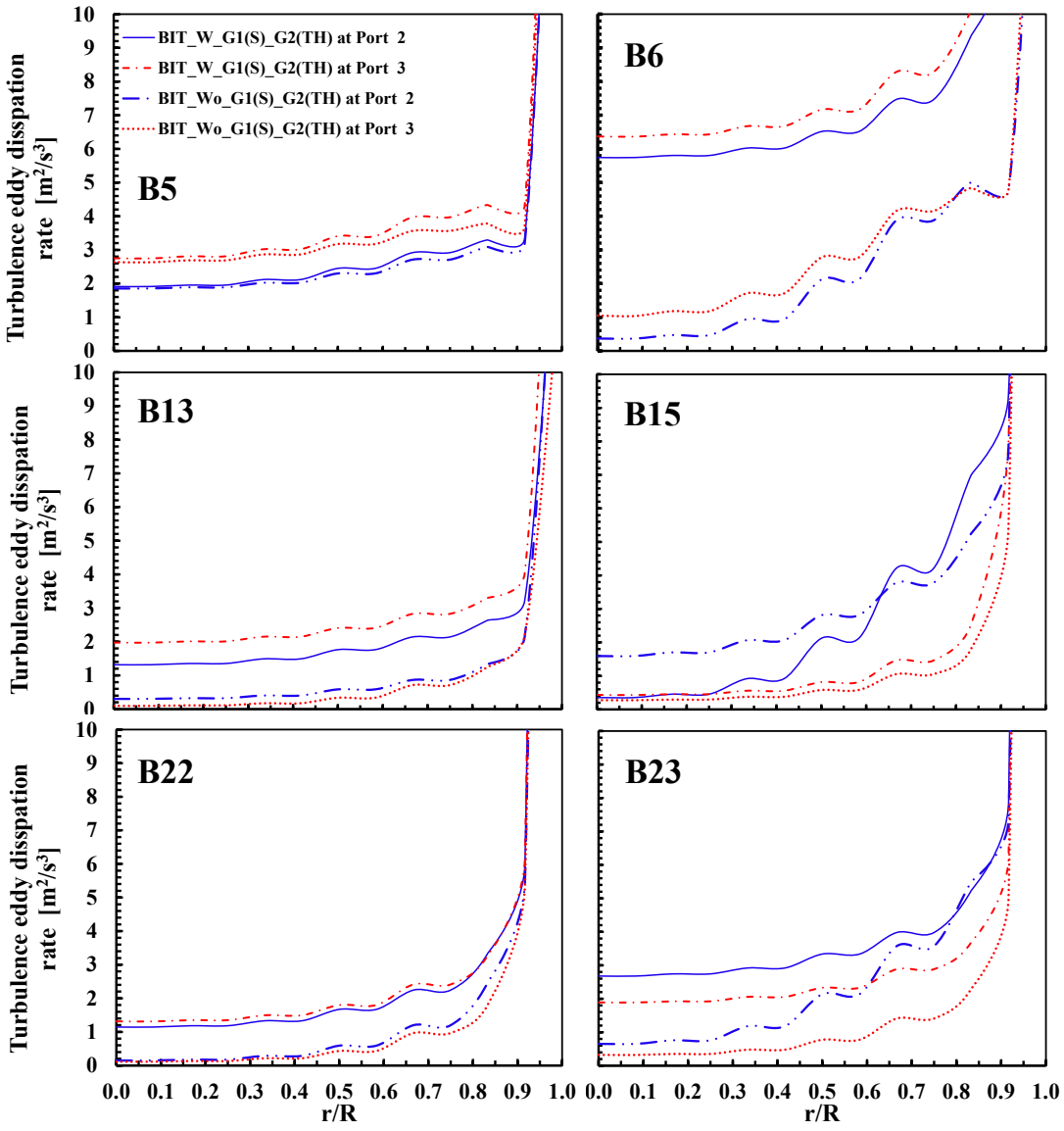

Figure 5.4. Effect of BIT on Turbulence Eddy Dissipation Rate Distribution for Flows in Churn-Turbulent Regime.

bigger differences in IAC distributions at port 2 and port 3 for group-1 and group-2 bubbles.

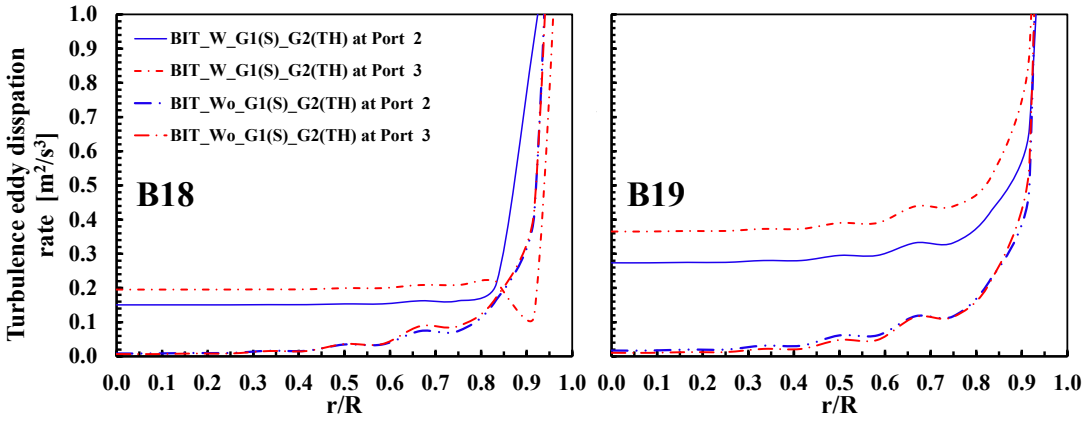

Figure 5.5. Effect of BIT on Turbulence Eddy Dissipation Rate Distribution for Flows in Transition Area: (a) is in a full scale, (b) is zoomed in scale.

Figure 5.9 presents IAC distributions in transition area. The effect of change in turbulent dissipation rate was significant for group-2 bubbles. The BIT source terms allowed more accurate prediction of IAC distribution for group-2 bubbles while the profile was underestimated without the BIT source terms.

5.4.1.5. Dominance of IATE mechanisms. Figure 5.10 through 5.13 indicate the effect of the BIT sources on dominance of 2G IATE components, which are interaction mechanisms (IM), mass transfer (MT), and volume expansion (VE). Figure 5.10 shows the comparison for the low flow conditions. B5 case at low superficial liquid and gas velocity did not show the effect of the BIT source terms on each IATE term, whereas the radial distributions of the 2G IATE component for B6 case varied a lot, and group-1 bubbles were impacted by the BIT source terms. The level of the distributions of the mass transfer (MT) and volume expansion (VE) terms were significantly decreased by implementing the BIT source terms, especially, near the wall region, and the changes in all three terms of the 2G IATE including interaction mechanism (IM), MT, and VE, at

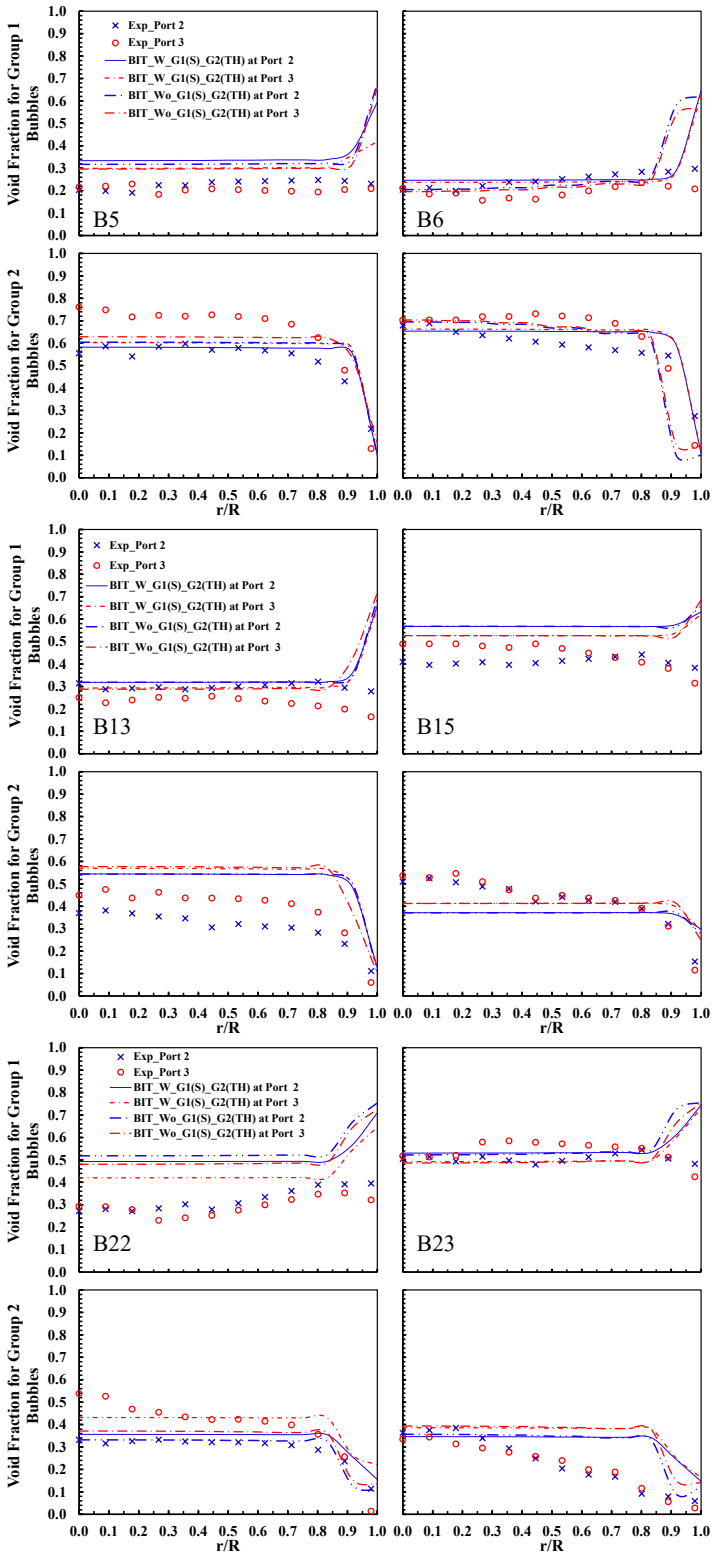

Figure 5.6. Effect of BIT on Void fraction Distribution for Flows in Churn-Turbulent Regime.

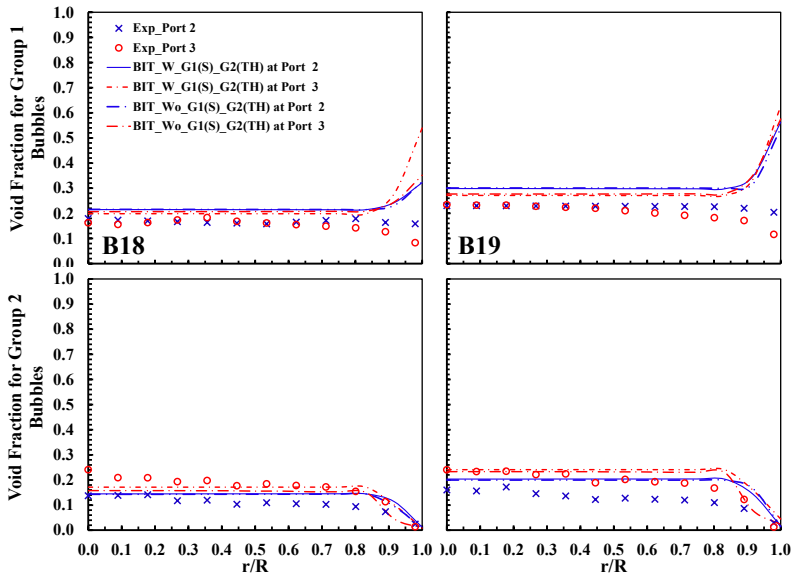

Figure 5.7. Effect of BIT on Void fraction Distribution for Flows in Transition Flow Regime.

port 3 were huge depending on the consideration of the BIT source terms for group-1 bubbles. For group-2 bubbles, there were changes in the profiles of MT and VE terms in the entire area of the pipe. The MT distribution was greater with the BIT source terms than the distribution without the source terms in the bulk area of the pipe, while the opposite trend appeared in the near-wall region. However, the distribution of the VE term with the BIT source terms was greater than the distribution without the source term from the center to the wall of the pipe. Very active changes in all IATE terms were found in the near wall region. These variations were induced by a huge difference in turbulent dissipation rate with the BIT source terms from the simulation conditions without the source terms.

As shown in the Figure 5.11, the response of group-1 bubbles was more dramatic to the BIT source terms than that of group-2. IM of the 2G IATE shows the largest variation among the other contributors. B13 case, which can be categorized as churn-

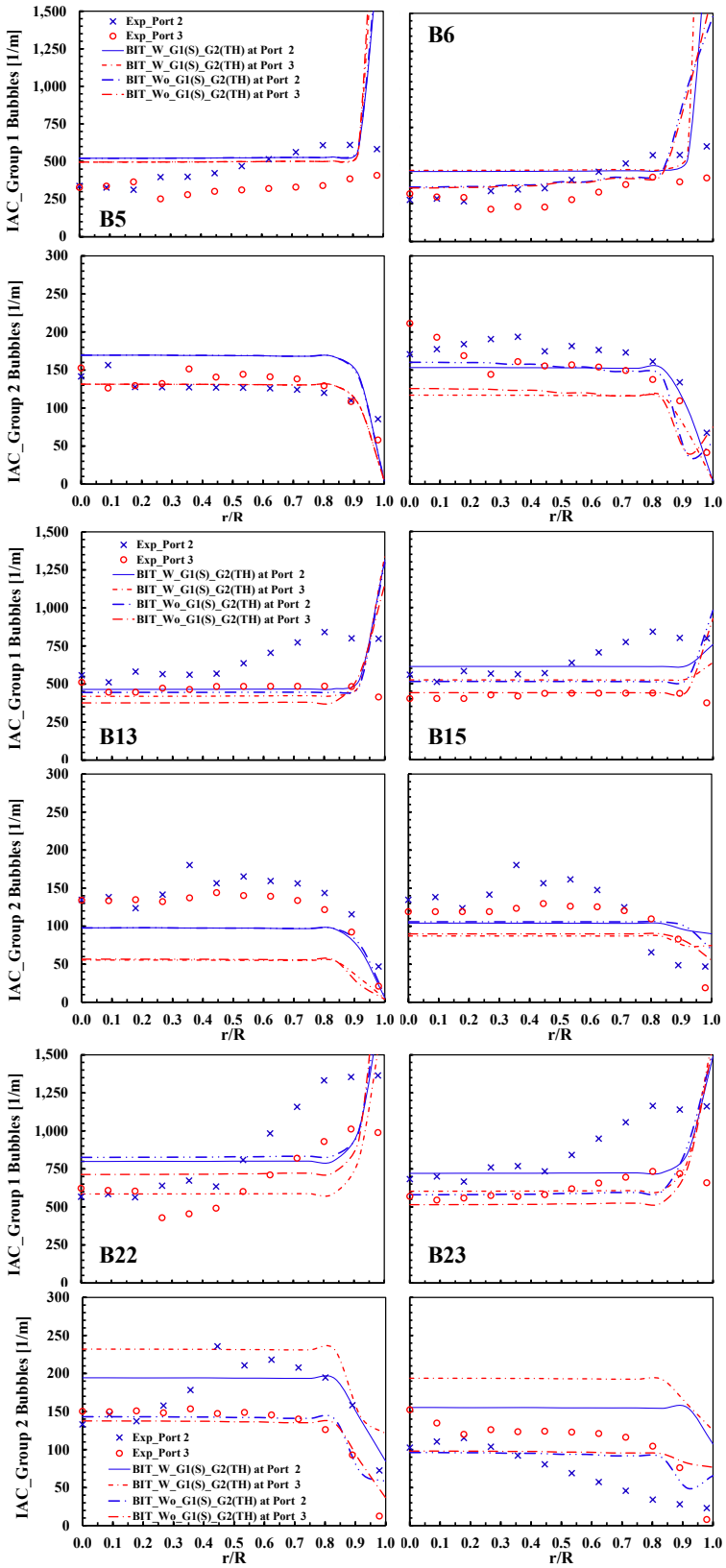

Figure 5.8. Effect of BIT on IAC Distribution for Flows in Churn-Turbulent Regime.

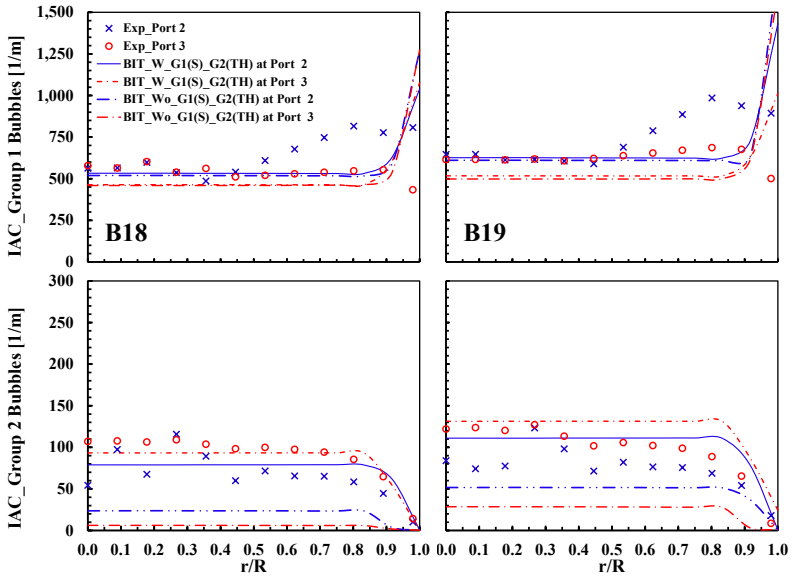

Figure 5.9. Effect of BIT on IAC for Flows in Transition Flow Regime.

turbulent flow regime in the transition area, IM term was dominantly affected by the BIT source terms and the distribution of IM term was increased. More bubble interactions, mass transfer and volume changes were caused by the BIT source terms, and those active changes in each term of the IATE induced variations in IAC distribution of group-1 bubbles. For group-2 bubbles, only VE term showed a noticeable changes in the comparison of the effect of the BIT source terms.

At high value of liquid flux conditions, a very active variation in the distributions of IATE terms was resulted by the BIT source terms as shown in Figure 5.12. B22 case showed that IM of group-1 bubbles had a big changes in its distribution, but VE term was the term significantly impacted by the BIT source terms for group-2 bubbles. B23 case also indicated that the BIT source terms mainly led to changing in the distribution of IM term for group-1 bubbles, but the distributions of all three terms of IATE for group-2 bubbles were impacted by the variations of turbulent kinetic energy and turbulent

dissipation rate. The large change in the turbulent dissipation rate in the center area of the pipe with the BIT source terms caused a huge enhancement of IM term for group-1 bubbles that resulted in the increase of the level of the IAC profile.

Figure 5.13 shows the results of the flow conditions in the transition area between cap/slug flow and churn-turbulent flow regimes. Mostly group-2 bubbles were affected by the BIT source terms. For group-1 bubbles of B18 case, the dominance of IM term in IAC distribution was decreased by the BIT source term, whereas the effect of the IM term on IAC distribution for group-2 bubbles was enhanced and became the most dominant term in the IAC profile. B19 case showed that, with BIT source terms, the effect of the IM term was decreased for group-1 bubbles, but the distribution of the IM term for group-2 bubbles was increased by the BIT source terms. Different from the trend of IM profile, the value of VE term was reduced with the BIT source terms.

5.4.2. Effect of the Two Approaches of BIT Model. Each effect of BIT model for each bubble group on local phase distributions was estimated by comparing four simulation conditions as with BIT model for both bubble groups, with BIT model for group-1 and without BIT model for group-2, without BIT model for group-1 and with BIT model for group-2, and without BIT models for both bubble groups.

5.4.2.1. Turbulent kinetic energy (KE or *k*). Figure 5.14 shows local radial distributions of square root of turbulent kinetic energy (√KE) in log scale at port 2 and port 3. As a reference model, the condition with considering BIT for both group-1 and group-2 bubbles is compared with other cases. When comparing the cases between the reference model and with considering BIT only for group-2 bubbles, BIM for group-1 bubbles does not much affect KE production at lower J_L for B4 and B6. However, at

higher J_L for B15 and B23 cases, BIM (group-1, Sato model) gave small increase in KE production. It seems that the Sato model works more sensitively at higher J_L condition. It is because of slightly higher relative velocity at higher J_L conditions, and there were more contribution of BIM for group-1 bubbles at port 3 compared to that at port 2. BIT for group-2 bubbles effects can be seen by comparing results between with the reference model and with BIM only for group-1 bubbles. Without considering BIT for group-2 bubbles, KE production decreased for B4 and B6 cases, whereas B15 and B23 cases at port 2 show slight increase of KE in particular area in transverse direction compared to the reference case. It is because of less void fraction of group-2 bubbles for B15 and B23 cases in bulk area of the pipe than the group-2 bubble void fraction for B4 and B6 cases. Group-2 bubbles cause more turbulent mixing, and higher void fraction of group-2 bubbles leads to more KE.

Without considering BIT for group-2 bubbles, KE is under- or over-estimated compared to the level of KE of the reference case, and those deviations can be found in distributions of void fraction and a_i in Figure 5.19 through Figure 5.22. Moreover, simulation results without considering BIT for both G1 and G2 bubbles follow trend of simulation case considering BIT only for group-2 bubbles. This indicates that considering BIT induced by group-2 bubbles is critical for accurate calculations of local phase distributions. All run cases, except for B15 and B23 at port 3, show KE production decaying away from a maximum value in the bulk area of the pipe to a minimum value near the wall region regardless of BIT model considered for group-1 or group-2 bubbles. The decreasing trend of KE production near the wall suggests that shear production is important to model. While B4 and B6 cases have a decreasing tendency of KE production

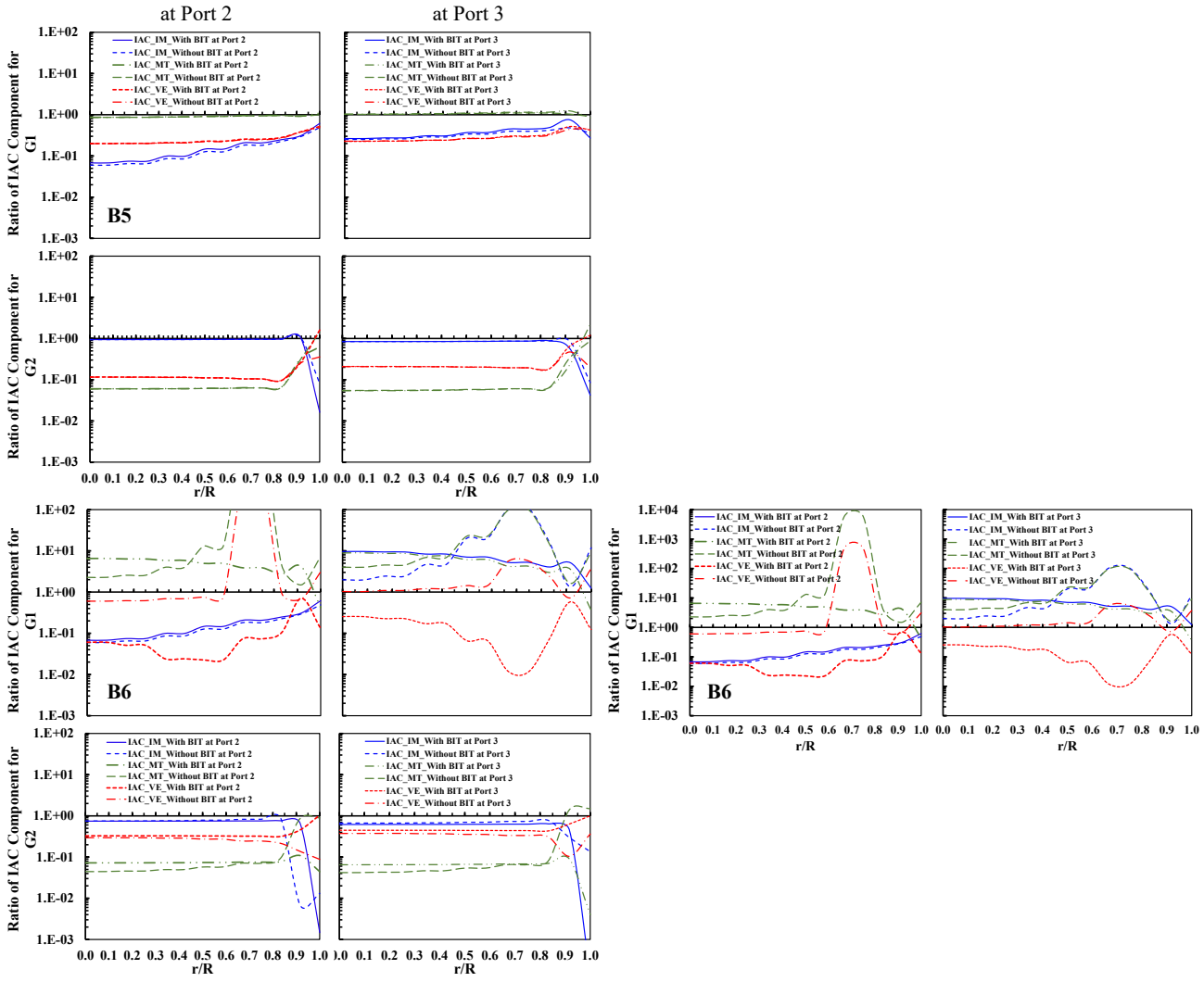

Figure 5.10. Effect of BIT on Dominance of Each IATE Component for Flows at Low Flow Conditions in Churn-Turbulent Regime.

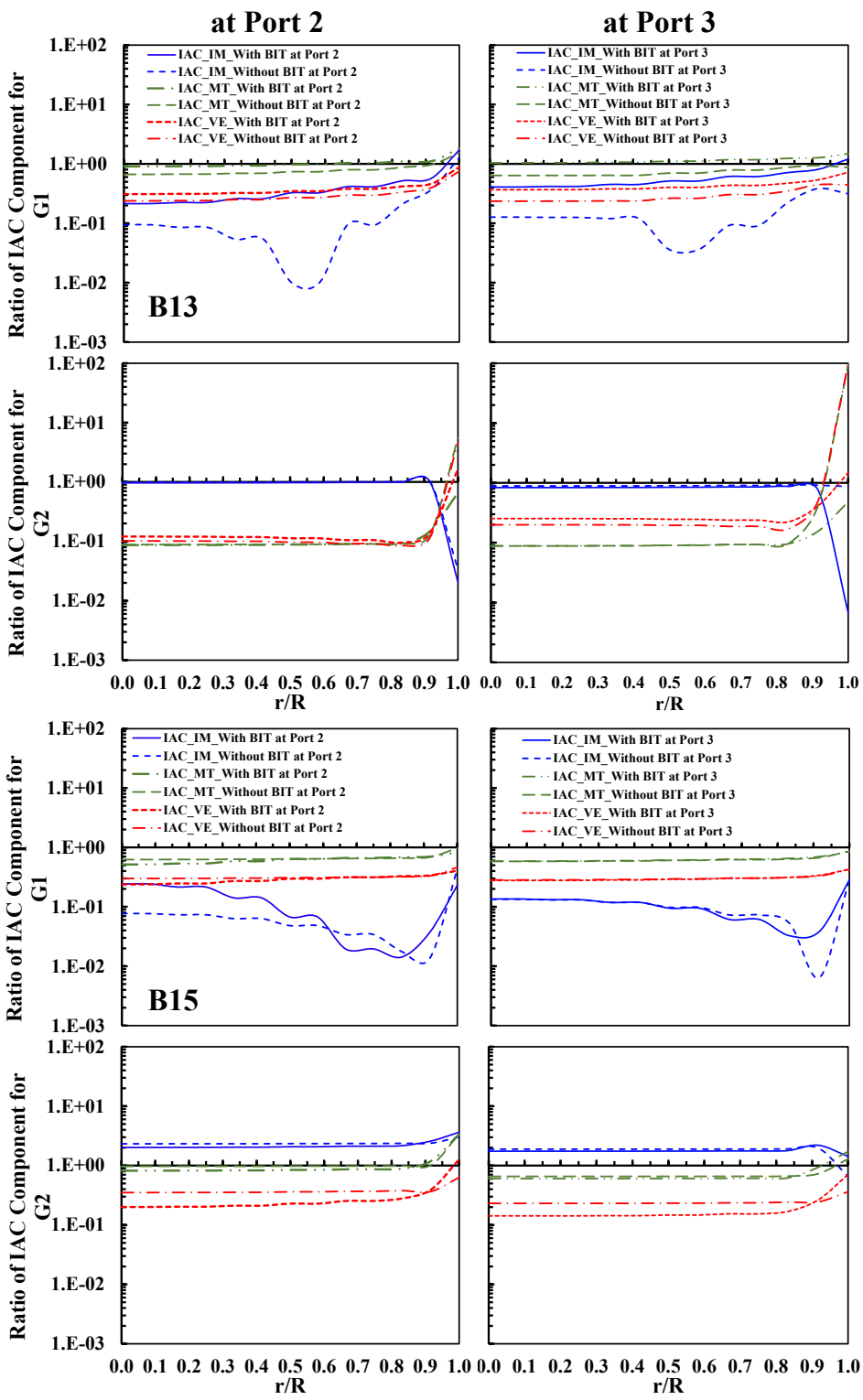

Figure 5.11. Effect of BIT on Dominance of Each IATE Component for Flows at Middle Flow Conditions in Churn-Turbulent Regime.

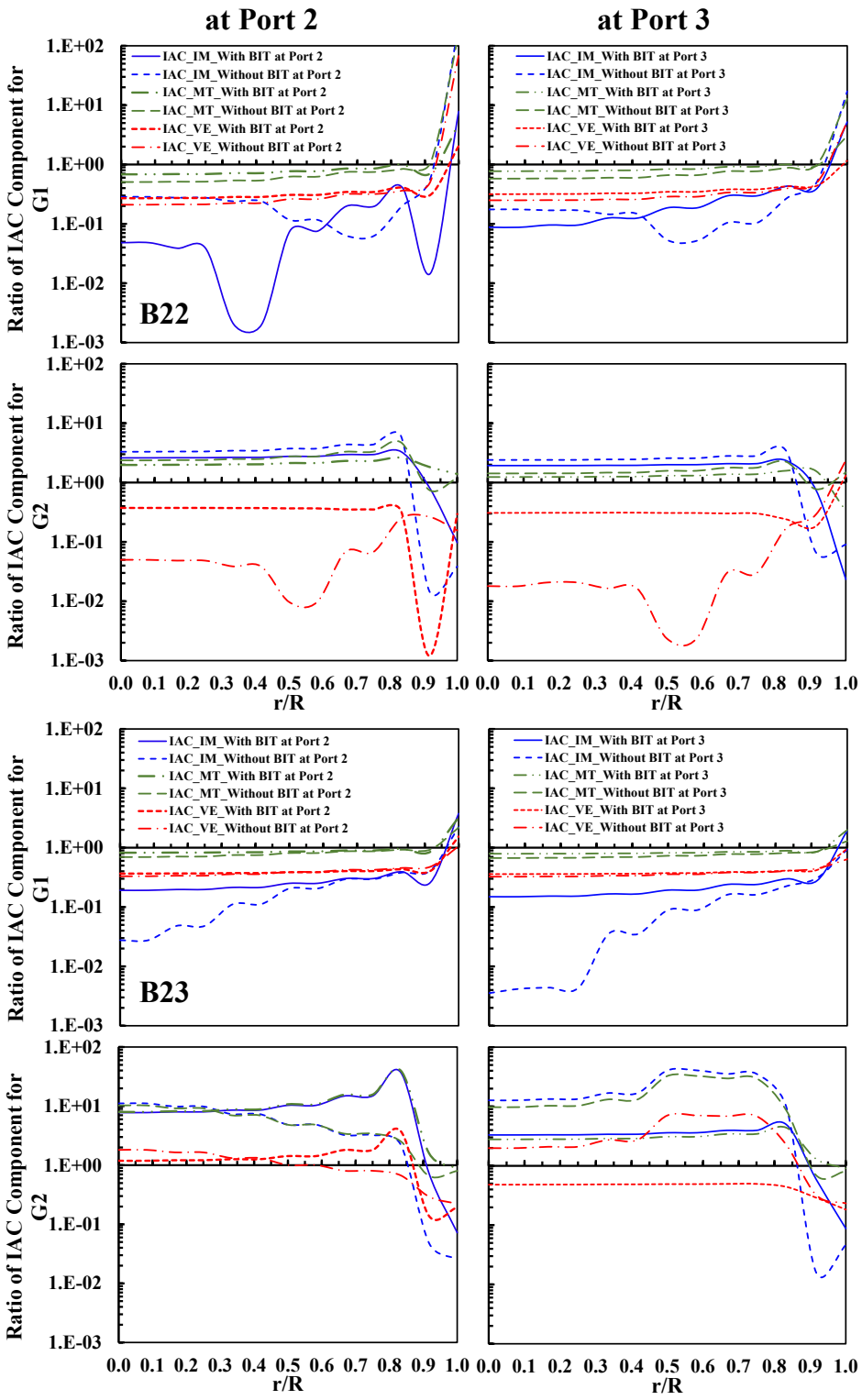

Figure 5.12. Effect of BIT on Dominance of Each IATE Component for Flows at High Flow Conditions in Churn-Turbulent Regime.

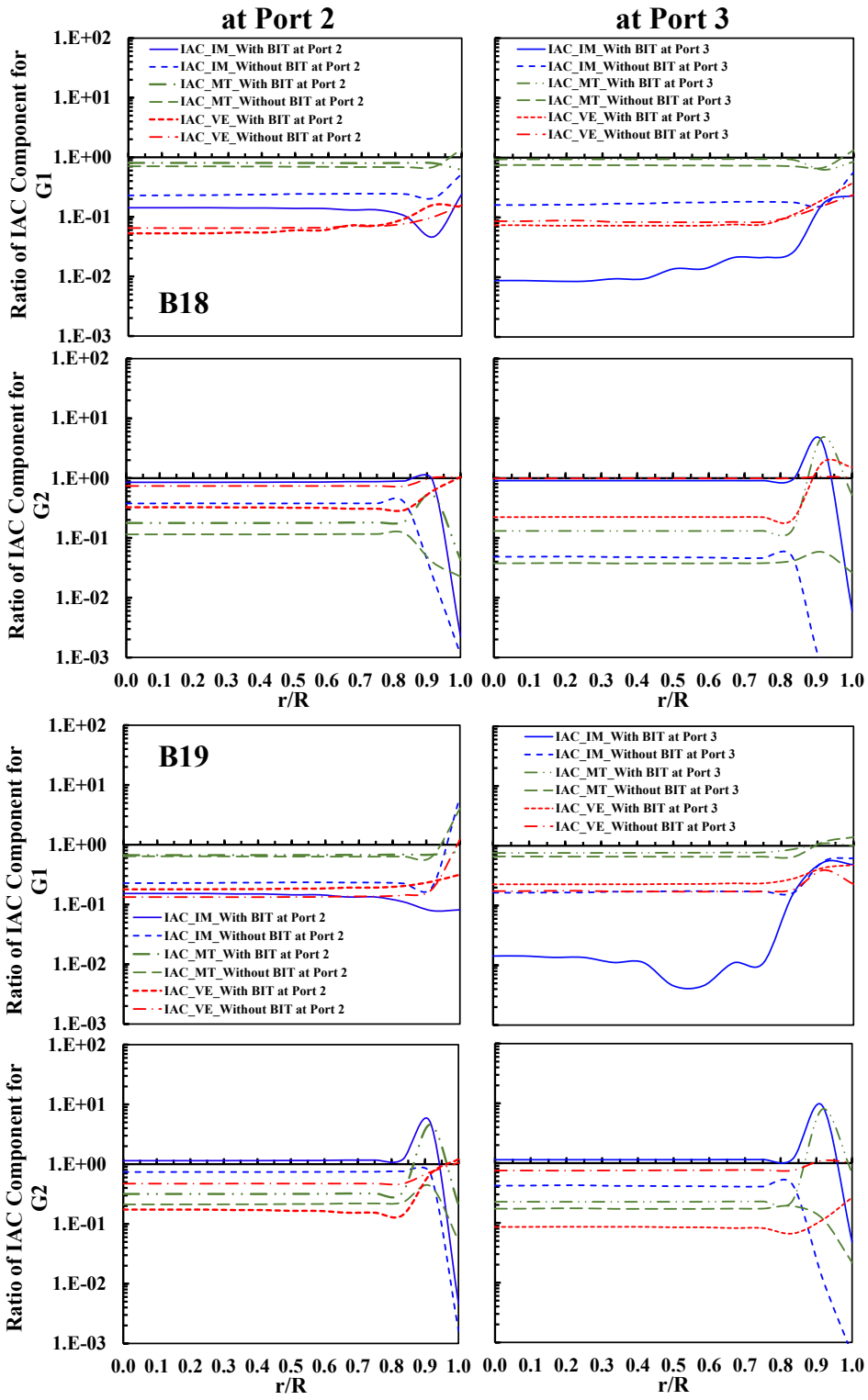

Figure 5.13. Effect of BIT on Dominance of Each IATE Component for Flows at Middle Flow Conditions in Transition Regime.

at near the wall region, KE production for B15 and B23 cases increased steadily even in the region near the wall and maximum production of KE occurred at the wall. Radial distributions of KE are flat in bulk area of the pipe. These tendency suggests that bubble dynamics driven by group-2 bubbles are the primary contributor of KE production in bulk area, which is evidenced by the quantity of √KE that varies with level of void fraction of group-2 bubbles. Moreover, at low velocity conditions (B4 and B6), there is a gap between the two cases considering BIT for group-2 bubbles and the other two cases without considering BIT for group-2 bubbles, whereas high velocity conditions exhibit KE productions seems converged. The reason of the difference between low and high velocity conditions can be explained as the lower liquid velocity environment allows relatively longer time for gases to interact more actively and the higher velocity condition is more likely to depend on the shear production mechanisms.

The Tchen model gives significant production of KE and flatter distributions for all B4, B6, B15, B23 cases. It may be due to turbulent dispersion effect included in the Tchen model, which has a tendency of equalizing distribution of bubbles. From the comparisons of TR model between B4 and B6 case results and between B15 and B23 case results, as increasing J_G, KE increases, and as decreasing J_G, KE decreases even though J_L increased, respectively.

5.4.2.2. Turbulent dissipation rate (ε). Effect of BIT on local distributions of turbulent dissipation rate (ε) is presented in log scale in Figure 5.15. For all B4, B6, B15, B23 cases, ε has an increasing tendency near the wall region and steadily increases without considering BIT for group-2 bubbles as location changes toward wall. B4 and B6 cases present an ignorable effect of BIM for group-1 bubbles on the ε distributions from

the comparison between the reference case (BIT for both group-1 and group-2 bubbles) and the case only with BIT for group-2 bubbles, whereas ε was calculated to be lower without BIT for group-2 bubbles than the value of the reference case. B15 and B23 cases show that the effect of BIM for group-1 bubbles is also very small which is similar with B4 and B6 cases. The effect of BIT for group-2 bubbles is weaker than that for B4 and B6 cases, but the B15 and B23 cases also calculated lower ε without BIT for group-2 bubbles comparing to the reference case. The Tchen model expects much higher and further flatter lateral profiles of ε than the various comparison cases. It is the same tendency shown in KE comparisons. Similar to KE comparisons, the trend of increasing ε with increasing J_G is also captured.

5.4.2.3. Turbulent viscosity ($\mu_{L,t}$). Turbulent viscosity ($\mu_{L,t}$) profiles are compared with different BIT conditions in Figure 5.16 Increase of turbulent viscosity enhances turbulent stresses. The predicted value of $\mu_{L,t}$ is expected to influence liquid velocity profile and may indirectly cause lift force change that impacts lateral distribution of void fraction. Moreover, greater $\mu_{L,t}$ signifies more turbulent flow by increasing KE and ε, which drives flatten velocity profile due to higher turbulent dispersion force. For all simulation cases and running conditions, $\mu_{L,t}$ tends to be higher in the center of the pipe and lower near the pipe wall and decreases as location moves toward near the wall, as seen in Figure 5.16 by comparing the cases between the reference and only with BIT for group-2 bubbles. While BIM for group-1 bubbles barely affects $\mu_{L,t}$ profiles, lower values of $\mu_{L,t}$ are calculated without BIT for G2 bubbles than the values for the reference case. It is expected that the big group-2 bubbles will cause more turbulence than the small group-1 bubbles, both due to bigger size and higher slip velocity.

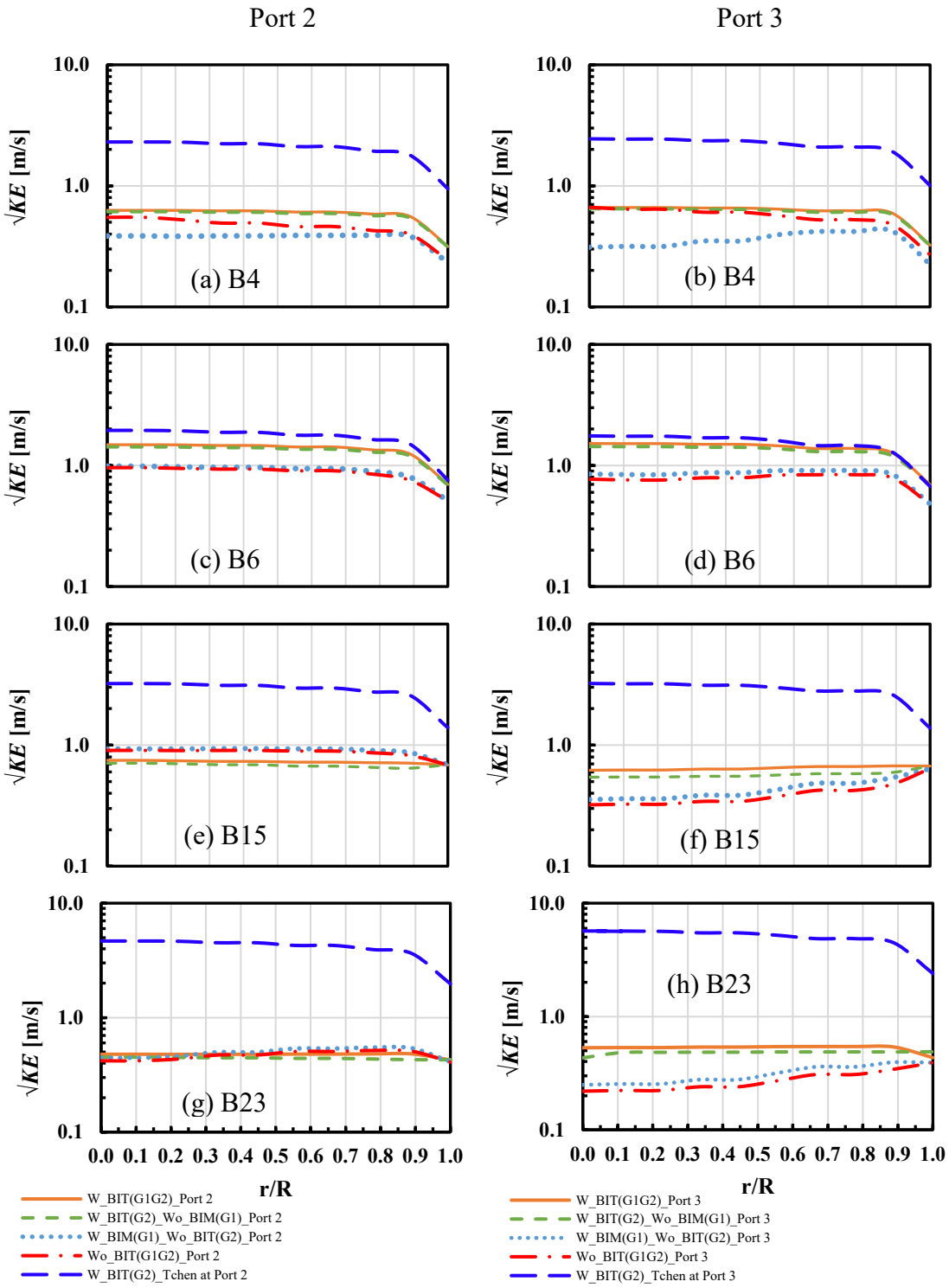

Figure 5.14. Effect of Bubble-Induced Turbulence on Local Distribution of Square Root of Turbulent Kinetic Energy (√KE) for B4, B6, B15, and B23 Cases at Port 2 and Port 3.

Also, it is expected that the bubble induced turbulence effect will be more at center as group-2 bubbles have affinity to go towards the channel center. The figures show that the CFD results of turbulent viscosity predict the right trend. From the comparison between simulation conditions of no BIT effect and only with BIM for group-1 bubbles, it is predicted that the Sato model increases $\mu_{L,t}$ due to linear algebraic relationship between bubble-induced turbulent viscosity ($\mu_{L,t}^{BI}$) and shear- induced turbulent viscosity ($\mu_{L,t}^{SI}$). However, at the lowest J_L condition (B4), the condition without any BIT effects delivered locally greater values of $\mu_{L,t}$ than the values under the condition only with BIM for group-1 bubbles. This is because turbulent flow is not strong enough only with BIM for group-1 bubbles, and the presence of higher void fraction of group-1 bubbles may observe turbulence energy at bubble interfaces through collision with turbulent eddies. The weakened turbulent flow leads to higher void fraction of group-2 bubbles due to less bubble breakup process as shown in Figure 5.20 (a) and (b). The Tchen model also predicts higher values comparing the different conditions except for B6 case at port 3. However, the influence of $\mu_{L,t}$ variation seems relatively small in comparison with the effect of *KE* and ε on void fraction distribution. Aforementioned, directly adding source terms to turbulence model may be more significantly affect local phase distribution than introducing $\mu_{L,t}^{BI}$ does, and the effect of $\mu_{L,t}^{BI}$ could be unnoticeable or ignorable. Although the effect of $\mu_{L,t}^{BI}$ could be very small, the effect of BIM for group-1 bubbles still affects velocity profile of gas phase and can be confirmed in Figure 5.17 and Figure 5.18.

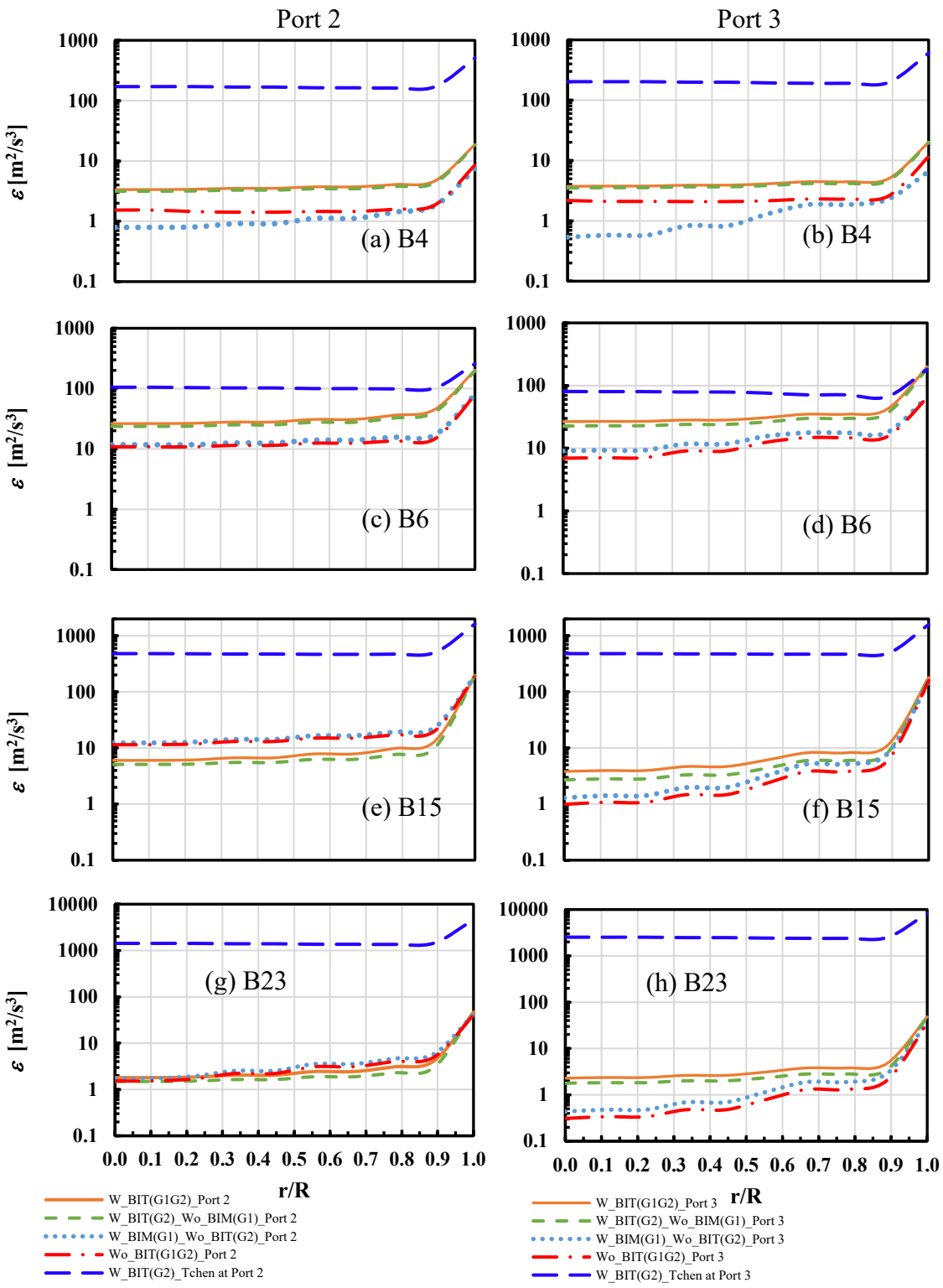

Figure 5.15. Effect of Bubble-Induced Turbulence on Local Distribution of Turbulent Dissipation Rate (ε) for B4, B6, B15, and B23 Cases at Port 2 and Port 3.

5.4.2.4. Gas velocity profile. Figure 5.17 and Figure 5.18 show local velocity profiles predictions in comparison with measurements for group-1 and group-2 bubbles, respectively. While the liquid velocity were not measured directly, the gas velocity profile is strongly linked to liquid velocity profile through slip. As discussed in the previous sections, increase in turbulence parameters enhances $\mu_{L,t}^{SI}$ and $\mu_{L,t}$, and makes turbulence dispersion force stronger, which is proportional to $\mu_{L,t}$. In addition, $\mu_{L,t}$ drives momentum equations change. This effect can be confirmed in Figure 5.17 and Figure 5.18. Commonly, with BIT for group-2 bubbles, all four cases give flatter gas velocities. Effect of BIT for group-2 bubbles is stronger than that of BIM for group-1 bubbles. Both conditions only with BIT for group-2 bubbles and with BIT for group-1 and group-2 bubbles show similar distribution to each other and follow trends of experimental velocity profiles, while rest conditions without BIT for group-2 model and without BIT for group-1 and group-2 expect larger gradient in radial direction. Without BIT for group-2 bubbles, higher velocities are calculated in bulk region of the pipe and lower values of velocity are expected as the location is close to the pipe wall than the velocities with considering BIT only for group-2 bubbles.

Drag interfacial force also plays a major role in the prediction of the gas velocity. Therefore, over- or under-estimation of gas velocity may occur due to inaccurate modeling of drag coefficient, and this would be a future work for evaluating the drag coefficient models.

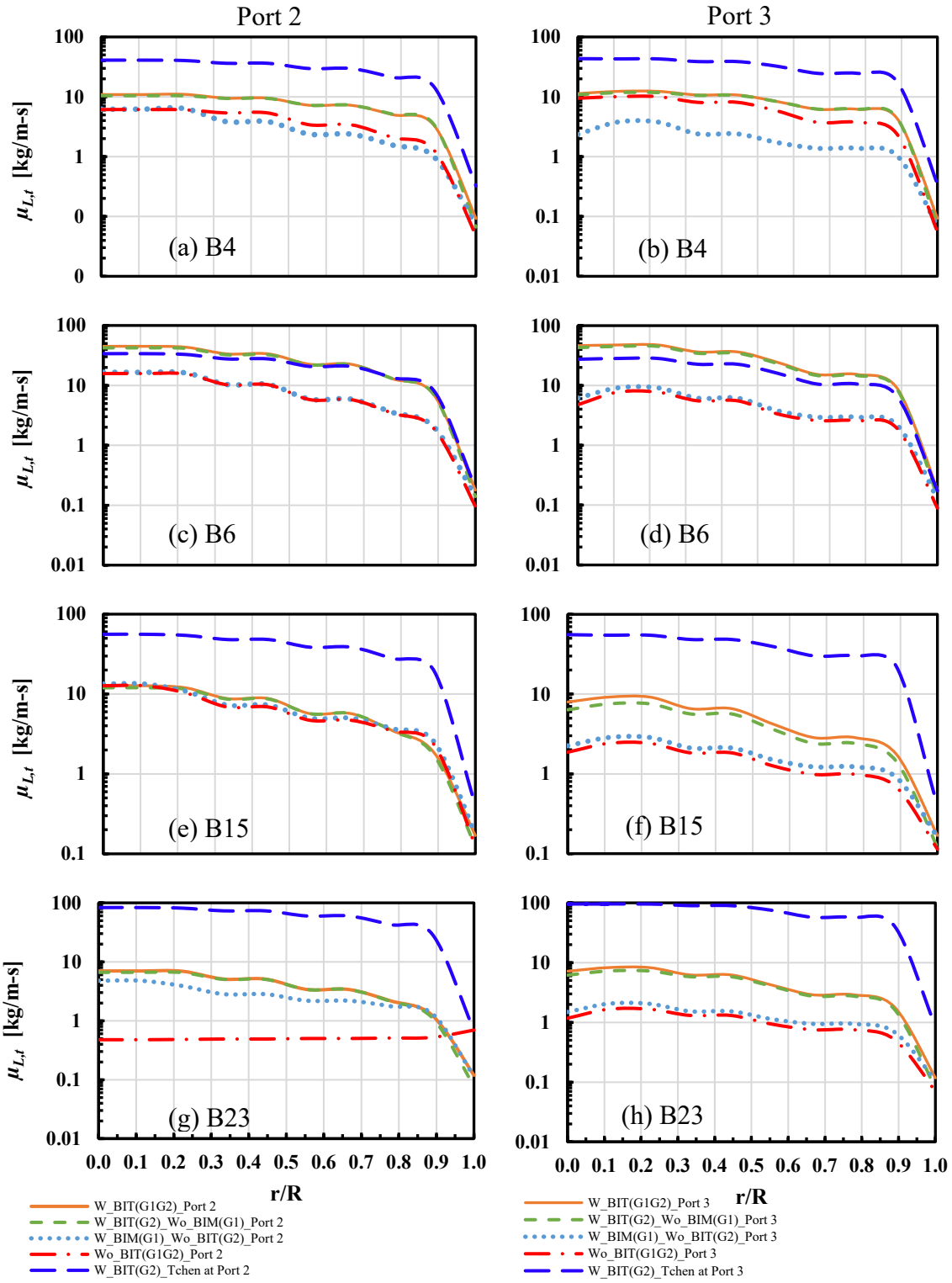

Figure 5.16. Effect of Bubble-Induced Turbulence on Local Distribution of Turbulent Viscosity ($\mu_{L,t}$) for B4, B6, B15, and B23 Cases at Port 2 and Port 3.

5.4.2.5. Void fraction. Simulation results of void fraction with considering BIT for group-2 bubbles or BIT for both group-1 and group-2 bubbles in Figure 5.19 and Figure 5.20 concur with the experiment dataset in the bulk area of the pipe except for near the pipe wall. As opposed to experiment dataset, however, the CFD calculation shows sharp increase of void fraction for group-1 bubbles near the pipe wall. This increasing tendency of void fraction profile for group-1 bubbles near the wall, again, point out the limits of Eulerian-Eulerian (E-E) model and turbulence model since the E-E model is not able to capture the characteristics of all discrete size of bubbles and k-ε turbulence model is hard to describe large eddies that could have the same size with a diameter of a channel in a large diameter pipe in real phenomena and may help to redistribute small bubbles by carrying them from near the wall region to bulk area of the pipe. This tendency also can be explained by an increasing trend of ε, which leads to active bubble breakup mechanisms. Lower production of KE and ε caused lower values of void fraction for group-1 bubbles and higher values of void fraction for group-2 bubbles in comparison with the reference case. Effect of BIT for group-2 bubbles on void fraction distributions for group-1 bubbles is relatively more remarkable at lower J_L conditions of B4 and B6 cases than that at higher J_L conditions of B15 and B23 cases. Indeed, void fraction profile for group-2 bubbles seems to be more dependent on BIT for group-2 bubbles. Without BIT for group-2 bubbles, void fractions for both group-1 and group-2 bubbles show larger differences at lower J_G and J_L conditions, such as B4 and B6, with measured void fractions when it compares to those at higher J_G and J_L conditions, such as B15 and B23. For group-1 bubbles void fraction decreases whereas void fraction for group-2 bubbles increases with comparisons of the void fractions of the

reference case. For all four simulation cases, without considering BIT for group-2 bubbles, higher values of void fraction for group-2 bubbles are predicted in the center of the pipe, which are driven by lower productions of *KE* and ε.

Without any BIT sources ($\mu_{L,t}^{BI}$, S_{k_C}, and S_{ε_C}), large gradient of void fractions for group-1 and group-2 bubbles is found at low J_G condition, B4 case, due to weaken turbulence dispersion force resulted from simulation condition without any BIT sources. For the rest of B6, B15 and B23 cases, void fractions for group-1 and group-2 bubbles without any BIT sources follow trends of the simulation conditions considering BIT for group-2 bubbles. This indicates that $\mu_{L,t}^{BI}$ is important for relatively lower J_G conditions while for relatively higher J_G and J_L conditions $\mu_{L,t}^{SI}$ is much higher and effect of BIM for group-1 bubbles is ignorable.

5.4.2.6. Interfacial area concentration (IAC or a_i). Figure 5.21 and Figure 5.22 show the effect of particle or bubble induced turbulence (PIT or BIT) models on IAC of group-1 and group-2 bubbles (a_{i_G1} and a_{i_G2}). The Sato model and Troshko Hassan model were used as a reference for G1 and G2 bubbles, respectively. As can be seen, the IAC distributions follows trends of void fraction profiles.

Firstly, IACs for group-1 and group-2 bubbles (a_{i_G1} and a_{i_G2}) at port 2 and at port 3 were evaluated by considering BIT model under conditions with BIT model and without BIT model for each bubble group, and then the a_{i_G1} and a_{i_G2} were investigated with two different BIT models of the Troshko Hassan model and Tchen model. The Sato model acts through enhanced effective viscosity of the continuous phase by adding Sato bubble-induced viscosity term to continuous phase turbulent viscosity. For lower liquid velocity flow conditions of B4 and B6 cases, the effect of BIT for group-2 bubbles seems

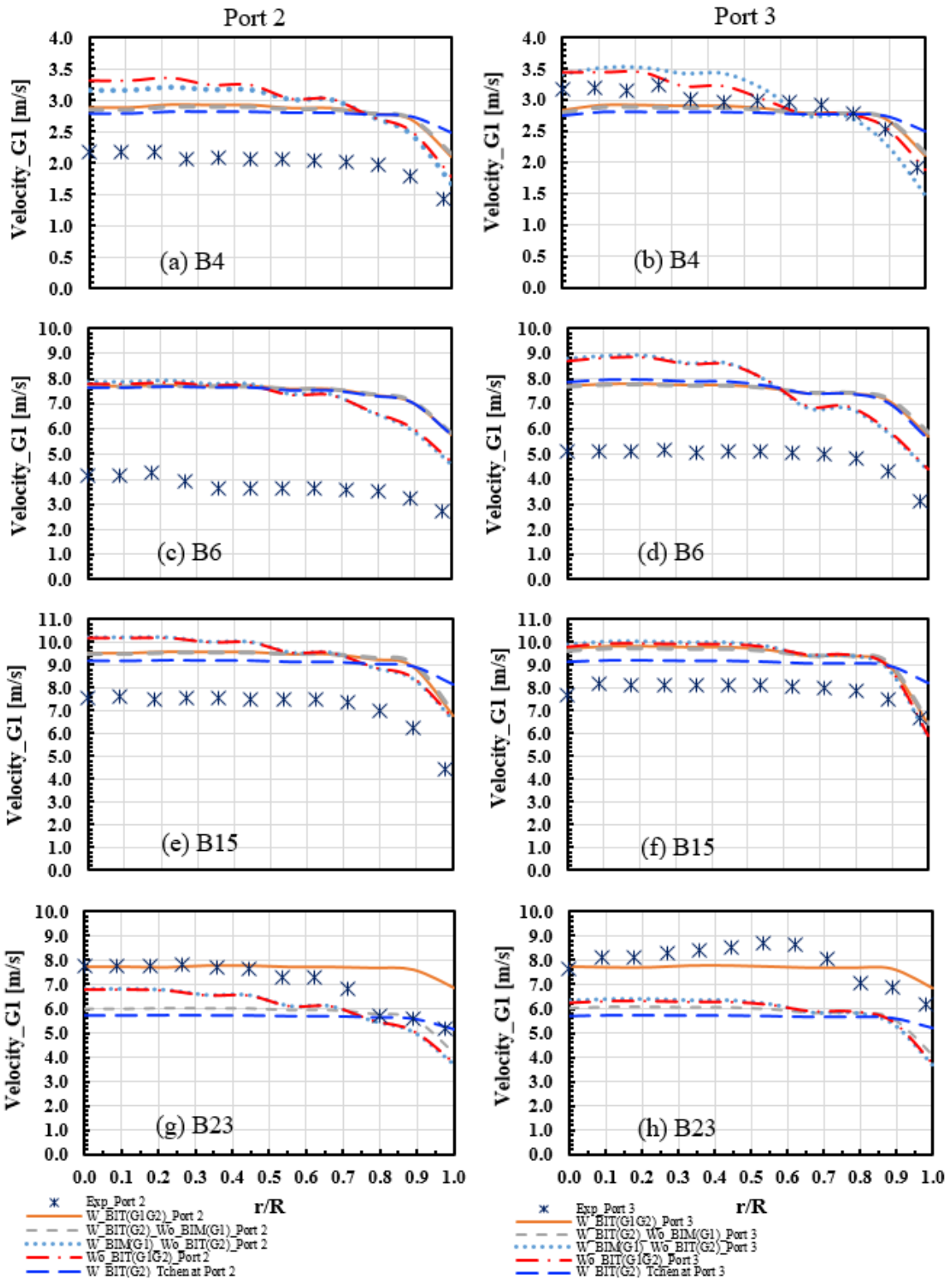

Figure 5.17. Effect of Bubble-Induced Turbulence on Local Distribution of Velocity for G1 Bubbles for B4, B6, B15, and B23 Cases at Port 2 and Port 3.

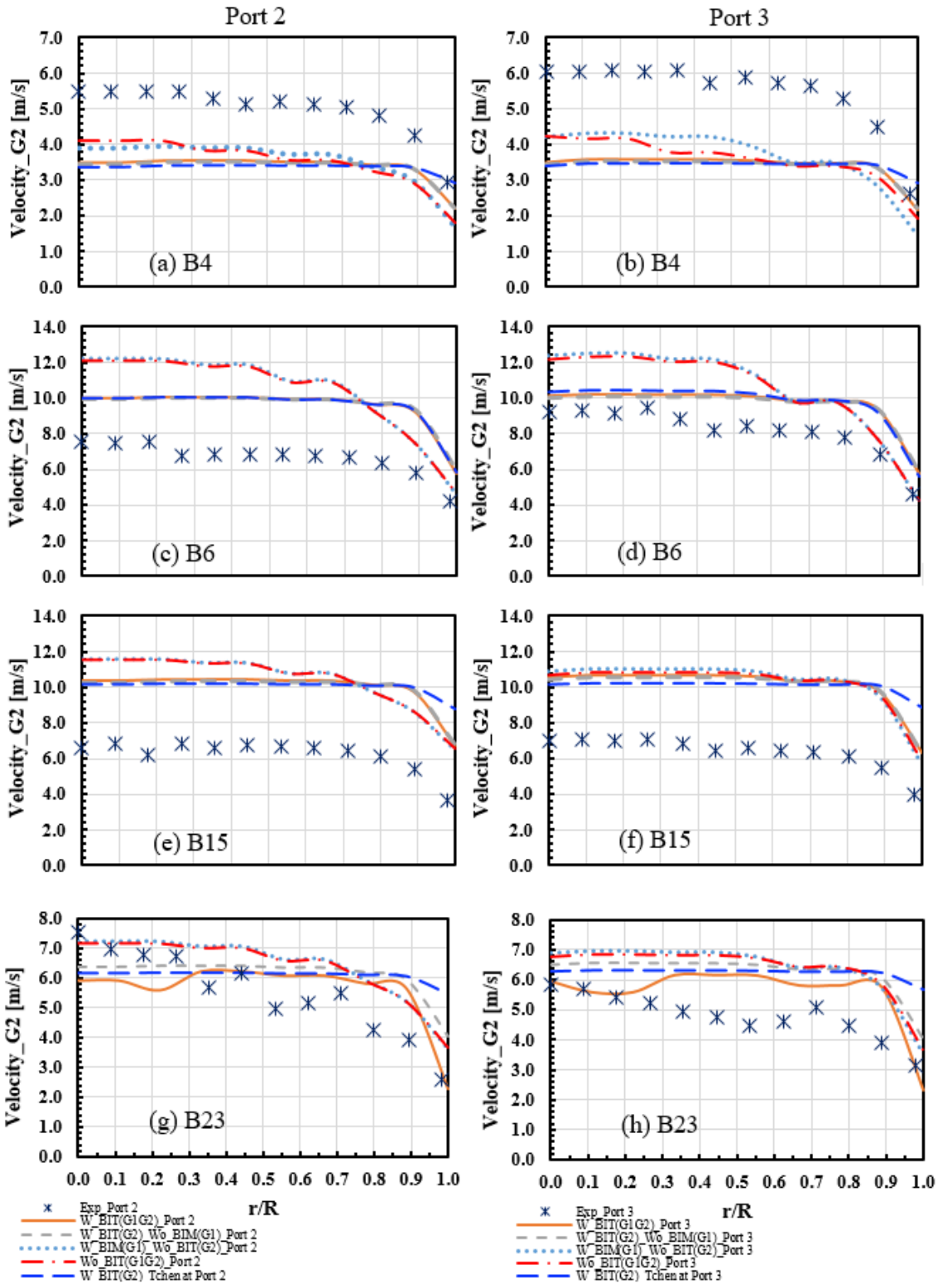

Figure 5.18. Effect of Bubble-Induced Turbulence on Local Distribution of Velocity for G2 Bubbles for B4, B6, B15, and B23 Cases at Port 2 and Port 3.

large as shown in Figure 5.21 and Figure 5.22 ((a)-(d)), and it gives significant radial gradient of IAC for group-1 and group-2 bubbles.

Figure 5.21 and Figure 5.22 show the effect of particle or bubble induced turbulence (PIT or BIT) models on IAC of group-1 and group-2 bubbles (a_{i_G1} and a_{i_G2}). The Sato model and Troshko Hassan model were used as a reference for G1 and G2 bubbles, respectively. As can be seen, the IAC distributions follows trends of void fraction profiles.

Firstly, IACs for group-1 and group-2 bubbles (a_{i_G1} and a_{i_G2}) at port 2 and at port 3 were evaluated by considering BIT model under conditions with BIT model and without BIT model for each bubble group, and then the a_{i_G1} and a_{i_G2} were investigated with two different BIT models of the Troshko Hassan model and Tchen model. The Sato model acts through enhanced effective viscosity of the continuous phase by adding Sato bubble-induced viscosity term to continuous phase turbulent viscosity. For lower liquid velocity flow conditions of B4 and B6 cases, the effect of BIT for group-2 bubbles seems large as shown in Figure 5.21 and Figure 5.22 ((a)-(d)), and it gives significant radial gradient of IAC for group-1 and group-2 bubbles.

It may be because at lower liquid velocity less turbulence effect is expected and results in less turbulent dispersion force generation that induces a large gradient of void fraction in radial direction. Moreover, difference in relative velocity of group-1 and group-2 bubbles may affect level of a_{i_G1}. The driving mechanism of BIT production (KE) term (S_{k_C}) is assumed drag of bubbles and results in a proportional power-law relationship of the KE, $\mu_{L,t}$, and ε with the relative velocity as shown in Equation (26),

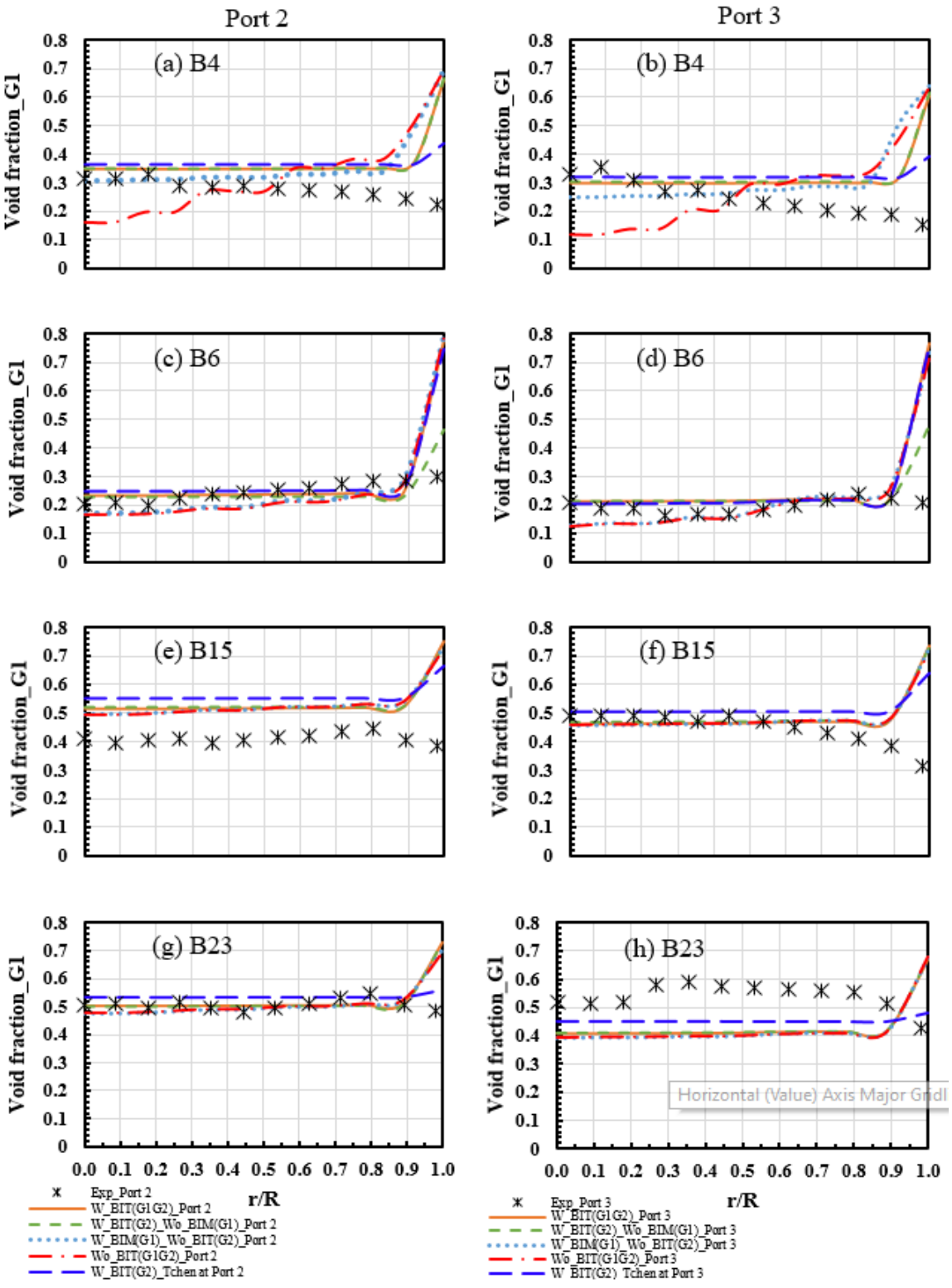

Figure 5.19. Effect of Bubble-Induced Turbulence on Void Fraction Distribution for G1 Bubbles for B4, B6, B15, and B23 Cases at Port 2 and Port 3.

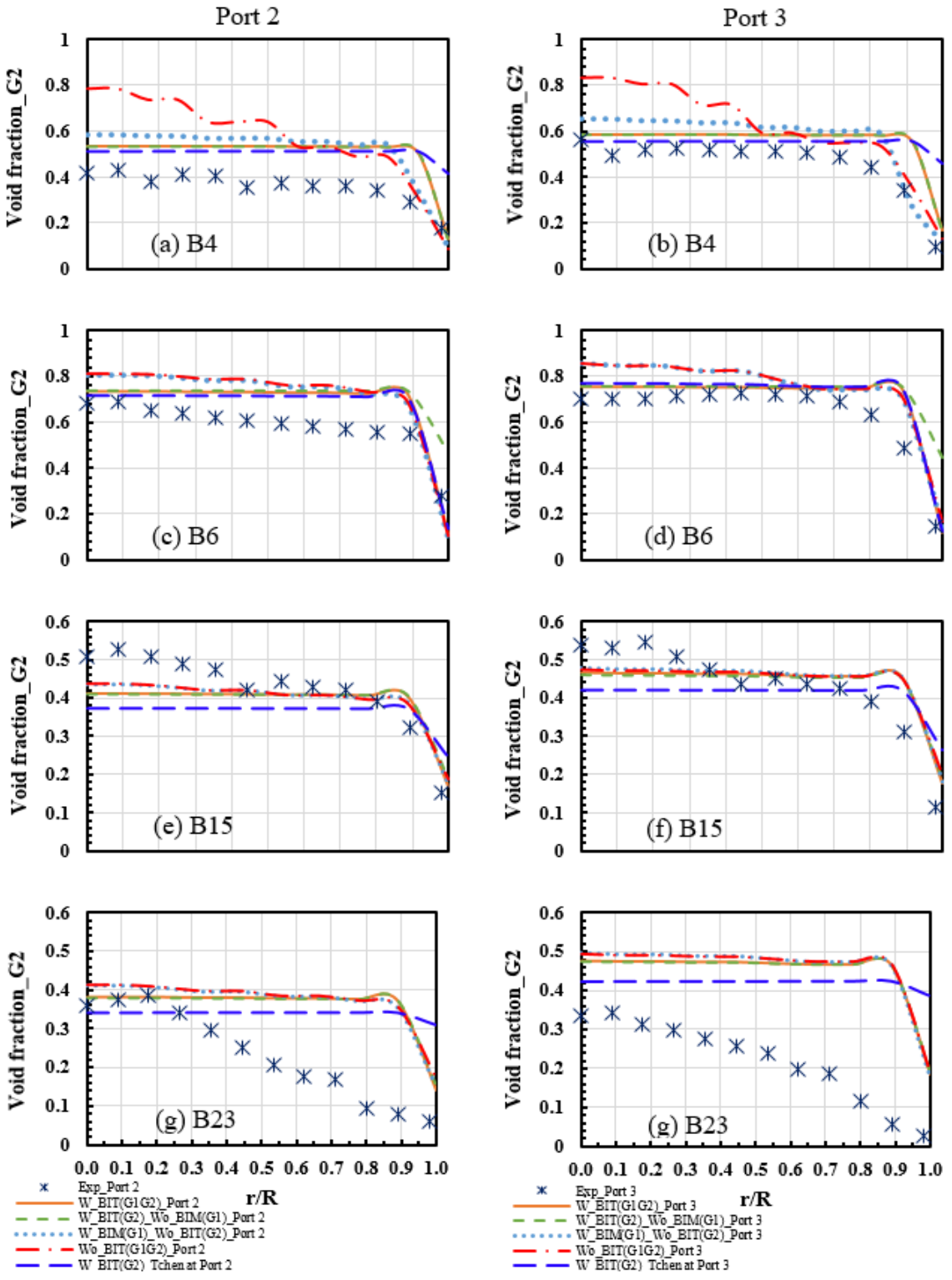

Figure 5.20. Effect of Bubble-Induced Turbulence on Void Fraction Distribution for G2 Bubbles for B4, B6, B15, and B23 Cases at Port 2 and Port 3.

Equations (28), and Equation (52), and prediction of the KE, $\mu_{L,t}$, and ε relies on the relative velocity. Therefore, Figure 5.21 (a)-(d) show that the case considering only BIM for group-1 bubbles underestimates a_{i_G1} compared to the cases with BIT for group-2 bubbles, whereas under the higher liquid velocity conditions (B15 and B23 cases) no significant deviations are obtained between the case of considering only BIM for group-1 bubbles and the cases with BIT for group-2 bubbles as shown in Figure 5.21 (e)-(h).

In contrast, Figure 5.22 indicates that a_{i_G2} is overestimated without BIT for group-2 bubbles for all B4, B6, B15, and B23 cases due to higher value of void fraction of group-2 bubbles caused by lower production of KE and ε. It can also be found in Figure 5.22 (e)-(h) that small deviations of a_{i_G2} still exist even under high velocity conditions for liquid phase (B15 and B23 cases) without BIT for group-2 bubbles from the values of a_{i_G2} for the cases considering BIT by group-2 bubbles, which is caused by missing BIT effect of group-2 bubbles.

From the results, it can be induced that BIM for G1 bubbles played a role only for B4 case, which is the lowest velocity conditions and BIT for group-2 bubbles is an important factor for accurate prediction of interfacial area profile in a large diameter pipe. This is the same trend with void fraction profiles in Figure 5.19 and Figure 5.20.

5.5. CONCLUSIONS

5.5.1. The Effect of BIT Models. The effects of BIT source terms in the turbulent kinetic energy and turbulent dissipation rate on the distributions of void

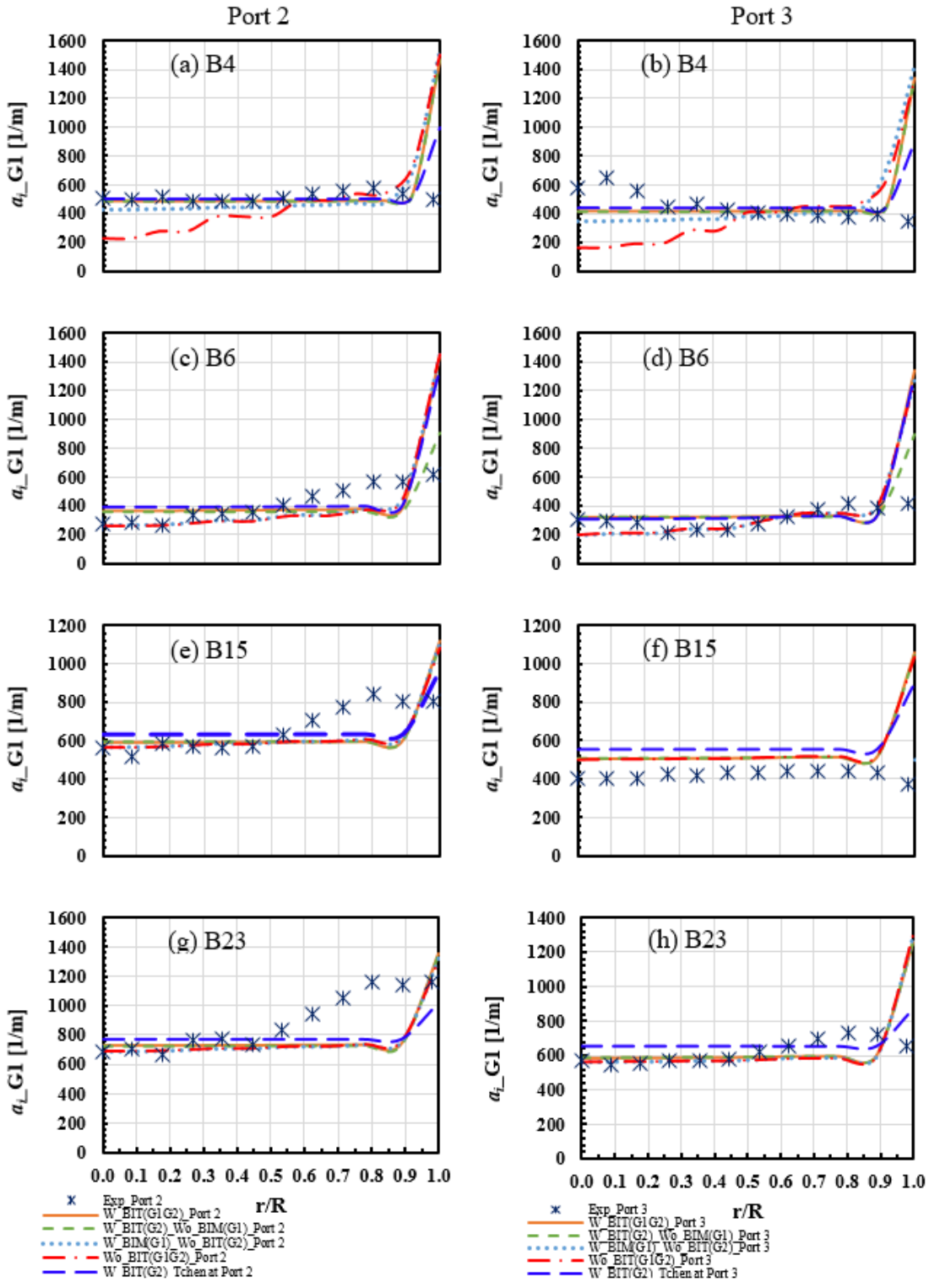

Figure 5.21. Effect of Bubble-Induced Turbulence on IAC (a_{i_G1}) for G1 Bubbles for B4, B6, B15, and B23 Cases at Port 2 and Port 3.

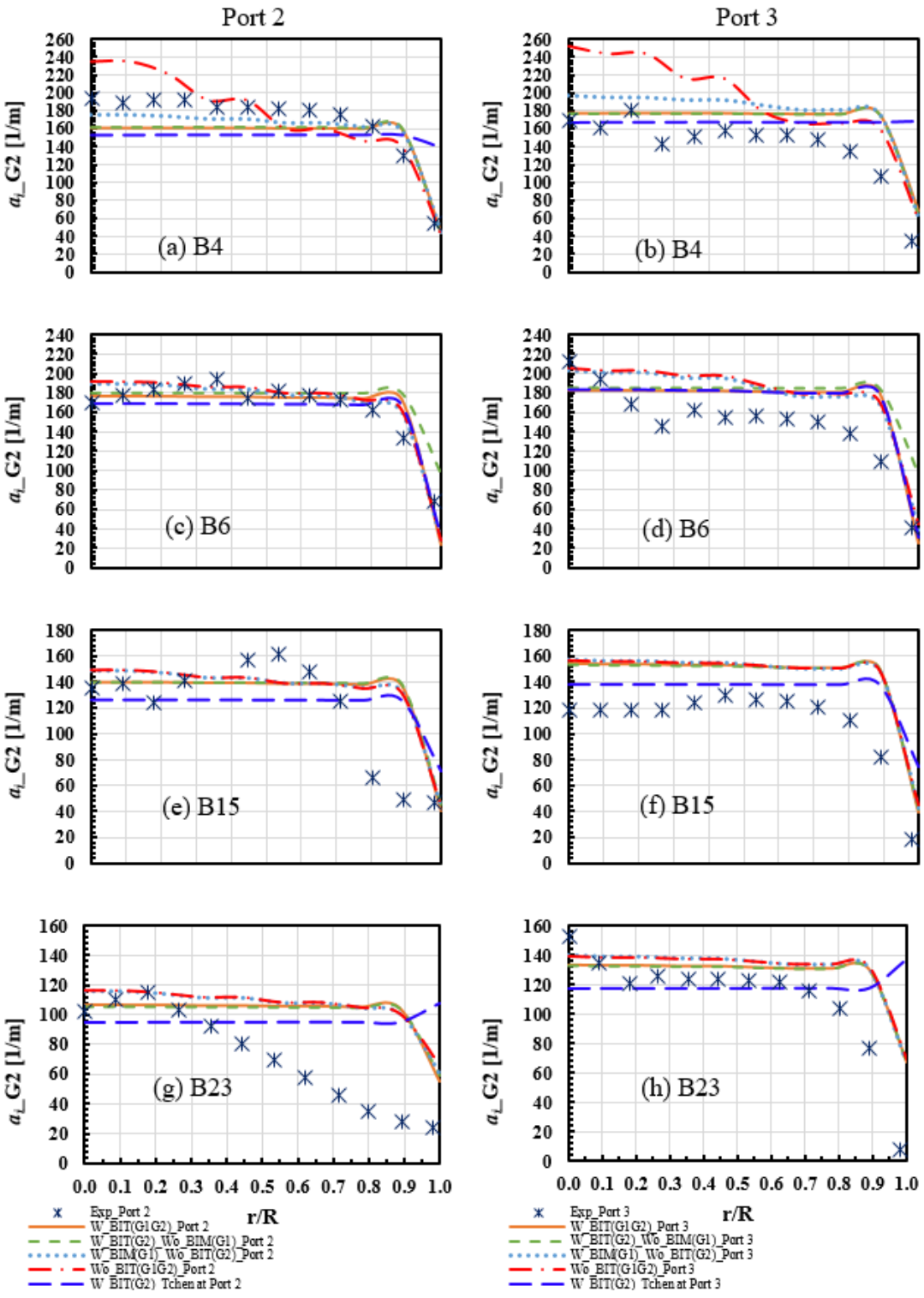

Figure 5.22. Effect of Bubble-Induced Turbulence on IAC (a_{i_G2}) for G2 Bubbles for B4, B6, B15, and B23 Cases at Port 2 and Port 3.

fraction, IAC, and each terms of 2G IATE were evaluated. The consideration of BIT source terms improved the prediction in the local distribution of IAC, especially for group-2 bubbles. The following points mainly can be concluded for the details of the BIT effect on turbulent parameters and two-phase flow parameters. For the turbulent kinetic energy distributions, in churn-turbulent flow regime, first, the turbulent kinetic energy varied more with higher superficial velocity. Second, by BIT source term, core peak distribution of turbulent kinetic energy were induced. Third, wall peak of the turbulent kinetic energy was found near the wall, without the BIT source terms.

In transition area, without BIT source term, higher turbulent kinetic energy was predicted in a large area of the pipe.

For the turbulent dissipation rate, in churn-turbulent flow regime, first, the effect of the BIT source term on the distribution of the turbulent dissipation rage was similar to the distributions of the turbulent kinetic energy. However, different from the turbulent kinetic energy distribution, the turbulent dissipation rate increased as close to the pipe wall and exponentially increased near the wall. In transition area, with the BIT source terms, flatter distributions and higher values of turbulent dissipation rate were predicted in the bulk area of the pipe than these without the source terms.

Void fraction profile did not sensitively react to the BIT source terms at low, middle, and high flow conditions in both churn-turbulent flow regime and transition area.

For the effect on the dominance of each IATE component, the BIT source terms affected the mechanisms of the 2G IATE. First, in churn-turbulent flow regime, the increase in superficial gas velocity causes more sensitive reaction of 2G IATE terms to the BIT sources, and small bubbles (Group-1 bubbles) more actively response to the BIT

source terms. Second, at middle flow conditions, in the transition area or regime close to the transition area, more bubble interactions, mass transfer and volume changes were caused by the BIT source terms, and IM term was dominantly affected. Those active changes in each term of the IATE induced variations in IAC distribution of group-1 bubbles. At high flow conditions, BIT source term affected the distributions of all three terms of IATE. In the transition area, the BIT source terms affected changes in all three mechanisms of 2G IATE for both group-1 and group-2 bubbles.

5.5.2. Effect of the Two Approach of BIT Model. In this work, the effect of BIT was investigated with different BIT conditions and with two different BIT models by implementing 2G IATE based on *Sγ* PBE model. Four different superficial velocity flow conditions of gas and liquid phases were adapted for model comparison with experiment dataset developed by Schlegel et al. (2012). BIT models change *KE* and ε values. Change in *KE* and ε leads to variations of source terms in void fraction transport equation and 2G IATE. Therefore, it is worth evaluating how BIT models change profiles of *KE*, ε, $\boldsymbol{\mu_{L,t}}$ and effect of those changes on variation of profiles for void fraction and ai. When BIT is considered for both group-1 and group-2 bubbles for beyond bubbly flows in a large diameter channel, the Sato model does not much affect local phase distributions of turbulent parameters and hydraulic parameters of two-phase flows, such as *KE*, ε, $\boldsymbol{\mu_{L,t}}$, and void fraction and a_i, respectively. However, the direct approach of introducing source terms to turbulence transport equation significantly impacts local profiles of dispersed phase.

The effect of BIT induced by group-2 bubbles is important for prediction of the local phase distributions. The significance of BIT by group-2 bubbles is enhanced at

lower J_L and J_G conditions as well as under higher level of void fraction for group-2 bubbles condition. As increase more gas velocity, effect of BIT from group-2 was more significant. For higher liquid velocity flow conditions,

BIT from group-1 or group-2 bubbles contributes a little to void fraction distribution, which means that at a certain point of liquid velocity turbulence by liquid flows is strongly developed and turbulence induced by bubbles is not significant enough to affect liquid phase trubulent flows. By considering BIT for group-2 bubbles, more active bubble interaction mechanisms, such as WE, TI, and SO that depend on turbulence intensity or relative velocity, may lead to satisfactory results. Therefore, BIT is an important factor that should be accounted for accurate prediction of local phase distribution, especially in large diameter channels, where various bubble shapes present.

BIBLIOGRAPHY

Antal, S. P., R. T. Lahey Jr, and J. E. Flaherty. "Analysis of phase distribution in fully developed laminar bubbly two-phase flow." International journal of multiphase flow 17, no. 5 (1991): 635-652.

Auton, T. R., J. C. R. Hunt, and M. Prud'Homme. "The force exerted on a body in inviscid unsteady non-uniform rotational flow." Journal of Fluid Mechanics 197 (1988): 241-257.

Behzadi, A., R. I. Issa, and H. Rusche. "Modelling of dispersed bubble and droplet flow at high phase fractions." Chemical Engineering Science 59, no. 4 (2004): 759-770.

Bestion, D. "Applicability of two-phase CFD to nuclear reactor thermalhydraulics and elaboration of Best Practice Guidelines." Nuclear Engineering and Design 253 (2012): 311-321.

Bove, Stefano, Tron Solberg, and Bjørn H. Hjertager. "Numerical aspects of bubble column simulations." International Journal of Chemical Reactor Engineering 2, no. 1 (2004).

Brooks, Caleb S., Sidharth S. Paranjape, Basar Ozar, Takashi Hibiki, and Mamoru Ishii. "Two-group drift-flux model for closure of the modified two-fluid model." International journal of heat and fluid flow 37 (2012): 196-208.

Buffo, Antonio, Marco Vanni, Peter Renze, and Daniele L. Marchisio. "Empirical drag closure for polydisperse gas–liquid systems in bubbly flow regime: Bubble swarm and micro-scale turbulence." Chemical Engineering Research and Design 113 (2016): 284-303.

Burns, Alan D., Thomas Frank, Ian Hamill, and Jun-Mei Shi. "The Favre averaged drag model for turbulent dispersion in Eulerian multi-phase flows." In 5th international conference on multiphase flow, ICMF, vol. 4, pp. 1-17. Japan: ICMF, 2004.

CD-ADAPCO, User Guide: STAR-CCM+ Version 11.02 CD-ADAPCO

Chen, Shao-Wen, Christopher Macke, Takashi Hibiki, Mamoru Ishii, Yang Liu, Peng Ju, Subash Sharma et al. "Experimental Study of Horizontal Bubble Plume With Computational Fluid Dynamics Benchmarking." Journal of Fluids Engineering 138, no. 11 (2016).

Chuang, Tien-Juei, and Takashi Hibiki. "Interfacial forces used in two-phase flow numerical simulation." International Journal of Heat and Mass Transfer 113 (2017): 741-754.

Clift, Roland, John R. Grace, and Martin E. Weber. "Bubbles, drops, and particles." (2005).

Colombo, Marco, and Michael Fairweather. "Influence of multiphase turbulence modelling on interfacial momentum transfer in two-fluid Eulerian-Eulerian CFD models of bubbly flows." Chemical Engineering Science 195 (2019): 968-984.

Deen, Niels Gerbrand, Tron Solberg, and Bjørn Helge Hjertager. "Large eddy simulation of the gas–liquid flow in a square cross-sectioned bubble column." Chemical engineering science 56, no. 21-22 (2001): 6341-6349.

Hibiki, Takashi, and Mamoru Ishii. "Lift force in bubbly flow systems." Chemical Engineering Science 62, no. 22 (2007): 6457-6474.

Hibiki, Takashi, Mamoru Ishii, and Zheng Xiao. "Axial interfacial area transport of vertical bubbly flows." International Journal of Heat and Mass Transfer 44, no. 10 (2001): 1869-1888.

Hosokawa, Shigeo, and Akio Tomiyama. "Multi-fluid simulation of turbulent bubbly pipe flows." Chemical Engineering Science 64, no. 24 (2009): 5308-5318.

Ishii, M., and S. Kim. "Development of one-group and two-group interfacial area transport equation." Nuclear science and engineering 146, no. 3 (2004): 257-273.

Ishii, Mamoru, and Novak Zuber. "Drag coefficient and relative velocity in bubbly, droplet or particulate flows." AIChE journal 25, no. 5 (1979): 843-855.

Ishii, Mamoru, and Takashi Hibiki. Thermo-fluid dynamics of two-phase flow. Springer Science & Business Media, 2010.

Khan, Irfan, Mingjun Wang, Yapei Zhang, Wenxi Tian, Guanghui Su, and Suizheng Qiu. "Two-phase bubbly flow simulation using CFD method: A review of models for interfacial forces." Progress in Nuclear Energy 125 (2020): 103360.

Kim, Seungjin, X. Y. Fu, X. Wang, and M. Ishii. "Development of the miniaturized four-sensor conductivity probe and the signal processing scheme." International journal of heat and mass transfer 43, no. 22 (2000): 4101-4118.

Kocamustafaogullari, G., and M. Ishii. "Foundation of the interfacial area transport equation and its closure relations." International Journal of Heat and Mass Transfer 38, no. 3 (1995): 481-493.

Krepper, Eckhard, Matthias Beyer, Thomas Frank, Dirk Lucas, and Horst-Michael Prasser. "CFD modelling of polydispersed bubbly two-phase flow around an obstacle." Nuclear Engineering and Design 239, no. 11 (2009): 2372-2381.

Krepper, Eckhard, Roland Rzehak, and Dirk Lucas. "Validation of a closure model framework for turbulent bubbly two-phase flow in different flow situations." Nuclear Engineering and Design 340 (2018): 388-404.

Kuidjo, EV Kuidjo, M. G. Rodio, R. Abgrall, and P. Sagaut. "Comparison of bubbles interaction mechanisms of two-group Interfacial Area Transport Equation model." International Journal of Multiphase Flow 163 (2023): 104399.

Liao, Yixiang, and Dirk Lucas. "Investigations on bubble-induced turbulence modeling for vertical pipe bubbly flows." In International Conference on Nuclear Engineering, vol. 44984, pp. 519-527. American Society of Mechanical Engineers, 2012.

Liao, Yixiang, Tian Ma, Eckhard Krepper, Dirk Lucas, and Jochen Fröhlich. "Application of a novel model for bubble-induced turbulence to bubbly flows in containers and vertical pipes." Chemical Engineering Science 202 (2019): 55-69.

Liu, T. J. "The role of bubble size on liquid phase turbulent structure in two-phase bubbly flow." In Proc. Third International Congress on Multiphase Flow ICMF, vol. 98, pp. 8-12. 1998.

Lucas, D., M. Beyer, J. Kussin, and P. Schütz. "Benchmark database on the evolution of two-phase flows in a vertical pipe." Nuclear engineering and design 240, no. 9 (2010): 2338-2346.

Lucas, D., M. Beyer, L. Szalinski, and P. Schütz. "A new database on the evolution of air–water flows along a large vertical pipe." International Journal of Thermal Sciences 49, no. 4 (2010): 664-674.

Lucas, Dirk, E. Krepper, and H-M. Prasser. "Use of models for lift, wall and turbulent dispersion forces acting on bubbles for poly-disperse flows." Chemical Engineering Science 62, no. 15 (2007): 4146-4157.

Ma, Tian, Claudio Santarelli, Thomas Ziegenhein, Dirk Lucas, and Jochen Fröhlich. "Direct numerical simulation–based Reynolds-averaged closure for bubble-induced turbulence." Physical Review Fluids 2, no. 3 (2017): 034301.

Manera, Annalisa, Basar Ozar, Sidharth Paranjape, Mamoru Ishii, and H-M. Prasser. "Comparison between wire-mesh sensors and conductive needle-probes for measurements of two-phase flow parameters." Nuclear Engineering and Design 239, no. 9 (2009): 1718-1724.

Morel, Christophe. "Turbulence modelling and first numerical simulations in turbulent two-phase flows." In Proc. 11 th Symp. on Turbulent Shear Flows, Grenoble, France, 1997, vol. 3. 1997.

Oberkampf, William L., and Timothy G. Trucano. "Verification and validation in computational fluid dynamics." Progress in aerospace sciences 38, no. 3 (2002): 209-272.

Ohnuki, Akira, and Hajime Akimoto. "Experimental study on transition of flow pattern and phase distribution in upward air–water two-phase flow along a large vertical pipe." International journal of multiphase flow 26, no. 3 (2000): 367-386.

Pan, Y., M. P. Dudukovic, and M. Chang. "Dynamic simulation of bubbly flow in bubble columns." Chemical Engineering Science 54, no. 13-14 (1999): 2481-2489.

Pfleger, D., and S. Becker. "Modelling and simulation of the dynamic flow behaviour in a bubble column." Chemical engineering science 56, no. 4 (2001): 1737-1747.

Politano, M. S., P. M. Carrica, and J. Converti. "A model for turbulent polydisperse two-phase flow in vertical channels." International Journal of Multiphase Flow 29, no. 7 (2003): 1153-1182.

Pourtousi, M., J. N. Sahu, and P. Ganesan. "Effect of interfacial forces and turbulence models on predicting flow pattern inside the bubble column." Chemical Engineering and Processing: Process Intensification 75 (2014): 38-47.

Rabha, Swapna, Markus Schubert, and Uwe Hampel. "Intrinsic flow behavior in a slurry bubble column: a study on the effect of particle size." Chemical Engineering Science 93 (2013): 401-411.

Rzehak, Roland, and Eckhard Krepper. "Bubble-induced turbulence: Comparison of CFD models." Nuclear Engineering and Design 258 (2013a): 57-65.

Rzehak, Roland, and Eckhard Krepper. "CFD modeling of bubble-induced turbulence." International Journal of Multiphase Flow 55 (2013): 138-155.

Sato, Y., and K. Sekoguchi. "Liquid velocity distribution in two-phase bubble flow." International Journal of Multiphase Flow 2, no. 1 (1975): 79-95.

Schiller, Links. "A drag coefficient correlation." Zeit. Ver. Deutsch. Ing. 77 (1933): 318-320.

Schlegel, Joshua P., P. Sawant, S. Paranjape, B. Ozar, T. Hibiki, and M. Ishii. "Void fraction and flow regime in adiabatic upward two-phase flow in large diameter vertical pipes." Nuclear Engineering and Design 239, no. 12 (2009): 2864-2874.

Schlegel, Joshua P., S. Miwa, S. Chen, T. Hibiki, and M. Ishii. "Experimental study of two-phase flow structure in large diameter pipes." Experimental Thermal and Fluid Science 41 (2012): 12-22.

Schlegel, Joshua P., S. Sharma, R. M. Cuenca, T. Hibiki, and M. Ishii. "Local flow structure beyond bubbly flow in large diameter channels." International journal of heat and fluid flow 47 (2014): 42-56.

Schwer, Leonard E. "Guide for verification and validation in computational solid mechanics." (2009).

Scott, D., M. Sabourin, S. Beaulieu, B. Papillon, and C. Ellis. "CFD model of an aerating hydrofoil." In IOP Conference Series: Earth and Environmental Science, vol. 22, no. 6, p. 062008. IOP Publishing, 2014.

Sharma, S. L., T. Hibiki, M. Ishii, Joshua P. Schlegel, J. R. Buchanan Jr, K. J. Hogan, and P. W. Guilbert. "An interfacial shear term evaluation study for adiabatic dispersed air–water two-phase flow with the two-fluid model using CFD." Nuclear Engineering and Design 312 (2017): 389-398.

Sharma, Subash L. "Investigation of gas-liquid two-phase flow using three-field two-fluid model and two-group interfacial area transport equation in CFD code." (2016).

Sharma, Subash L., Mamoru Ishii, Takashi Hibiki, Joshua P. Schlegel, Yang Liu, and John R. Buchanan Jr. "Beyond bubbly two-phase flow investigation using a CFD three-field two-fluid model." International Journal of Multiphase Flow 113 (2019): 1-15.

Shaver, D. R., and M. Z. Podowski. "Modeling of interfacial forces for bubbly flows in subcooled boiling conditions." Transactions of the American Nuclear Society 113, no. 10 (2015): 1368-1371.

Shawkat, M. E., C. Y. Ching, and M. Shoukri. "Bubble and liquid turbulence characteristics of bubbly flow in a large diameter vertical pipe." International Journal of Multiphase Flow 34, no. 8 (2008): 767-785.

Shih, T-H., William W. Liou, Aamir Shabbir, Zhigang Yang, and Jiang Zhu. A new k-epsilon eddy viscosity model for high Reynolds number turbulent flows: Model development and validation. No. CMOTT-94-6. 1994.

Smith, T. R., Joshua P. Schlegel, T. Hibiki, and M. Ishii. "Mechanistic modeling of interfacial area transport in large diameter pipes." International journal of multiphase flow 47 (2012): 1-16.

Sun, Xiaodong, Mamoru Ishii, and Joseph M. Kelly. "Modified two-fluid model for the two-group interfacial area transport equation." Annals of Nuclear Energy 30, no. 16 (2003): 1601-1622.

Sun, Xiaodong, Seungjin Kim, Mamoru Ishii, and Stephen G. Beus. "Development of two-group interfacial area transport equation for confined flow-1. Modeling of bubble interactions," The 11th Int. Conf. on Nuclear Engineering, Shinjuku, Tokyo, Japan, April 20–23, 2003.

Sun, Xiaodong, Seungjin Kim, Mamoru Ishii, and Stephen G. Beus. "Development of two-group interfacial area transport equation for confined flow-2. Model evaluation," The 11th Int. Conf. on Nuclear Engineering, Shinjuku, Tokyo, Japan, April 20–23, Paper No.: ICONE11-36115, 2003.

Sun, Xiaodong, Seungjin Kim, Mamoru Ishii, and Stephen G. Beus. "Modeling of bubble coalescence and disintegration in confined upward two-phase flow." Nuclear Engineering and Design 230, no. 1-3 (2004): 3-26.

Sun, Xiaodong, Todd R. Smith, Seungjin Kim, Mamoru Ishii, and Jennifer Uhle. "Interfacial area of bubbly flow in a relatively large diameter pipe." Experimental thermal and fluid science 27, no. 1 (2002): 97-109.

Sun, Xiaodong. "Two-group interfacial area transport equation for a confined test section." PhD diss., Purdue University, 2001.

Tabib, Mandar V., Swarnendu A. Roy, and Jyeshtharaj B. Joshi. "CFD simulation of bubble column—an analysis of interphase forces and turbulence models." Chemical Engineering Journal 139, no. 3 (2008): 589-614.

Tomiyama, A., G. P. Celata, S. Hosokawa, and S. Yoshida. "Terminal velocity of single bubbles in surface tension force dominant regime." International journal of multiphase flow 28, no. 9 (2002): 1497-1519.

Tomiyama, Akio, Hidesada Tamai, Iztok Zun, and Shigeo Hosokawa. "Transverse migration of single bubbles in simple shear flows." Chemical Engineering Science 57, no. 11 (2002): 1849-1858.

Tomiyama, Akio, Isao Kataoka, Iztok Zun, and Tadashi Sakaguchi. "Drag coefficients of single bubbles under normal and micro gravity conditions." JSME International Journal Series B Fluids and Thermal Engineering 41, no. 2 (1998): 472-479.

Tomiyama, Akio. "Drag, lift and virtual mass forces acting on a single bubble." In 3rd Int. Symp. on Two-Phase Flow Modeling and Experimentation, 2004.

Tomiyama, Akio. "Struggle with computational bubble dynamics." Multiphase Science and Technology 10, no. 4 (1998): 369-405.

Troshko, A. A., and Y. A. Hassan. "A two-equation turbulence model of turbulent bubbly flows." International Journal of Multiphase Flow 27, no. 11 (2001): 1965-2000.

Wu, Q., S. Kim, M. Ishii, and S. G. Beus. "One-group interfacial area transport in vertical bubbly flow." International Journal of Heat and Mass Transfer 41, no. 8-9 (1998): 1103-1112.

Yao, Wei, and Christophe Morel. "Volumetric interfacial area prediction in upward bubbly two-phase flow." International Journal of Heat and Mass Transfer 47, no. 2 (2004): 307-328.

Yun, Byong-Jo, Andrew Splawski, Simon Lo, and Chul-Hwa Song. "Prediction of a subcooled boiling flow with advanced two-phase flow models." Nuclear engineering and design 253 (2012): 351-359.

Zhang, D., N. G. Deen, and J. A. M. Kuipers. "Numerical simulation of the dynamic flow behavior in a bubble column: a study of closures for turbulence and interface forces." Chemical Engineering Science 61, no. 23 (2006): 7593-7608.

VITA

Sungje Hong was born in Seoul, South Korea. Sungje was awarded a B.S. in Mechanical Engineering with minor in Electrical Engineering from Handong Global University in 2009. He began research on development of experimental apparatus for surface temperature measurements of pebbles and local heat flux of pebbles in pebble bed modular reactor (PBMR) and performed computational fluid dynamics (CFD) analysis using ANSYS CFD code for the thermal analysis of the PBMR as a graduate research assistant for his M.S. degree at Handong Global University and completed M.S. degree in Mechanical Engineering in 2014.

Sungje started his job as an engineer in a nuclear company. After working over five years in the nuclear industry, he attended Missouri University of Science and Technology in pursuit of a Ph.D. degree in Nuclear Engineering and focused on CFD analysis for beyond bubbly gas-liquid two-phase flows in a large diameter pipe. He was awarded a Ph.D. in Nuclear Engineering from Missouri S&T for the effort in May of 2023.

Sungje has had the great pleasure of sharing this journey with many special people which he cannot thank enough for their support. One person in particular, a wife of Sungje, has been at his side along the way since they came to Missouri state nearly six years ago. They are excited to begin the next chapter of their lives.